P-14-22

Tests and simulations of THM processes relevant for the buffer installation

Lars-Erik Johannesson, Ola Kristensson, Mattias Åkesson
Clay Technology

Peter Eriksson, Svensk Kärnbränslehantering AB

Mikael Hedin, ÅF

March 2014

Svensk Kärnbränslehantering AB
Swedish Nuclear Fuel
and Waste Management Co

Box 250, SE-101 24 Stockholm
Phone +46 8 459 84 00

ISSN 1651-4416
SKB P-14-22
ID 1343697

Tests and simulations of THM processes relevant for the buffer installation

Lars-Erik Johannesson, Ola Kristensson, Mattias Åkesson
Clay Technology

Peter Eriksson, Svensk Kärnbränslehantering AB

Mikael Hedin, ÅF

March 2014

Keywords: Buffer, relative humidity, deposition hole.

Abstract

The SKB reference design states that we are to install all buffer components and canisters in a disposal tunnel before initiating the backfilling. This results in a situation where the installed canisters and buffer components will need to be protected for a time of up to three months before the backfilling covers all of the deposition holes. During this time, the bentonite blocks will be protected by a buffer protection made of a plastic or of rubber in order to protect the bentonite from water and high relative humidity. The covering is removed just before the start of the backfilling.

The heat from the canister will affect the buffer blocks and cause a redistribution of the water in the buffer during the three month period. Small scale laboratory experiments were conducted to study this redistribution process. Based on the results of these small scale experiments a decision was made to repeat the experiments in full scale. The reason for this decision was challenges with scaling factors and the fact that we could not achieve both the correct temperature and temperature gradient simultaneously in the small scale tests.

The full-scale test setup consisted of a thermally insulated steel container holding two full sized buffer rings with five heater in the centre. The temperature of the steel container (simulating the rock temperature) was controlled using a water mantel while the temperature of the heaters were directly controlled using a power controller. Temperature and humidity sensors were installed both in, and on the surfaces of the buffer.

Dismantling of the test was done after a period of four months after initiation. At this time we could identify a number of cracks in the bentonite blocks, especially close to the heater. We could also identify changes in density and water content which were determined over several profiles of the buffer blocks.

The observations and the data from the laboratory test show that a redistribution of the water and dry density had occurred and this caused the observed damages on the block. The changes in the dry density were caused by local volume changes of the buffer. Although the cracks in the blocks were extended and large; no larger pieces of bentonite had fallen off from the blocks.

A modelling of the test was done after the dismantling using both Code_Bright and Comsol. The purpose of the modelling was to see if the simulations could describe the behaviour of the bentonite during the test. The models could fairly well describe the desiccation of the buffer.

Sammanfattning

Enligt SKB:s referensdesign ska vi installera alla buffertkomponenter och kapslar i en depositionstunnel innan man påbörjar återfyllnaden. Detta resulterar i en situation där de installerade kapslarna och buffertkomponenterna måste skyddas under en tid på upp till tre månader innan återfyllningen täcker alla deponeringshål. Under denna tid kommer bentonitblocken vara skyddade av ett buffertskydd tillverkat av plast eller gummi. Buffertskyddets uppgift är att skydda bentoniten från vatten och från hög relativ fuktighet. Buffertskyddet avlägsnas strax före återfyllning.

Den termiska effekten från kapseln kommer att påverka buffertblocken inuti buffertskyddet och orsaka en omfördelning av vattnet i bufferten under tremånadersperioden. Småskaliga laboratorieförsök genomfördes för att studera denna omfördelningsprocess. Baserat på resultaten från dessa småskaliga experiment fattades beslut om att upprepa experimenten i full skala. Anledningen till detta beslut var problem med att identifiera lämpliga skalfaktorer samt det faktum att vi inte kan uppnå både rätt absolut temperatur och temperaturgradient samtidigt i småskaliga tester.

Den fullskaliga testuppställningen bestod av en värmeisolerad stålbehållare innehållandes två fullstora buffertringar med fem värmare placerade i centrum av testuppställningen. Stålbehållarens temperatur (simulering av bergtemperaturen) kontrollerades med hjälp av en vattenmantel medan temperaturen på värmarna styrdes genom att kontrollera värmarnas effekt. Temperatur- och fuktgivare installerades både i blocken samt på buffertblockens ytor.

Brytning av försöket gjordes efter en period av fyra månader av förslutning. Vid brytning kunde man identifiera ett antal sprickor i bentonitblocken, speciellt i närheten av värmarna . Man kunde också identifiera förändringar i densitet och vattenhalt som bestämdes genom flertalet profiler i buffertblocken.

Observationer och data visar att en omfördelning av vattnet och torrdensitet hade inträffat och att detta i sin tur orsakat sprickorna i buffertblocken. Förändringarna i torrdensiteten var orsakade av lokala volymförändringar för bufferten.

Även fast sprickorna i blocken var genomgående och relativt stora så lossnade aldrig några större bitar av buffertblocken.

En modellering av testet genomfördes efter brytning med både Code_Bright och Comsol. Syftet med att modellera var att se om simuleringarna kunde beskriva beteendet hos bentoniten under testet. Modelleringen lyckades väl beskriva de uttorkningsprocesser som observerats.

Contents

1 Introduction

According to the Swedish concept for disposal of radioactive waste, KBS-3V the buffers surrounding the copper canister consist of highly compacted blocks of bentonite, Figure 1-1. The outer slot between the surface of deposition hole and the blocks is filled with bentonite pellets.

The upper part of the deposition hole and the central part of the tunnel is filled with blocks of backfill material.

According to SKB's reference design we are installing all canisters and buffer components in a complete tunnel before initiating the backfilling of the tunnel.

After installation of canisters and bentonite blocks in a deposition hole, there will be a time period of up to approximately three months (Wimelius and Pusch 2008) before the backfilling of the tunnel, above the deposition hole, is completed. During this time, the bentonite blocks will be covered with a buffer protection made out of a special sheet of plastic or rubber in order to protect the bentonite from water and high relative humidity. Just before the start of the backfilling, the covering sheet will be removed and the slot between buffer blocks and rock will be filled with pellets.

During the three month period, before the pellet and backfill installation, it is possible that the heat from the canister will affect the buffer blocks and cause a redistribution of the water in the blocks. In order to investigate this phenomenon, a laboratory test has been performed in a small scale with the outer diameter of the buffer blocks of about 300 mm, see Appendix 1. Numerical analyses of the processes in the small scale test have also been made.

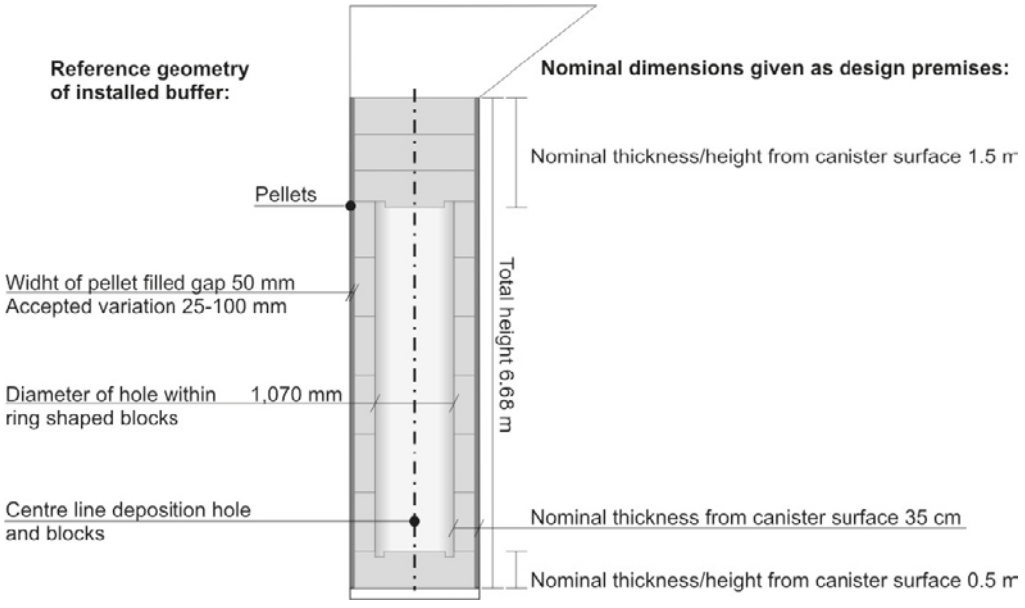

Figure 1-1. *Reference geometry of the installed buffer and the nominal dimensions given as design premises. Note that the installed dimensions and density will depend on the geometry of the deposition hole (from SKB 2010).*

There were uncertainties in the conclusions from the laboratory tests. These laboratory tests could either simulate the actual temperature fall over the buffer i.e. the temperature on the inner and outer surfaces of the buffer or the temperature gradient in a full scale deposition hole. In order to be able to simulate the correct temperature in all parts of the buffer in a real repository, i.e. both correct temperature level and temperature gradient, a laboratory test with full size buffer blocks is required. This was the reason for starting the planning of the test described in this report (see test setup in Chapter 2). The installation of the test was preceded by numerical simulation of the temperature evolution in a repository at the installation of a canister in order to get input for the temperature control of the test (described in Chapter 3).

The test was excavated after approximately four months at which point we conducted both ocular inspection of the test and performed density and water content measurements (described in Chapter 4). Further simulations were finally done after the dismantling using both Code_Bright and Comsol with the purpose to see if the simulations could describe the observed behavior of the bentonite during the test (described in Chapter 5).

2 Test setup

2.1 General

The test is designed to study the effects of the temperature gradient that is created over the buffer after the installation of a canister but before the pellet and backfill has been installed. During this time there will be a buffer protection installed to protect the buffer material from the surrounding environment in the deposition hole. The focus of the study is two of the buffer rings positioned close to the centre of the canister as see in Figure 2-1.The goal is to study the effects of the temperature gradient over the bentonite. But rather than trying to analyse a worst case scenario[1], focus is in the centre of the canister, see Figure 2-1.

The result of the test is a description of the development of the temperature in the buffer during the experiment and a mapping of the redistribution of water.

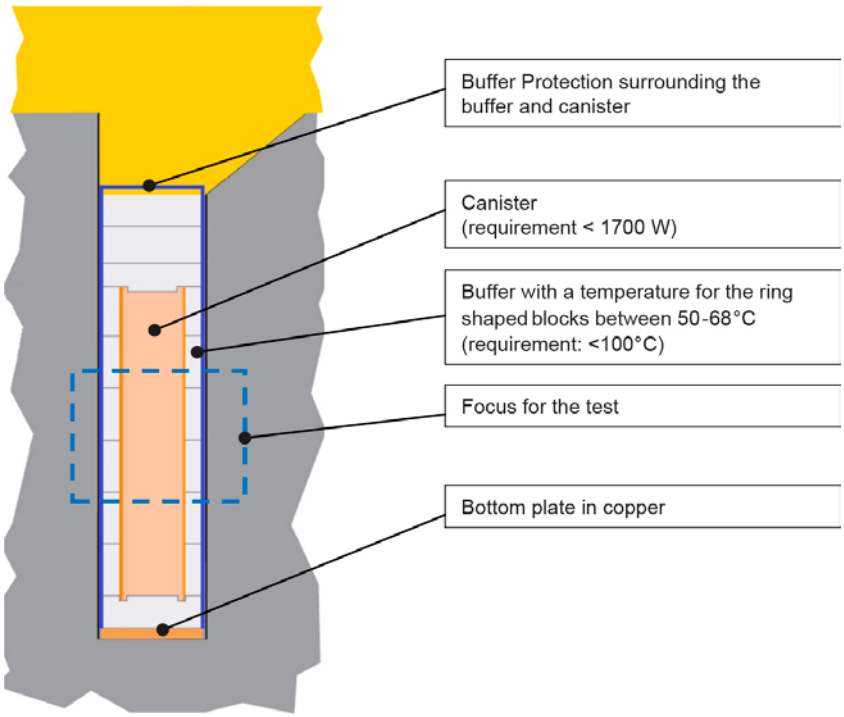

Figure 2-1. *Focus of the study is two of the buffer rings close to the centre of the canister.*

[1] Worst case scenario is expected to be at the top and bottom of the canister and buffer or if the buffer protection comes in direct contact with the buffer but this has not been verified within this test.

2.2 Test equipment

The test setup as shown in Figure 2-2:

1. Styrofoam isolation covered with a steel lid > 250 mm.
2. Glass wool isolation 100 mm (also covered top of container).
3. The tank is outfitted with a 150 mm thick temperature controlled water mantel which enabled us to set the temperature on the outside of the buffer; simulating the temperature of the buffer protection and rock wall. To ensure an even temperature over the complete cylinder we used a circulation pump during the complete experiment to circulate the water.
4. Space between buffer blocks and water mantel.
5. Upper buffer ring.
6. Lower buffer ring.
7. 5+5 layers of Styrofoam (Sundolitt XPS300) T=100 mm.
8. Upper steel assembly for lifting and stabilization. Welled to the water mantel (3).
9. Water level.
10. Four threaded rods welded to the lifting cross of the heater (adjustment of heater placement).
11. 50 mm of glass wool isolation between buffer block and Styrofoam; and between the heater and Styrofoam.
12. Lower lifting cross for heater.
13. Five thermal units placed 250 mm from the outer edge; and 200 mm from the bottom of the sand filled heater.
14. Space between heater and buffer blocks.
15. Sand for even distribution of heat.
16. 50 mm glass wool isolation to protect the Styrofoam from the thermal load of the heater.

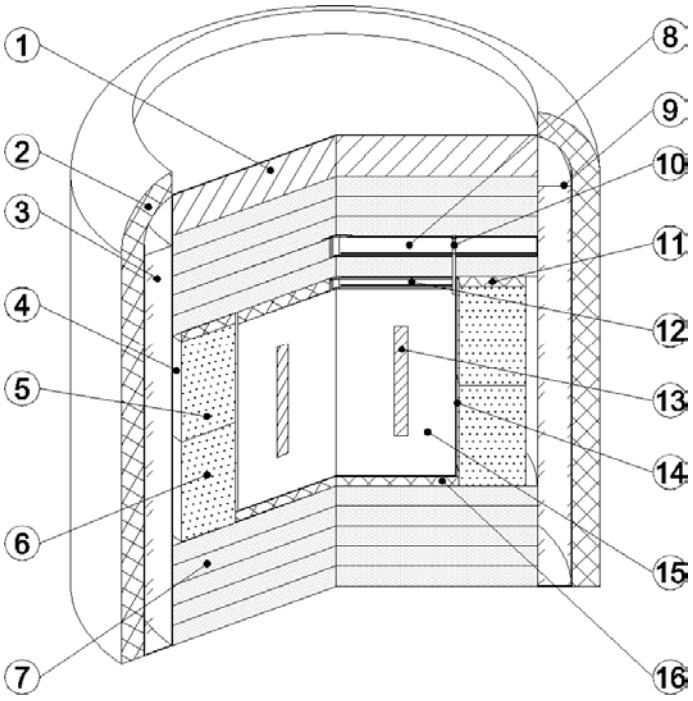

Figure 2-2. *The test setup.*

Table 2-1. Dimensions.

Total height	**2,250 mm**
Cylinder width (outside):	2,050 mm
Cylinder width (inside):	1,750 mm
Heater:	1,050 mm
Insulation:	500 mm each for top and bottom
	Thermal conductivity of Styrofoam 0,033 W/(m*K)
Extra outer insulation:	250 mm
	Thermal conductivity of Glass wool 0.04 W/(m*K)
Buffer:	2 rings totalling 1,000 mm

Figure 2-3. *Test setup for the temperature gradient test.*

2.3 Buffer material

The buffer consists of two ring shaped blocks of MX-80 with an average water content of 17%. The bentonite was delivered to Äspö during 2012 with an initial water content of about 11%. It was mixed with tap water in an Eirich-mixer situated at Äspö to its final water content. The blocks were compacted uniaxially in a press at GEA Heat Exchangers AB in Ystad, Sweden. The density and water content of the blocks are shown in Table 2-2. After the compaction the blocks were machined to its final shape at Sorvikivi Oy in Savitaipale, Finland. The final densities of the blocks after machining are also shown in Table 2-2.

Table 2-2. Data from the manufacturing of the blocks for the test.

Block No	Water cont. (%)	Density at compaction (kg/m^3)	Density after machining (kg/m^3)
B1 (bottom block)	17.3	2,131	2,129
B2 (top block)	17.4	2,110	2,134

2.4 Instrumentation

To monitor the progress of the experiment we installed a basic set of sensors listed in Table 2-3.

The sensors for measuring temperature and relative humidity were installed in four perpendicular directions at the upper surface of the lower bentonite block, see Figure 2-4. At the installation of the sensors, holes were drilled for the sensors and grooves for the cables coming from the sensors, on the upper surface of the lower block towards the outer surface of the block were made, see Figure 2-4.

The RH sensors were of the type KIMO TH200 with built in temperature sensors (Pt100 thermo couples). The principle of the sensor is measurement of the capacitance. In total, 8 RH sensors were installed in two sections of the block. These sensors were placed in the block with a mutual distance of about 60 mm, see Figure 2-4. Another 2 sensors were installed for measuring the Relative humidity in the outer slot between the bentonite blocks and the test cylinder.

The thermo couples, Pentronic Type K, were also installed in two sections of the block, in total 8 sensors, see Figure 2-4. The thermo couples T1, T4 T5 and T8 had its sensors tips placed at boundaries of the block i.e. the temperatures were measuring on the surfaces of the block. Another 4 thermo couples were placed at mid height on the surface of the heater and 4 thermo couples measured the temperature on the outer surface of the test cylinder.

Table 2-3. Sensors used in the experiment.

Description	Type	Placement
RH1...RH8: KIMO TH200 incl. Pt100 thermo couples	Temp+RH	Inside the bottom block
RH10...11: KIMO TH200 incl. Pt100 thermo couples	Temp+RH	outer slot
T1, T4, T5 and T8: Pentronic Type K thermo couples	Temperature	Surface of the blocks
T2, T3, T6 and T7: Pentronic Type K thermo couples	Temperature	Inside the bottom block
4 additional Temp-sensors: Pentronic Type K thermo couples	Temperature	mid height on the surface of the heater
4 additional Temp-sensors: Pentronic Type K thermo couples	Temperature	outer surface of the test cylinder

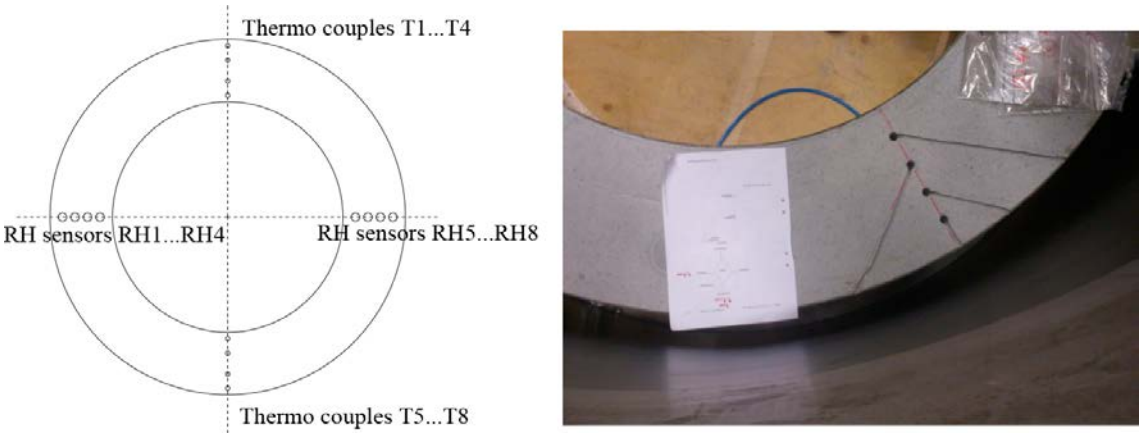

Figure 2-4. *The position of the sensors installed from the upper surface of the bottom block.*

The power to the heating elements inside the heater was also possible to adjust during the test period. Furthermore the temperature on the outer surface of the test cylinder was adjusted by circulating the water in the outer slot of the test cylinder, see Section 2.1. The data from the installed sensors, and the applied power on the heating elements were collected continuously during the test period.

2.5 Experiment Control System

A TYA 201 effect controller was used to adjust the heat during the experiment to ensure that the correct temperature on the inner buffer surface was reached.

The temperature on the outer surface of the test cylinder was adjusted by controlling the temperature of the circulating water in the water mantel.

The data from the installed sensors, and the applied power on the heating elements were collected continuously during the test period.

3 Pre operational simulations of the test

3.1 Introduction

In order to develop a thermal protocol for the experiment, modelling of a KBS-3V deposition hole during installation was first performed to obtain boundary conditions which were prescribed on a model of the actual experiment.

The experiment design consisted of two full size ring shaped bentonite blocks, a steel pipe equipped with heaters inside simulating the canister, and a water tank surrounding the blocks which allowed for controlling the outer wall temperature. The top and bottom was heavily insulated to avoid thermal leakage so that radial heat flow was obtained.

The geometry can be summarized as:

- Heater radius: $r_h = 0.525$ m
- Inner bentonite surface radius: $r_{in} = 0.535$ m
- Outer bentonite surface radius: $r_{out} = 0.825$ m
- Rock wall/Water tank radius: $r_w = 0.875$ m
- Inner slot width: $a_{in} = r_{in} - r_h = 0.01$ m
- Outer slot width: $a_{out} = r_{in} - r_h = 0.05$ m

In order to obtain a representative temperature evolution in the buffer, the experiment has to be adjusted thermally. The thermal adjustment of the experiment can be done by:

(1) Setting the heater power, which gives a certain radial heat flux, q_r. Increase of q_r gives a steeper temperature profile as indicated in Figure 3-1.

(2) Setting the temperature at the outer wall, T_w, as given in Appendix 2. An increase of T_w gives a shift upwards of the profile as indicated in Figure 3-2.

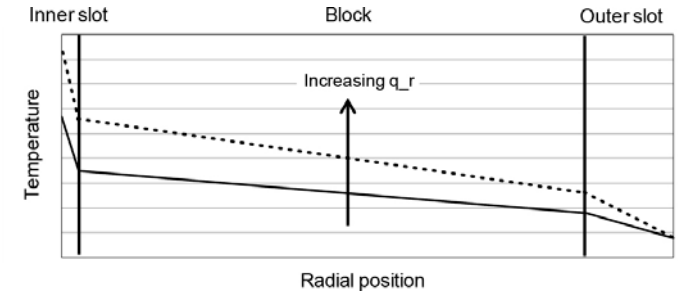

Figure 3-1. *Schematic radial temperature profiles over the experiment for two different heat fluxes.*

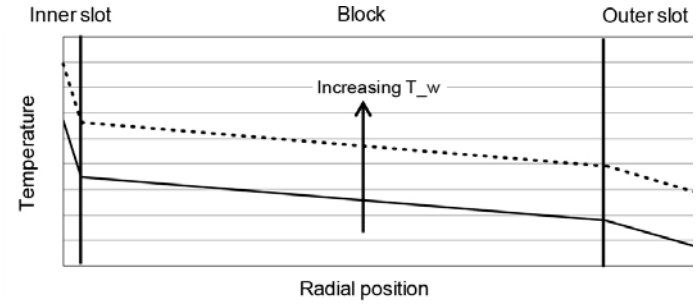

Figure 3-2. *Schematic radial temperature profiles over the experiment for two different temperatures at the outer boundary.*

3.2 Defining representative temperature evolutions

Before considering the experiment representative temperature evolutions had to be defined so that suitable boundary conditions could be obtained for the model of the experiment. A thermal model in 3D (2D with axisymmetry) of a general KBS-3V design, see Figure 3-3, was used for generating representative temperature evolutions.

The KBS-3V model, described in more detail in Appendix 2, was modelled using two different values for the rock thermal conductivity, 3.63 and 2.00 W/(m·K). The former choice results in *rock temperatures* that agree well with measurements of the Prototype Repository and the latter generates *buffer temperatures* that agree better with measurements in the Prototype Repository.

It was decided that the model using 2.00 W/(m·K) should be regarded as the base case producing the temperatures to aim for. The temperature evolutions for both choices of thermal conductivity are shown in Figure 3-4 and the heater powers per length unit are shown in Figure 3-5.

Temperatures obtained after three months are listed in Table 3-1 for the two choices of thermal conductivities.

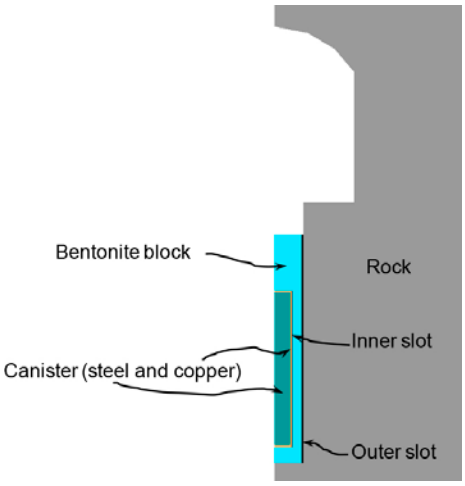

Figure 3-3. *Close up of the geometry of the tunnel and deposition hole in the KBS-3V model.*

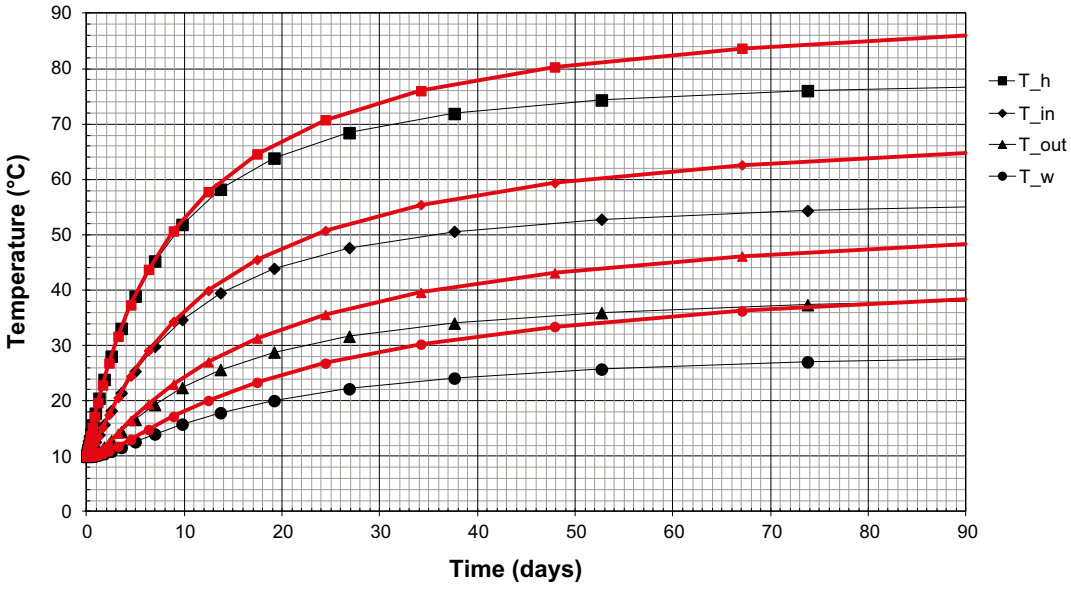

Figure 3-4. *Temperature evolutions from the thermal KBS-3V model using a rock thermal conductivity of 3.63 W/(m·K) (black) and 2.00 W/(m·K) (red).In the legend: T_h=heater temperature, T_in=inner block surface temperature, T_out=outer block surface temperature, and T_w=wall temperature.*

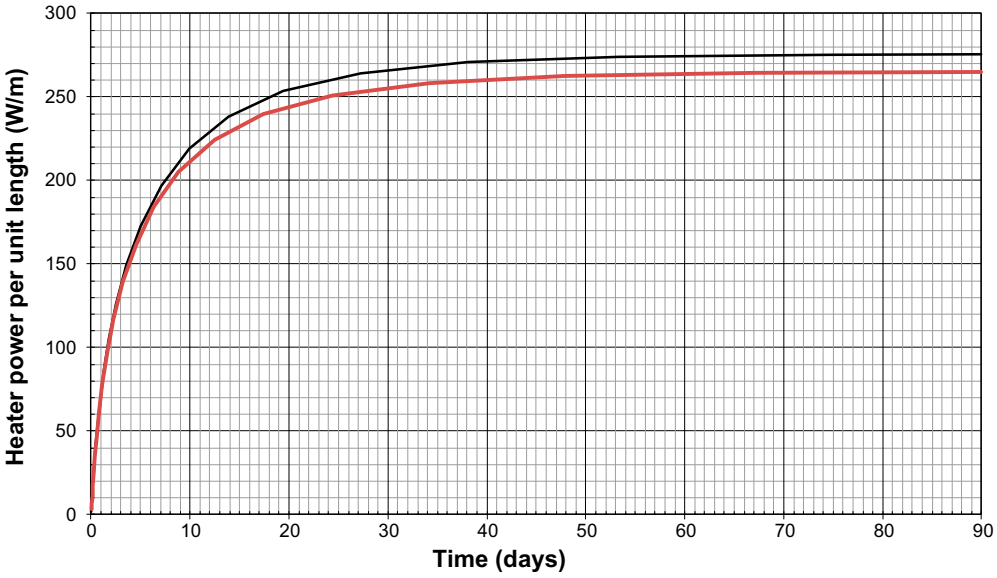

Figure 3-5. *The heater power per length unit obtained from the KBS-3V model using a rock thermal conductivity of 3.63 W/(m·K) (black) and 2.00 W/(m·K) (red).*

Table 3-1. Temperatures after three months.

Feature	T_w	T_{out}	T_{in}	T_h
3.63 W/(m·K)	27.6	38.0	55.0	76.7
2.00 W/(m·K)	38.3	48.3	64.8	86.0

3.3 Modelled experiment with an adopted water temperature protocol

To get an idea of how the experiment could be controlled so that the temperature in the buffer became representative for KBS-3V a model of the experiment as described in Appendix 2 was developed. The model simulated the thermal and hydraulic processes in a disc at mid-height of the experiment.

As can be seen in Figure 3-6 showing the model geometry, the “canister”, a sand-filled steel pipe, was also represented in the model, since this inherits a thermal inertia which affects the evolution of radial heat flux obtained at the steel pipe outer surface, and therefore also the buffer temperature evolution.

In the model of the experiment the protocol in Table 3-2, for the outer wall temperature, and a constant heater power of 265 W/m were used. In the experiment, the wall temperature protocol could be prescribed by letting water with the correct temperature flow in the water tank.

The desired result, the obtained temperatures when following the wall temperature protocol and applying a constant heater power of 265 W/m, are shown in Figure 3-7.

Figure 3-6. Geometry of the 1D_T experiment model.

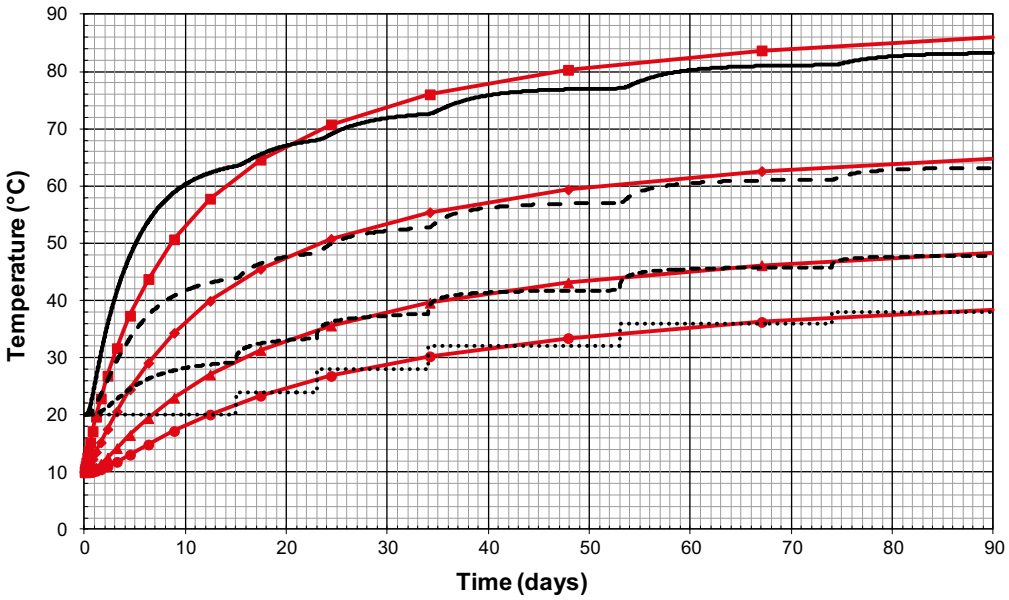

Figure 3-7. Temperature evolutions from the thermal KBS-3V model using a rock thermal conductivity of 2.00 W/(m·K) (red) and the thermo-hydraulic model of the experiment using the proposed protocol (black). Appearance from above: heater temperature; inner block surface temperature; outer block surface temperature; and wall temperature.

Table 3-2. Proposed wall temperature protocol for the experiment.

Interval no.	Start (day)	End (day)	Water temperature (°C)
1	0	15	20
2	15	23	24
3	23	34	28
4	34	53	32
5	53	74	36
6	74	90	38

4 Test results

4.1 The running of the test

In order to run the test at intended temperature and temperature differences in the buffer rings, at mid height of the experiment setup i.e. at the interface between the two bentonite blocks the power to the installed heating elements (Figure 4-1), the insulation of the outer diameter of the setup and the temperature on the water in the slot of the test cylinder were adjusted. But the temperature was not adjusted in accordance with the Table 3-4 since we had to adjust the power to the heater as well to achieve the correct temperature/temperature gradient. In Figure 4-2 the temperatures at different locations of the test are plotted as function of time together with the outcome from the simulations made, see Section 3.3.

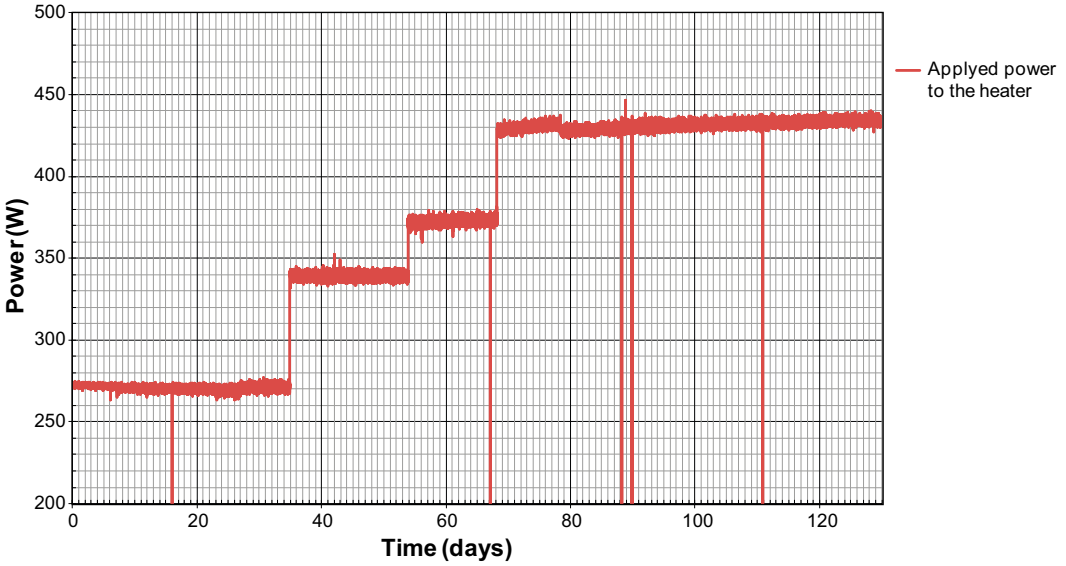

Figure 4-1. *The power applied to the heater as function of time.*

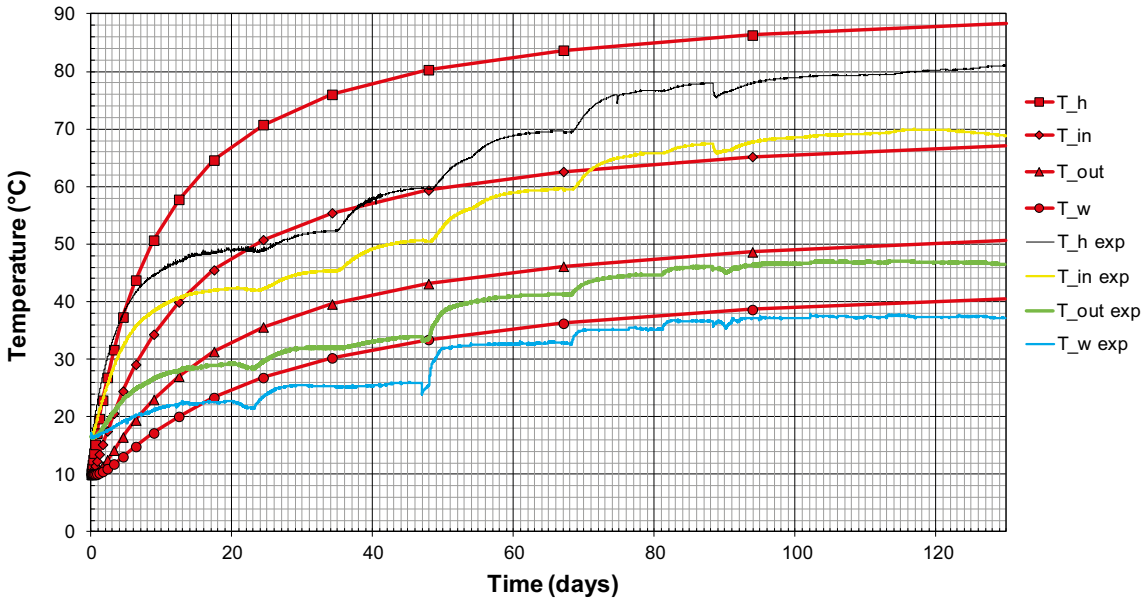

Figure 4-2. *The temperature development in the experiment together with the from FEM-analyses evaluated temperatures at different locations in the test setup. T_h is the temperature on the surface of the heater, T_in is the temperature on the inner surface of the block, T_out is the temperature on the outer surface of the block and T_wis the temperature on the surface of the test cylinder.*

Assuming that the simulation was accurate, the plan was to follow the temperature evolution from the simulation as well as possible, especially the temperatures on the surfaces of the block (T_in and T_out) and on the outer surface of the test cylinder (T_w). It was obvious from the start of the test that it would be difficult to mimic the simulated temperature on the surface of the heater (T_h) since the simulations were made with the assumption that the heater was made of copper while the test was running with a heater of steel and these two metals have different emissivity which affect the temperature on the surface. However, since the purpose of the test is to investigate the evolution of the buffer properties, e.g. the water content and the dry density, and not the heat transfer characteristics of the surface of the canister, this is not of concern. The differences between the simulated temperatures and the actual measured temperatures in the block are 5–10°C at the beginning of the test.

After several adjustments of the temperature of the outer surface of the test cylinder and three adjustments of the power of the heater, see Figure 4-1, the simulated and the measured temperatures approached each other. Around day 50 after the start of the test the temperature evolution followed the simulated temperatures fairly well. At the end of the test period the temperature at the inner surface (T_in) was about 3°C higher and the temperature at the outer surface was about 3°C lower than the temperatures from the simulation.

The power at the end of the test period was about 440 W corresponding to a heat flux of 133 W/m^2 when assuming only radial heat flow, thus about 50 W/m^2 larger than the heat flux used at the simulations (see Section 3.2). The simulations are made with the assumption that heat flow is only radial. It is obvious that there has also been a heat flow in axial direction in the test, which explains the need for the higher power in order to get the stipulated temperatures.

4.2 Data from installed sensors

The temperature gradient over the two profiles for which the temperature were measured (see Figure 2-1) are shown in Figure 4-3 and Figure 4-4. The figures show that the temperature gradients are larger in the profile with the thermo couples T5 to T8. At the end of the test period the average temperature gradient is about 0.64°C/cm for the T1-T4 profile and corresponding value for the other profile is about 0.81°C/cm. The reason for this might be that the side for the test setup in which the thermo couples T1..T4 were placed was facing towards the open space in the test hall while the other profile was closer to a wall. The figures show also that temperature gradients are higher close to the heater.

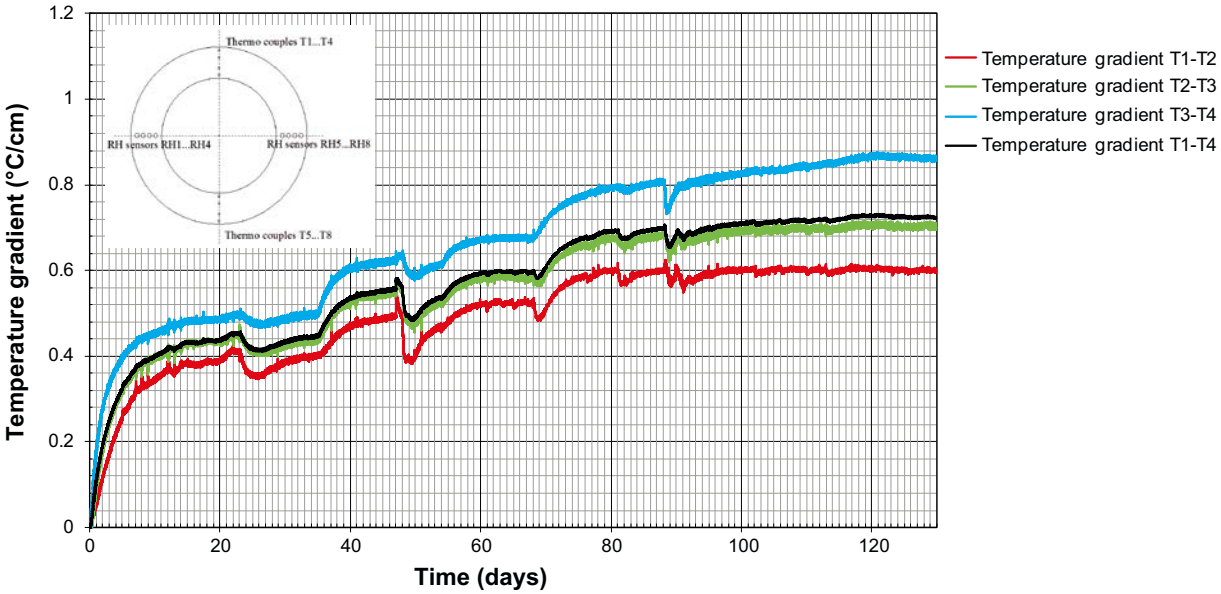

Figure 4-3. *The evaluated temperature gradient measured in the bentonite (profile 1 including the thermal couples T1…T4) as function of time.*

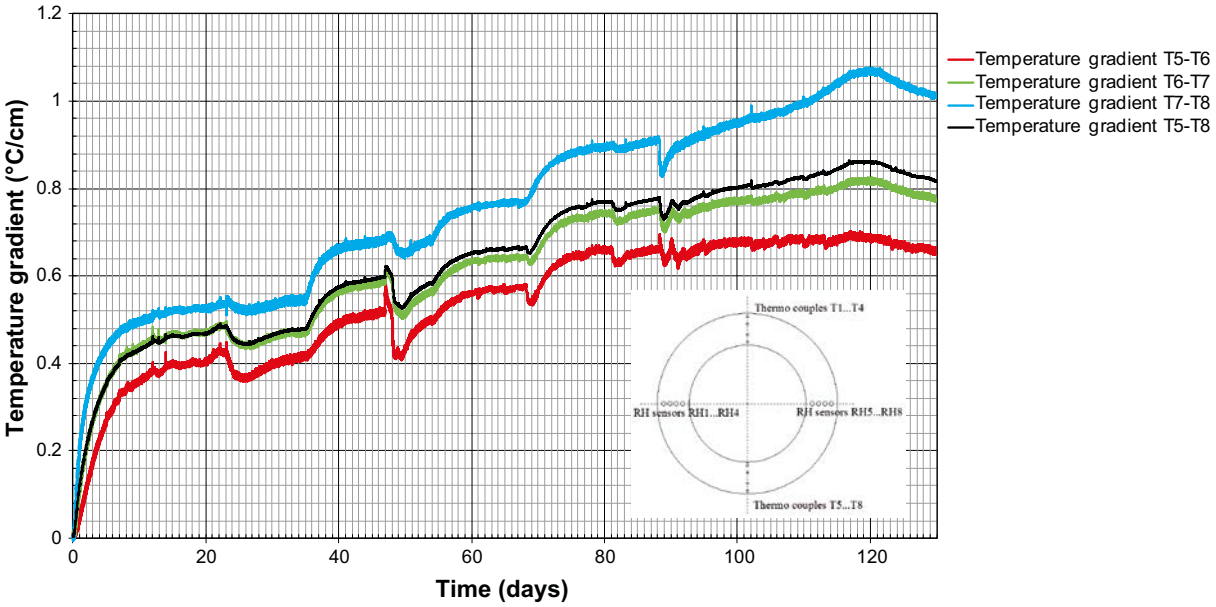

Figure 4-4. *The evaluated temperature gradient measured in the bentonite (profile 2 including the thermal couples T5…T8) as function of time.*

The measured Relative Humidity values (RH) in two profiles are shown in Figure 4-5 and Figure 4-6. All the installed sensors measured an increased RH during the first 10 days. During the next 40 days the RH was relatively constant although the temperature and the temperature gradient increase during this period. After that, the measured RH decreased, especially for the two sensors installed close to the heater (RH4 and RH8) which measured RH between 54–58% at the end of the test period. This indicates that a drying has occurred in the block during this period of 80 days.

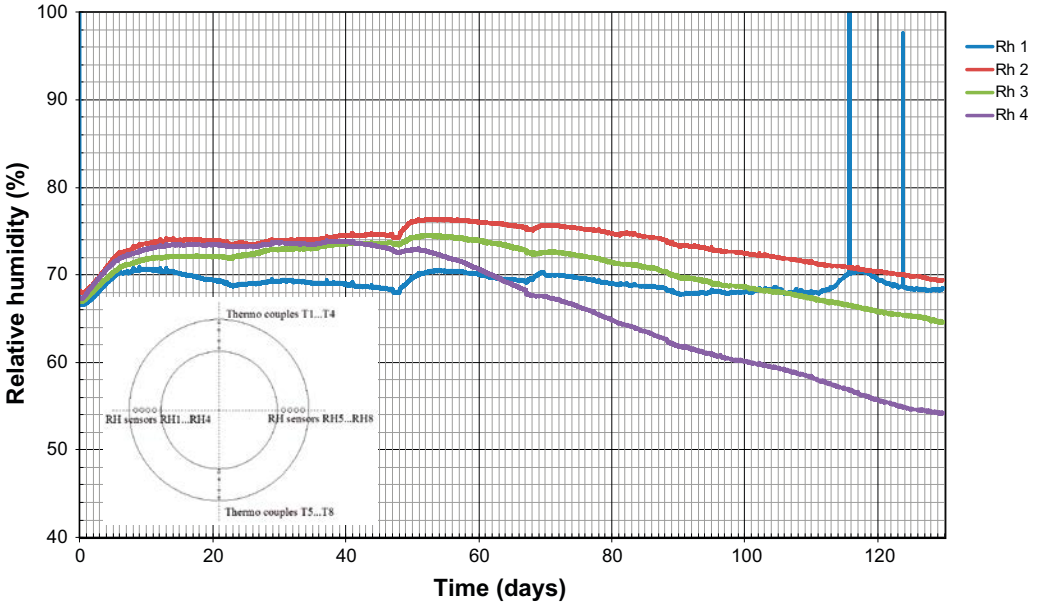

Figure 4-5. *The development of the Relative humidity inside the bentonite buffer as function of time (RH1…RH4).*

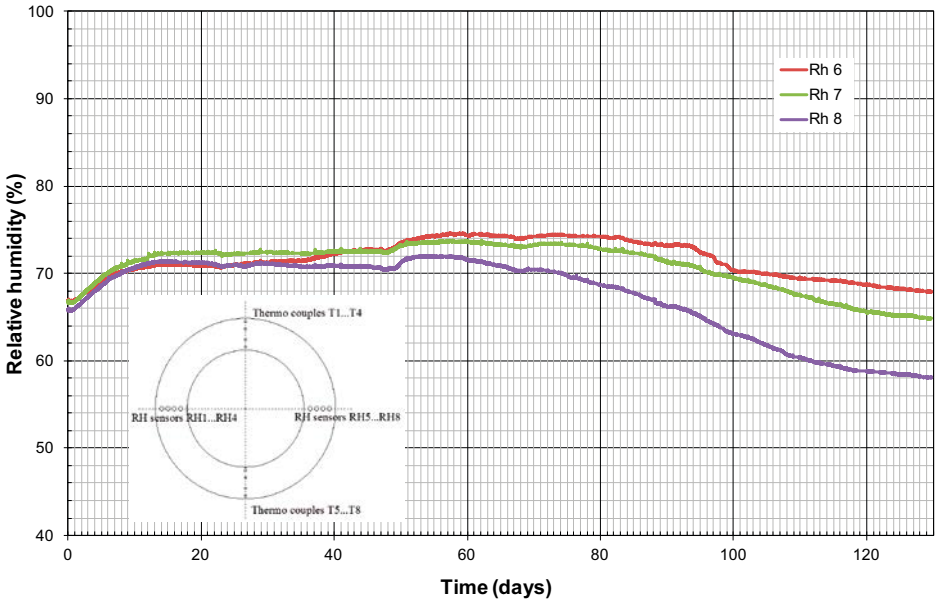

Figure 4-6. *The development of the Relative humidity inside the bentonite buffer as function of time (RH5…RH8).*

4.3 Data from the dismantling of the test

4.3.1 The technique used at the dismantling of the test.

The dismantling of the test was made in steps with the following observations:

1. The power to the heaters was switched off about one week before the actual dismantling started in order to get an acceptable working temperature on the buffer and heaters, maximum 20°C.
2. The upper steel lid and the isolation on top of the upper block and the top of the canister were removed. At the dismantling some puddles of water between the five layers of isolation were observed, see Figure 4-7.
3. The heater was lifted out from the centre of the buffer blocks with an over-head crane, see Figure 4-8.
4. Photos from the inside of the stack of blocks were taken for documenting the observed cracks in the blocks. Some of the cracks had a width of several centimetres and were going through the entire blocks, see Figure 4-9.
5. Water was observed in some areas at the bottom of the slot between the lower block and the inner surface of the test cylinder. The water had affected the lower part of the block and some bentonite with high water content was found at the bottom, see Figure 4-10. The amount of water was estimated by weighting the bentonite gathered at the bottom and determining its water content.
6. On one part of the upper block a wetter spot was observed. This spot was localized to a point where some cables fromthe installed sensors had touched the inner surface of the test cylinder and water which probably had condensate, had followed the cables and wetted the bentonite.
7. Larger pieces of the bentonite on four directions in each of the installed blocks were cut out on which the water content and the density were determined, see Figure 4-11. The large pieces were wrapped in plastic and transported to the laboratory. From the larger pieces specimens were taken with the use of a band saw on which the water content and density were determined. The results from these determinations are reporter in Section 4.3.2. The rest of the blocks were discarded.
8. Although an extensive amount of large cracks were observed in the blocks, no larger pieces of bentonite were found in the inner or outer slot i.e. between the heater and the bloc or between the block and the test cylinder. The bentonite observed in the outer slot was assumed to derived from the swelling of the lower part of the block when it took up the condensed water, see point 5 above.

Figure 4-7. *Some puddles of water between the upper layer of insulation and the steel lid.*

Figure 4-8. *The heater lifted up from the test cylinder.*

Figure 4-9. *Cracks observed from the inside of the ring shaped blocks.*

Figure 4-10. *Bentonite with high water content in the gap between the block and the test cylinder.*

Figure 4-11. *A large piece of bentonite cut out from the upper block with an alligator saw.*

4.3.2 Determination of the water content and density of the buffer

From the larger pieces taken of the bentonite rings an extensive sampling of the buffer was made, see Figure 4-12. This was made with the use of a band saw. The taken specimens had the following designations i.e. B1_190_752.5_b where:

B1 Block No. Block No B1 is the bottom block.

190 The direction in the blocks the specimens are taken. The investigated directions are 10, 100, 190 and 280 degrees.

752.5 The radial distance from the center of the block in mm.

B The vertical level in the block, A at the top, E at the bottom).

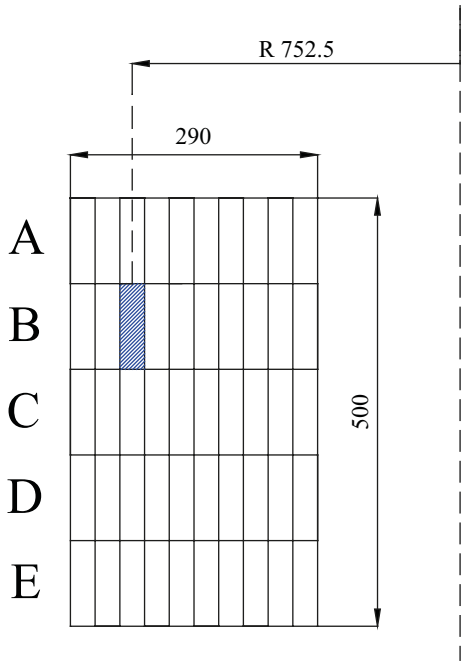

Figure 4-12. *Division of the collected larger sectors of the blocks into smaller pieces.*

From the taken samples smaller specimens were taken on which the water content and density were determined. These specimens were taken at the center of the samples A, B,…E and thus were taken at a distance of 50, 150, 250, 350 and 450 mm respectively from the upper surfaces of each block.

The determination of the water content was made in the following way:

1. The balance was checked with reference weights before the starting of the measurements.
2. A small baking tin of aluminum was placed on the balance and the weight (m_{bt}) was noted in a protocol.
3. The sample was placed in the baking tin and the weight of sample and tin is noted in a protocol ($m_{bt} + m_{bulk}$).
4. The tin with the sample was placed in an oven with a temperature of 105°C for 24 h.
5. After the drying the weight of the baking thin and the sample ($m_{bt} + m_{solid}$) was measured and noted in a protocol.

The mass of water dried from the sample was determined according to Equation 4-1:

$$m_{water} = m_{bulk} - m_{solid} \tag{4-1}$$

and the water content (w) was calculated according to Equation 4-2.

$$w = \frac{m_{water}}{m_{solid}} \tag{4-2}$$

The bulk density of the samples was determined by weighing the samples both in air and immerged in paraffin oil with known density. The determination was made as follows:

1. A piece of thread was weighed.
2. The sample was weighed hanging on the thread underneath the balance (m_{bulk}).
3. The sample was then submersed in the paraffin oil with the density $\rho_{paraffin}$ and the weight ($m_{paraffin}$) was noted.

The volume of the sample (V_{buk}) and the density (ρ_{bulk}) were calculated according to Equations 4-3 and 4-4.

$$V_{bulk} = (m_{bulk} - m_{paraffine}) / \rho_{paraffine} \quad (4\text{-}3)$$

$$\rho_{bulk} = \frac{m_{bulk}}{V_{bulk}} \quad (4\text{-}4)$$

The dry density (ρ_{dry}) and the degree of saturation (S_r) can be calculated according to Equations 4-5 and 4-6.

$$\rho_{dry} = \frac{\rho_{bulk}}{(1+w)} \quad (4\text{-}5)$$

$$S_r = \frac{w \times \rho_{bulk} \times \rho_s / \rho_w}{\rho_s \times (1+w) - \rho_{bulk}} \quad (4\text{-}6)$$

For calculating the degree of saturation the values of the density of the solid particles ρ_s = 2,780 kg/m^3 and the density of water to ρ_w = 1,000 kg/m^3 are used. The void ratio (e) can be calculated according to Equation 4-7.

$$e = \frac{\rho_s - \rho_{bulk}}{\rho_{bulk} - \rho_w \times S_r} \quad (4\text{-}7)$$

Altogether about 400 determinations of water content and density on the taken specimens were executed. The results from these determinations are provided in Appendices 3–10. An example of data from the determinations is shown in Figure 4-13. The red curves in the figure are describing the conditions of the block at the installation. The measurements are showing the following:

- A considerable drying of the buffer close to the heater was observed in all profiles. The initial water content was about 17%. In some points close to the heater the measured water content was as low as 7%.
- In most of the profiles the total water content of the buffer has decreased compared to its initial water content, see below about the exceptions.
- The measurement of the water content in the lower profiles (depth 450 mm from the upper surface of the block) in block B1 close to its outer surface shows an increase in water content. This is probably caused by the water which was condensed on the inner surface of the test cylinder and flowed down to the bottom and then taken up by the bentonite.
- The measured water content at the upper profile of block B2 shows an increase in water at a radial distance of 550–650 mm in direction 10 and 280°. An explanation to this might be that a colder area has occurred by a local thermal bridge formed by the device, in which the heater was hanging, see Figure 4-8. This resulted in a condensation of water in that area.
- The water content of the buffer in all measuring point on the outer diameter of the blocks was about 15%. This is an indication that the Relative humidity close to the outer surface of the bentonite blocks was relatively constant in all parts of the slot at the dismantling.
- The dry density of the bentonite has increased in most parts of the blocks, due to shrinkage i.e. the pore volume of the buffer has decreased at the drying. The exceptions are those parts of the blocks were the water content has increased. The most extensive increase of the dry density was measured on the parts of the blocks close to the heater.

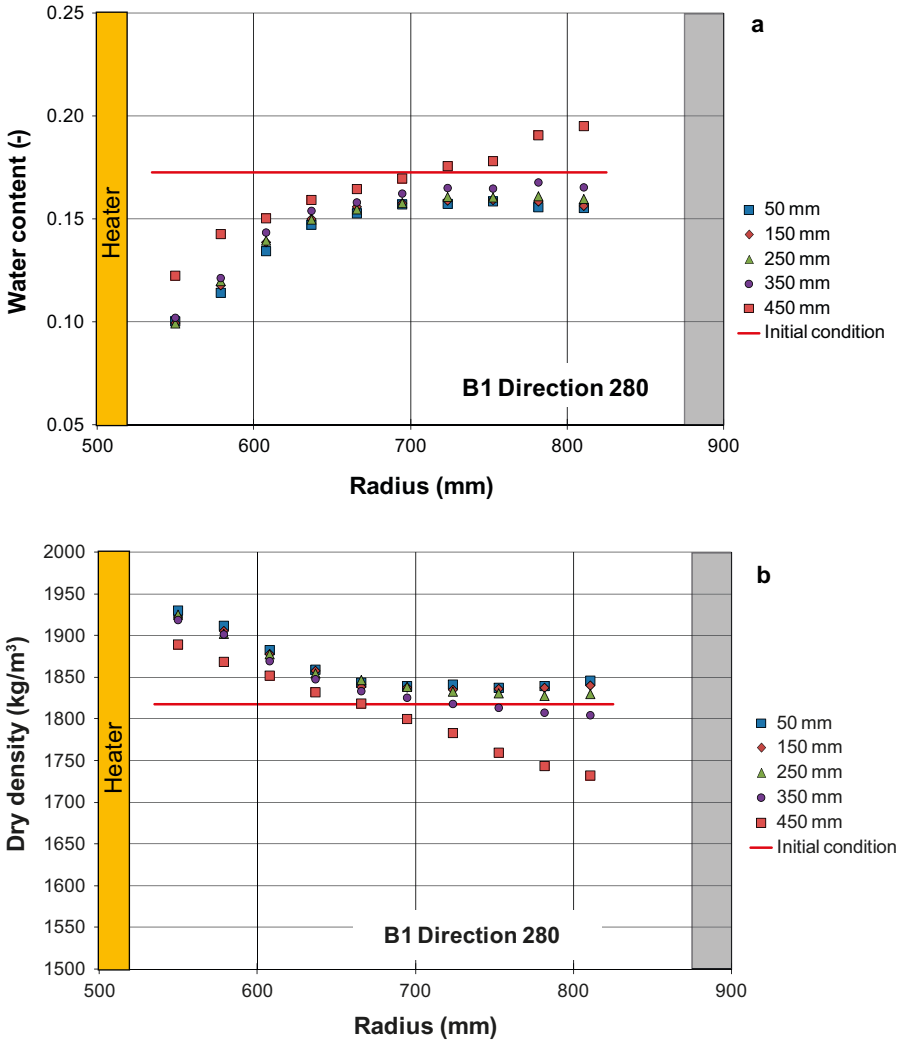

Figure 4-13. *Measured water content a) and dry density b) for the lower block (B1) at direction 280°. The measurements are made at four different depths in the block.*

The data from the profiles taken in the four directions can also be plotted as contour plots, see Appendices 11–14. The plots are showing the following:

- Beside the radial gradient both in water content and in dry density there is an axial gradient in these parameters as well, indicating that the thermal flow was not only radial in the test setup.
- The wetter parts of the buffer, at a radial distance of 650 mm at the top of the upper block and at the outer part of the lower block, are distinct in these plots.

When the blocks were removed the bentonite at the bottom of the test cylinder was collected and weighted, see Figure 4-14. Furthermore the water content of the bentonite was determined. This water content was used to estimate the amount of water which has condensed on the outer surface of the test cylinder. The amount of water in the bentonite, gathered at the bottom of the test cylinder, was determined to about 15 kg and the estimated amount of water condensed in the isolation measured at the dismantling was about 5 kg, i.e. the condensed water in the test setup was about 20 kg.

Figure 4-14. *The "wet" bentonite at the bottom of the test cylinder.*

From the measured water contents of the two blocks it was possible to determine the average water content of the bentonite at the dismantling and compare it with its initial water content at the installation. These calculations show that buffer had, out of initial 390 kg water lost about 45 kg.

These measurements show that there has been a loss of about 25 kg water from the test (the loss of water in the bentonite blocks minus the observed condensed water) indicating that the test setup has not been totally vapour tight.

5 Post operational simulations of the test

5.1 Introduction

Three types of models were used for simulating the processes in the tests based on the data from the disassembly:

1. One dimensional axisymmetric model using Code_Bright.
2. Two dimensional axisymmetric model using Code_Bright.
3. Two dimensional axisymmetric model using Comsol Multi-physics.

The first modelling was done to investigate the evaporation in the inner part of the test and compare it to the results from the initial simulations.

The second and third modeling was performed to evaluate if the (a) axial leakage from the inner slot and out of the test or (b) radial leakage from the inner slot through fractures to the outer slot were the main contributor to the desiccation. The main difference between the two tools used is that the third modelling with Comsol Multi-physics includes support for including natural convection into the modelling of the experiment.

5.2 One dimensional simulations

5.2.1 Introduction

At the retrieval of the experiment it was found out that the water content of the bentonite at the outer diameter of the buffer rings has decreased from its initial value of about 17% to about 15–16% independent of the location on the outer surface. This indicates that the outer slot had a drying effect on the bentonite, which was caused by the temperature gap across the slot and the condensation on the cold side (see Figure 5-1). This process has been analysed with the FEM code Code_Bright (v4) and the results from the calculations are presented below.

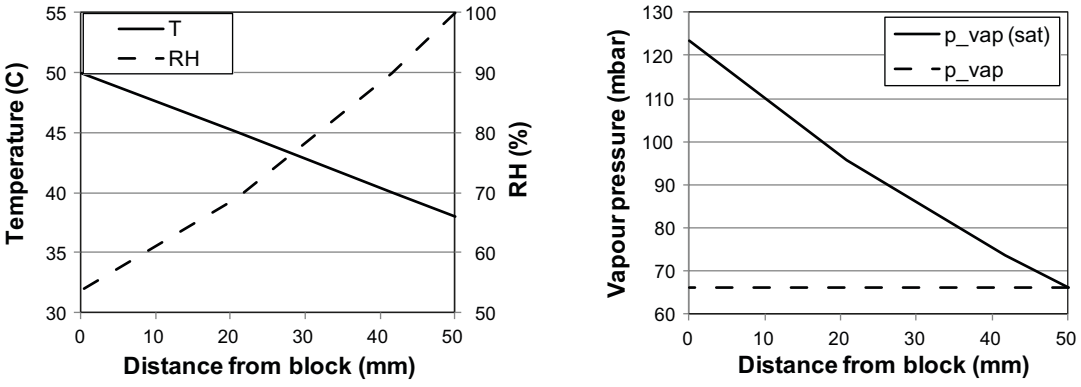

Figure 5-1. *Drying effect of the outer slot. Left graph shows an (assumed linear) temperature profile across the slot with measured values at the hot and cold side (solid line). This corresponds to a saturated vapour pressure distribution (solid line in right graph). The maximum equilibrated vapour pressure across the slot equals the saturated vapour pressure at the cold side (dashed line in right graph). The ratio between the equilibrated vapour pressure and the saturated vapour pressure distribution equals a specific RH distribution (dashed line in left graph). Bentonite blocks with an initial water content of 17% (corresponding to RH ~ 71%), would thereby dehydrate to a RH level of ~ 54% on the hot side of the slot, due to the condensation process on the cold side (RH = 100%), where water in liquid form could escape downwards due to gravity.*

5.2.2 Description of the model

A 1D axisymmetric model was used at the simulations; see Figure 5-2.The outer and inner diameter are those for the bentonite blocks.

The thermo-hydraulic processes were analysed including three transport processes:

i. Heat transport, controlled by the temperature gradient (Fourier´s law).

ii. Water transport, controlled by the liquid pressure gradient (Darcy´s law).

iii. Vapour transport controlled by vapour mass fraction gradient (Fick´s law).

See also Appendix 1, Equations (A1-1), (A1-6) and (A1-10).

The thermal part of the problem was simplified by applying a temperature boundary on the inner and outer surfaces. From an initial value of 20°C, the temperatures were increased to 66°C and 50°C on the inner and outer surfaces respectively during the first 24 hours and were then kept constant. These temperatures correspond to the measured temperatures in test setup at the end of the test period.

The initial condition for the hydraulic part of the problem was defined as an initial liquid pressure of –45.9 MPa which corresponds to a bentonite water content of 17%. The liquid pressure on the outer surface of the model was reduced to –74.9 MPa (corresponds to a Relative humidity of 60% at a temperature of 50°C) during the first 24 hours and kept constant. This liquid pressure corresponds to a water content of 15% which was observed on the outer surface of the blocks at the retrieval of the test. No water could pass through inner surface of the model.

The used material parameters for the simulations were adopted in accordance with Åkesson et al. (2010) and are listed in Table 5-1 and the chosen retention properties follow the “extended van Genuchten” curve, see Figure 5-3, which is implemented in the FEM-code.

Table 5-1 Material parameters for the MX-80 buffer blocks.

Void ratio	**e (–)**	**0.571**
Thermal conductivity	λ_{dry} λ_{sat} (W/mK)	0.7 1.3
Specific heat for solid	c (J/kgK)	800
Intrinsic permeability	k_0 (m^2)	1.2E–21
Relative permeability	k_r (–)	S_r^3
Vapour diffusion tortuosity	τ (–)	1
Water retention curve,	P_0 (MPa) λ (–) P_1 (MPa) λ_1 (–)	47.561 0.05 320 1
Particle density	ρ_s (kg/m^3)	2,780

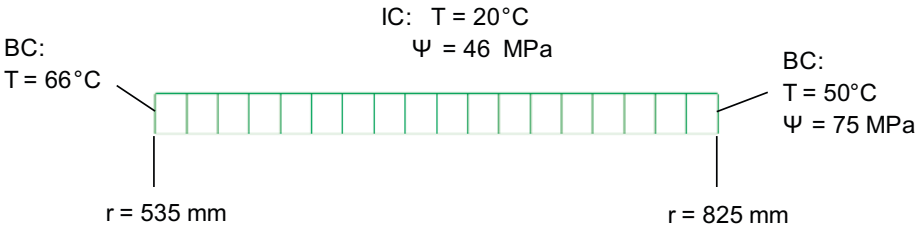

Figure 5-2. *Axisymmetric geometry, mesh, initial conditions (IC) and boundary conditions (BC) for the chosen model where T is the temperature and Ψ is the suction.*

$$\theta(\psi) := \left[1 + \left(\frac{\psi}{P_0}\right)^{\frac{1}{1-\lambda}}\right]^{-\lambda} \cdot \left(1 - \frac{\psi}{P_1}\right)^{\lambda_1} *$$

$P_0 \equiv 47.561$

$\lambda \equiv 0.05$

$P_1 \equiv 320$

$\lambda_1 \equiv 1$

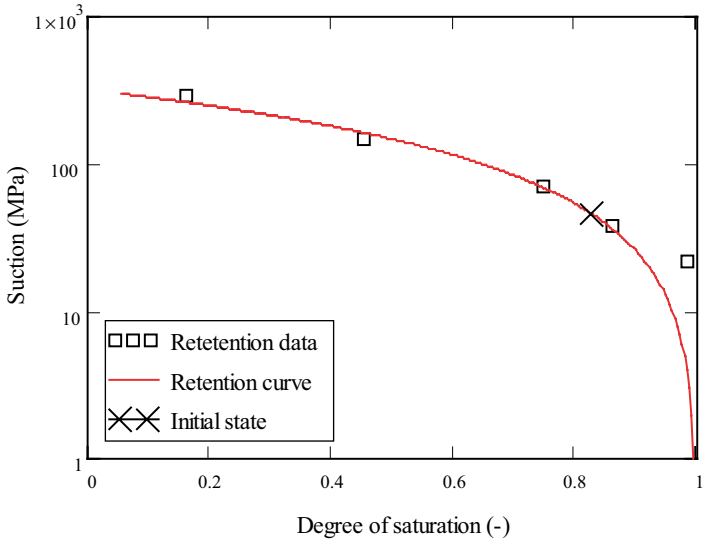

Figure 5-3. *Retention curve for the buffer blocks of MX-80.The suction (Ψ) is plotted as function of the degree of saturation (Θ).*

The simulated time for the model was in the first place 120 days which corresponds to the time the test was running. The simulated time was extended with another 600 days in order to get steady-state conditions.

Three cases were analysed:

i. Hydraulic boundary with the water content 15% on the outside, see Figure 5-2.

ii. Hydraulic boundary with the water content 17% on the outside (= 46 MPa in suction).

iii. No water could pass through the surfaces of the model (closed boundaries).

No gravity was included in the model and the gas pressure was kept constant to 0.1 MPa.

5.2.3 Results from the modelling

The results for the case “hydraulic boundary with the water content 15% on the outside” are presented as profiles of temperature, liquid pressure, vapour mass fraction and the water content at four different time periods, see Figure 5-3.

The following remarks can be made from Figure 5-4:

- The temperature profile is largely stable during the simulation time.
- The liquid pressure on the warmer inside is reduced to about –160 MPa at the end of the simulation while the vapour mass fraction is evened out with time although not totally since the steady-state condition requires that vapour transport is in balance with the liquid water transport.
- The water content is decreased in all parts of the profile and at the end of the simulation the water content is 15% on the outside and 9% on the inside.

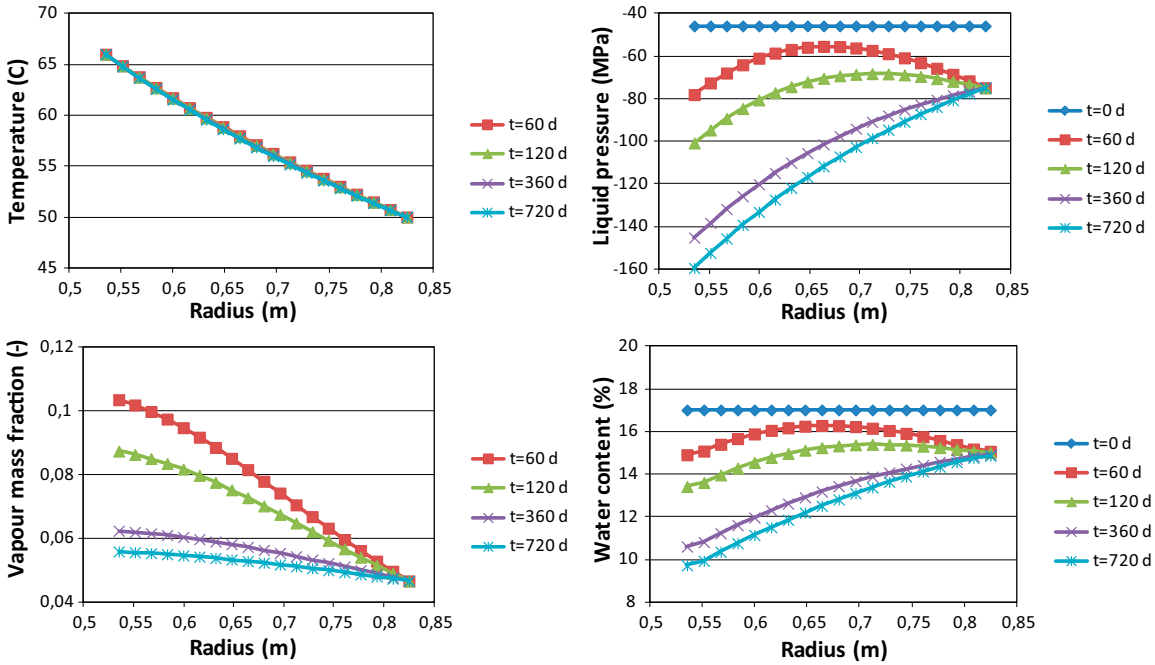

Figure 5-4. *The temperature, liquid pressure, vapour mass fraction and the water content as function the radial distance in the model.*

The water content profiles for the three different cases, see Section 5.1.2, are plotted in Figure 5-5. For the first case, with the water content 15% on the outer surfaces; the water content is decreasing towards 9% on the inside. For the case where the water content is 17% on the outside (suction 46 MPa) the water content decreases to 12% on the inside. For the case with closed boundaries the water is redistributed so that the water content varies between 13 and 19%.

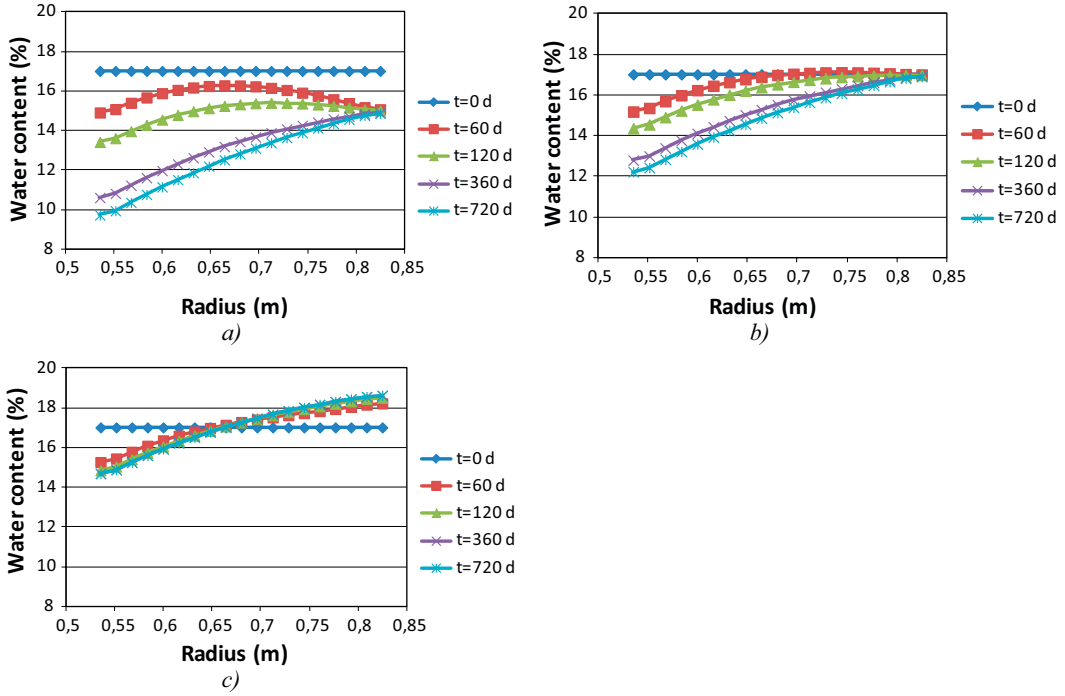

Figure 5-5. *The water content profiles from the simulations made at three different hydraulic boundaries: 15% water content (a), 17% water content (b) and closed boundaries (c).*

By integrating the water content profiles in Figure 5-4 the amount of water which has disappeared from the model can be calculated. For the case with two blocks (total height 1 m) the amount of water loss after day 60 is 27 kg. Corresponding values for 120 days, 270 days and 360 days are 45, 80 and 92 kg respectively.

The water content profile in the block at day 120, see Figure 5-4, looks similar to the profiles measured in the test, with a water content just above 15% at radius of 0.7 m. However, the inner part of the buffer of the test was dryer compare to the data coming from the simulation. A plausible explanation for this might be that vapour in the test was transported through passages which were not represented in the numerical model, i.e. axially in the inner slot (leakage) or radial through fractures in the blocks.

The difference between the water content in the mid-section of the "no leakage" model and the 1D model at different radii is less than 0.6%-units.

5.3 Two dimensional axisymmetric simulations

5.3.1 Introduction

The results from previous shown 1D simulation indicate that the evaporation in the inner part of the test was larger compare to the output from the simulations. The desiccation can be assumed to originate from two processes:

i. By axial leakage from the inner slot out from the test setup. This process supports by the water balance calculations made, see Section 4.3.2.

ii. By radial leakage from the inner slot through fractures to the outer slot. This process supports by the presence of fractures in the blocks.

The purpose with the 2D modelling is to find out which of these two processes are most relevant. The modelling has been done with two different FEM-codes the FEM code Code_Bright (v4) and Comsol Multi-physics respectively.

5.3.2 Description of the Code_Bright model

A 2D axisymmetric geometry was used for the problem (Figure 5-6). The thermo-hydraulic processes were analysed where three transport processes were includes in the model:

i. Heat transport, controlled by the temperature gradient (Fourier´s law).

ii. Water transport, controlled by the liquid pressure gradient (Darcy´s law).

iii. Vapor transport controlled by vapor mass fraction gradient (Fick´s law).

See also Appendix 1, Equations (A1-1), (A1-6) and (A1-10).

The thermal problem was simplified in order to recreate the temperatures which were measured on the inside and the outside of the bentonite blocks at the end of the test period:

- One power source of 435 W was applied evenly distributed along a 0.8 m line at the radius of 0.25 m.
- The boundary temperature of 20°C was applied on the outside of the insulation.
- The temperature on the test cylinder was set to 38°C.
- The thermal conductivity of the bentonite was kept constant (1.2 W/mK).
- The thermal conductivity of the inner and outer slot was evaluated from the measured temperatures *and the adopted conductivity value for the bentonite, by assuming a constant heat flux per unit length through all three materials* (Figure 5-7).
- The thermal conductivity for the isolation was set to 0.035 W/mK.
- The heater was represented in the modelled as one material and a thermal bridge with the same material as the heater was included in the model. The thermal conductivity of the heating material was calibrated to 4.5 W/mK (Figure 5-7).

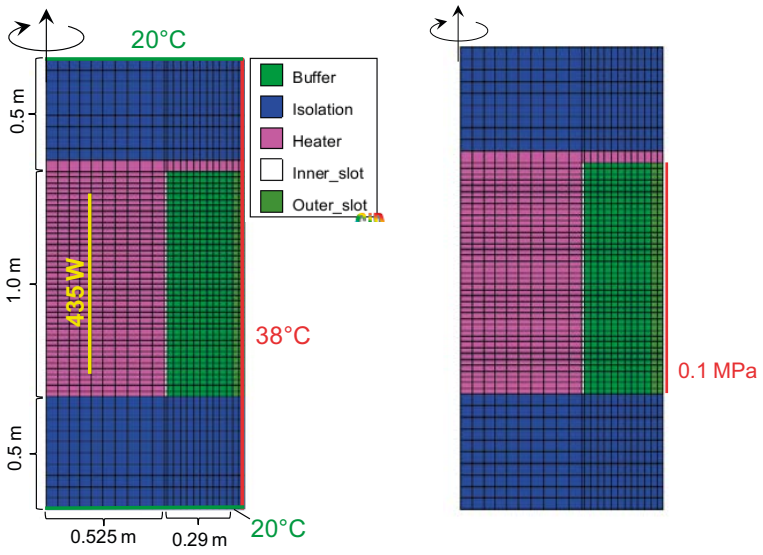

Figure 5-6. *The axisymmetric geometry with thermal boundaries and heat sources (Left) and the hydraulic boundaries (right).*

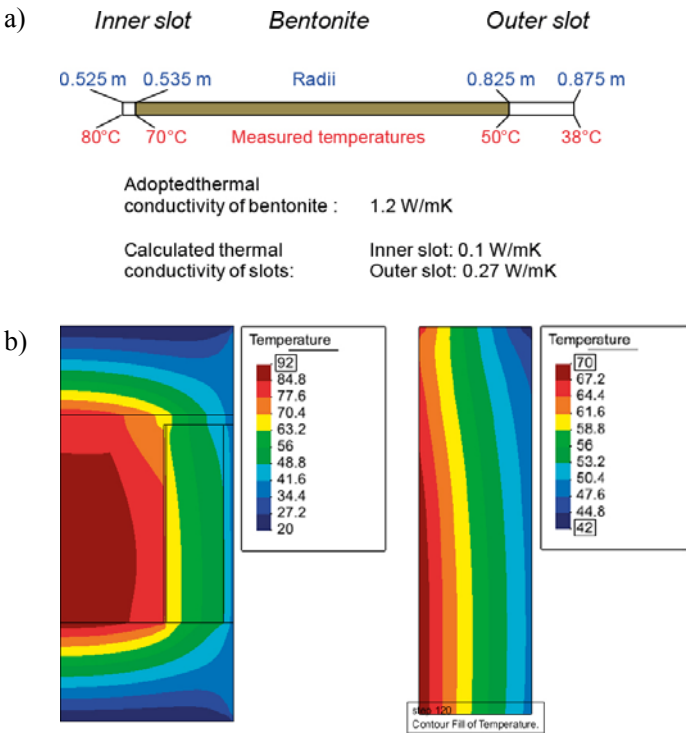

Figure 5-7. *Calibration of the thermal conductivity of the inner and outer slot (a). Contour plot of the temperature after 120 days (b): the test setup and the bentonite blocks.*

The initial conditions for the hydraulic problem was defined as an initial liquid pressure of –45.9 MPa (= suction 46 MPa), which corresponds to a water content of 17% for the buffer material. This initial condition was applied to all materials in the model. To be able to recreate the condensation, which occurred on the outside of the outer slot, a hydraulic boundary of liquid pressure of 0.1 MPa was applied on the outer boundary.

Parameter values for the bentonite blocks were adopted in accordance with Åkesson et al. (2010) with the exception for the thermal conductivity, which was kept constant. For the other materials the following assumptions were made (Table 5-1):

- The porosity of the material in the outer and inner gaps was set to a high value (0.99 = while the porosity for the heater and the isolation was set to a low value (0.001).
- The thermal conductivities were evaluated from the measured temperatures.
- The intrinsic permeability was set low (10^{-30} m^2) while a conventional function for the relative permeability was applied (S_r^3).
- The vapour diffusion tortuosity was set to the highest possible value for the two gap materials (1) while corresponding value for the heater and the isolation was set low (10^{-10}).
- The Specific heat, the density of the particles and the retention properties were set according to previous made modelling of tests, see Appendix 1. The retention properties for the outer gap were although modified so the maximum degree of saturation was set to 0.01 in order to limit the accumulated water in liquid phase for this material.

Three different cases were analysed:

i. A base case without any leakage paths, see Figure 5-8.

ii. A radial leakage was assumed to be present, see Figure 5-8. A horizontal gap (10 mm) going from the inner to the outer slot at mid height of the bentonite was added in the model. A vertical gap or fracture cannot be represented with an axisymmetric geometry. Still, the length of a horizontal gap (3–5 m) is of a similar order of magnitude as a vertical fracture (1m), and can therefore be regarded as relevant. The material properties for the gap were set to the same as for the materials in the slots.

iii. An axial leakage was assumed to be present, see Figure 5-8. A vertical gap (10 mm) going from the inner slot to the upper boundary was added in the model. The material properties for the gap were set to the same as for the materials in the slots. In addition to the temperature boundary of 20°C a hydraulic boundary condition of 100 MPa suction was set, corresponding to a RH of 48%.

No gravity was included in the model and the gas pressure was kept constant to at 0.1 MPa for simplicity and numerical convenience. The simulated time for the model was 120 days corresponding to the running time of the test.

Table 5-1. Parameters for the materials in the model.

		Buffer	Isolation	Heater	Inner gap	Outer gap
Porosity	n (–)	0.363	0.01	0.01	0.99	0.99
Thermal conductivity	λ_{dry} λ_{sat} (W/mK)	1.2 1.2	0.035 0.035	4.5 4.5	0.1 0.1	0.27 0.27
Specific heat for solid	c (J/kgK)	800	800	800	1,000	1,000
Intrinsic permeability	k_0 (m^2)	1.2E–21	1E–30	1E–30	1E–30	1E–30
Relative permeability	k_r (–)	S_r^3	S_r^3	S_r^3	S_r^3	S_r^3
Vapour diffusion tortuosity	τ (–)	1	10^{-10}	10^{-10}	1	1
Water retention curve,	P_0 (MPa) λ (–) P_1 (MPa) λ_1 (–)	47.651 0.05 320 1	0.1 0.6	0.1 0.6	0.1 0.6	0.1 0.6 S_{max} = 0.01
Particle density	ρ_s (kg/m^3)	2,780	30	2,650	1	1

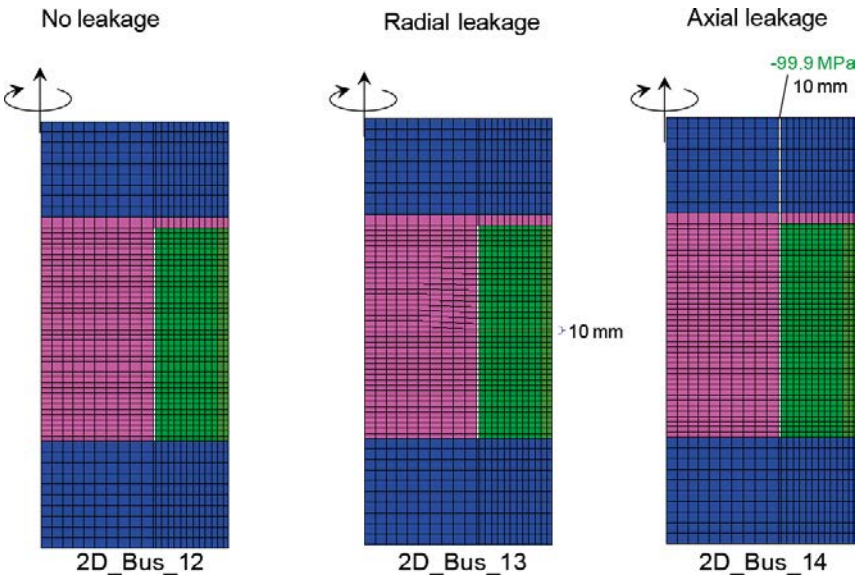

Figure 5-8. *The geometry for the three models.*

5.3.3 Results from the Code_Bright modelling

The contour plots of the water content in the bentonite blocks for the three models after 120 days are shown in Figure 5-9. The initial water content was 17% and the plots show thus that the bentonite has been subjected to general desiccation, besides for the upper corner where the water content was relatively unchanged. A comparison between the three models show that the modified geometries with radial or axial leakages admittedly caused an increase of the desiccation but this was limited.

The presented models show that the desiccation by the presence of a condensation boundary can be simulated by applying a simple hydraulic boundary condition of 0.1 MPa through which water can disappear from the model. No attempt to simulate the water transport along the walls on the test cylinder was made.

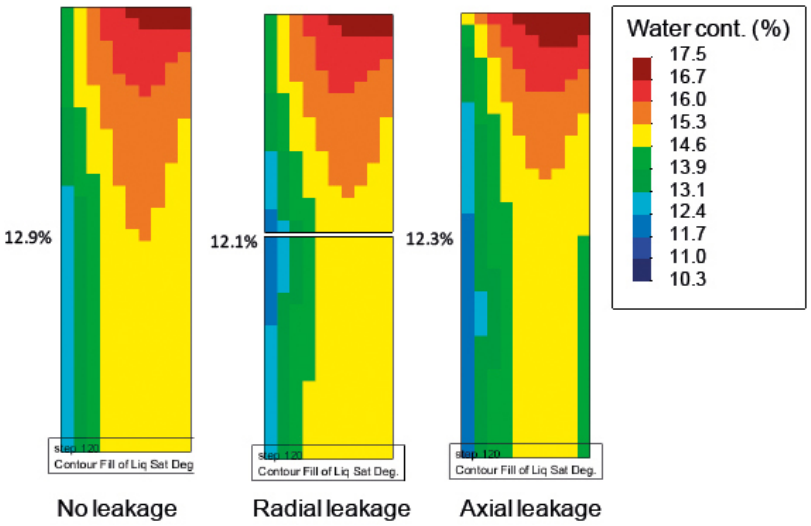

Figure 5-9. *Contour plots of the water content for the three models after 120 days.*

The presented models with radial and axial leakage show a larger desiccation of the bentonite compared to the base case where no leakage is present. This effect is however dependant on the width of the gaps. Wider gaps result in a larger desiccation of the buffer. However, none of the tested models showed as large desiccation as in the field experiment although the applied width of the gaps in the two models can be assumed to be large. This means that the models seem to lack some transport process/ mechanism which can explain the extensive desiccation in the field experiment. Natural convection might be such a process.

Finally, it can be pointed out that it is not possible from the made modelling to decide which of the proposed explanations (axial or radial leakage) is most relevant.

5.3.4 Description of the COMSOL Multi-physics model

A 2D axisymmetric geometry was used for the problem (Figure 5-10). The thermo-hydraulic processes were analysed where three transport processes were includes in the model:

a) Heat transport.

b) Water transport in the bentonite blocks.

c) Vapour transport in the bentonite blocks and the slots.

The governing Equations for the transport processes are described in Table 5-2.

The thermal boundary conditions used at the simulations are shown in Figure 5-11. At the thermal modelling the emissivity for the heater, bentonite and the test cylinder were set to 0.96, 0.8 and 0.6 respectively to fit with the experimental values. If other materials would be used than in the test setup these values would change.

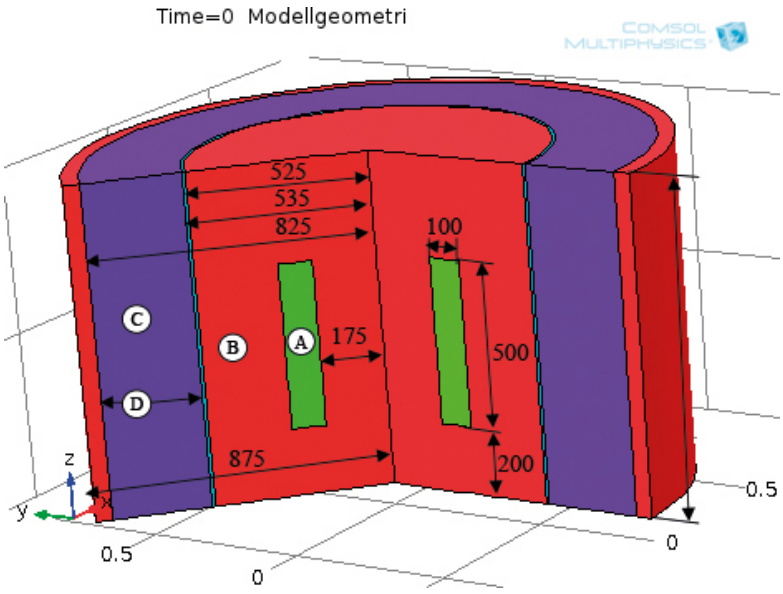

Id	Material	l (W/m/K)	C_p (J/Kg/K)	r (kg/m^3)	κ (m^2)
A	Steel	*	*	*	
B	Sand	0.3	800	1,400	
C	Bentonite	$0.5\cos^2(0.5S_e p)+1.3\sin^2(0.5S_e p)$	800	2,100	1.2×10^{-21}
D	Air	*	*	*	

Figure 5-10. *The geometry and the material parameters for the models. * marks the material parameters which were taken from COMSOL material library. Se is the degree of saturation of the bentonite.*

Table 5-2. The governing Equations used in the FEM-simulations.

Transport process	Governing equation	Parameters
Heat transport	$\rho C_p \frac{\partial T}{\partial t} + \rho C_p u \nabla T = \nabla(\lambda \nabla T) + Q$	Q = the heat source, u = the velocity of the gas (= zero in the blocks) is calculated with the Navier-Stokes equation. The difference in density with temperature creates the forces that drive the convection. λ, C_p, ρ see Figure 5-10.
Water transport	$\frac{C_m}{g}\frac{\partial(\theta\rho)}{\partial t} + \nabla\left(-\frac{\rho\kappa\kappa_r}{\mu}\nabla p\right) = Q_m$	$Q_m = A(P_w - P_a)\frac{0{,}089}{2272 * 10^3}$ An empiric description of the evaporation and condensation that is taken from ASHRAE Handbook where P_w the equilibrium vapor pressure is calculated with the Antoine equation with constants A=8.07131, B=1,730.63 and C=233.426. P_a is the actual vapor pressure and A is the area.
Vapor transport	$\frac{\partial c}{\partial t} + u\nabla c + \nabla(-D\nabla c) = R$	$D = n(1 - S_e)\frac{5.9x10^{-6}T^{2,3}}{P_g}$ where n is the porosity, S_e is the degree of saturation, P_g is the total gas pressure and T is the temperature (Åkesson et al. 2010) $R = -\frac{Q_m}{M_{H_2O}}$ An empiric description of the evaporation and condensation.

1: Symmetry line

2: The heat Q is the applied power on the heater.

3: The loss of power on this boundary is set to 0 in the first model and to 3 W/K/m^2 in the other models. The ambient temperature is set to 20°C.

4: The loss of power on this boundary is set to 0 in the first model and to 3 W/K/m^2 in the other models. The ambient temperature is set to 20°C.

5: This boundary is totally thermal isolated.

6: This boundary is totally thermal isolated.

7: The temperature on this boundary is set to the temperature measured in the test.

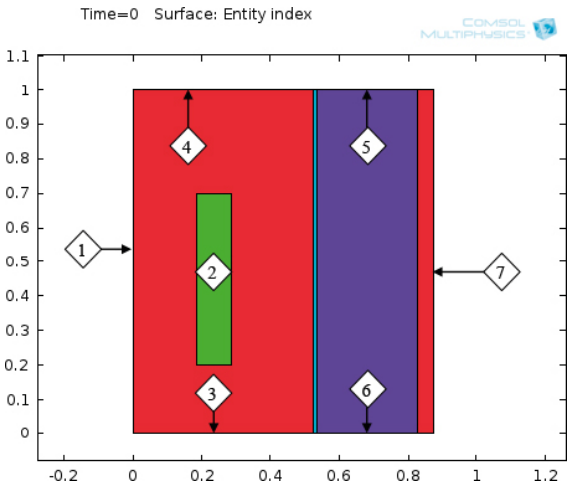

Figure 5-11. *The boundary conditions for the modelling.*

5.3.5 Results from the Comsol modelling

The results from the first modelling of the temperature, when assuming no heat losses in axial direction, are shown in Figure 5-12a, together with the measured temperatures in the test at different locations in the test setup. The figure shows that the temperatures from the modelling are higher (dotted lines) compared to the measured temperatures (solid lines), indicating that there has been some heat transport also in the axial direction of the test setup.

In Figure 5-12b the corresponding temperatures of the modelling are shown, when assuming the loss of power on the boundaries no 3 and 4 are set to 3 W/K/m^2, see Figure 5-11. The temperature evolution from the modelling corresponds well with the measured temperatures i.e. small differences between the solid and dotted lines. In Figure 5-13 the temperatures from the modelling at the end of the test period are plotted.

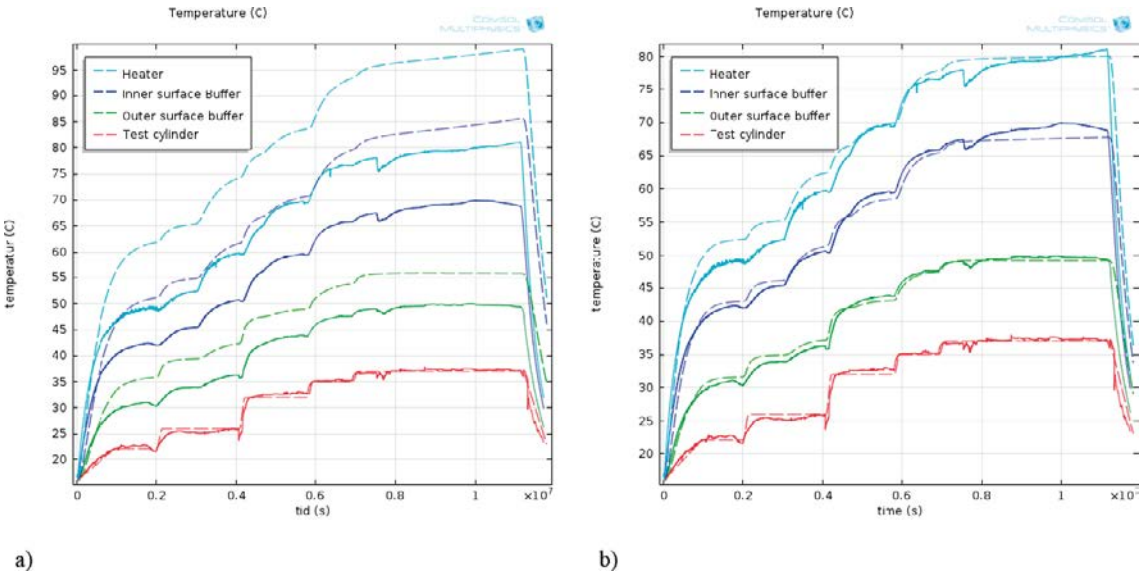

Figure 5-12. *The temperature evolution from the modelling (dotted lines) compared with the measured temperatures (solid lines) when a) assuming no heat loss in the axial direction and b) assuming a loss of 3 W/K/m^2 in axial direction.*

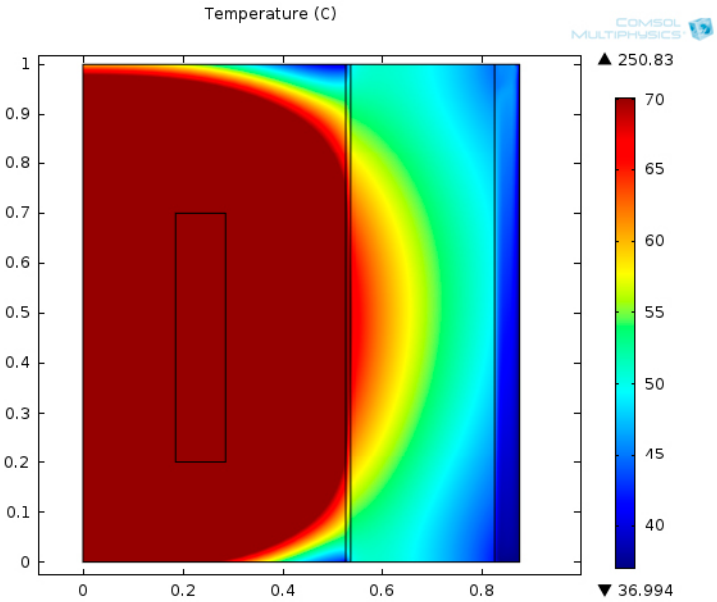

Figure 5-13. *Contour plots of the temperature from the modeling just before the heater was turned off.*

The measured water contents of the buffer at different heights from the bottom of the test setup at the dismantling represented by the dots, are considerably lower compared to those evaluated from the modelling represented by the lines, see Figure 5-14a. In order to reproduce the water content measurements of the buffer at the dismantling, a leakage of water vapour from the inner slot was introduced through a constant flux out of the inner slot. Since it is not possible to judge whether the leakage is radial or axial it is assumed at the modelling that the water vapour is removed from the model. In Figure 5-14b the results from the modelling when introducing a leakage, are compared with measured water content. The figure shows that a leakage of water probably occurred at the running of the test.

To get an even better compliance between the modelling data and the measured water content in the experiment, the assumed diffusion coefficient was increased with 30% while the leakage of water from the model decreased somewhat. The results from this simulation are shown in Figure 5-15(a) and (b). The contour plot of the water content and the water loss from the modelling in the buffer are shown in Figure 5-16.

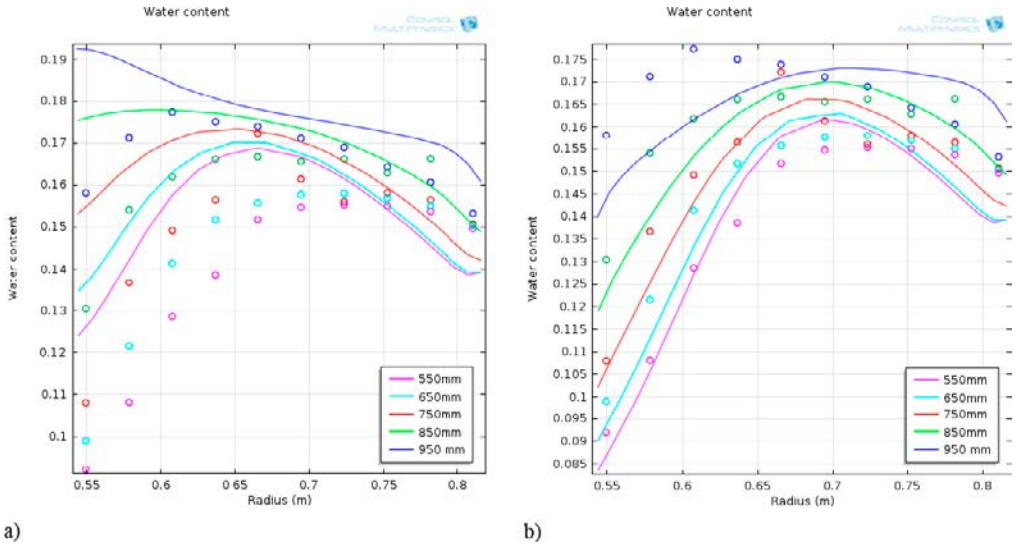

Figure 5-14. *The water content from the modelling (the lines) compared with the measured water content of the top block at the dismantling (the dots) as function of radial distance from the centre of the test setup when a) assuming no loss of water and b) when assuming a loss of water from the model. The legend shows the height from the bottom of the test.*

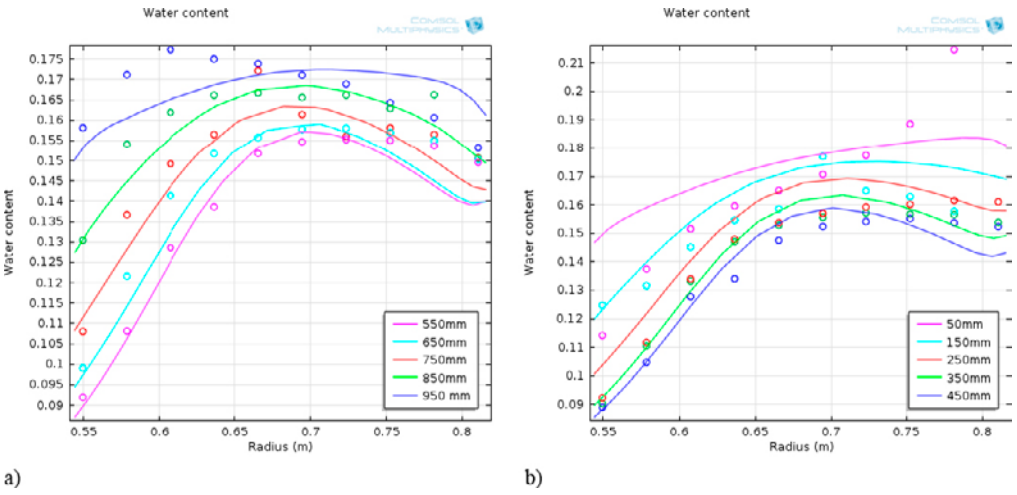

Figure 5-15. *The water content from the modeling compared with the measured water content at the dismantling when increasing the diffusion coefficient increased with 30% compared to the initial assumption a) the upper block b) the lower block.*

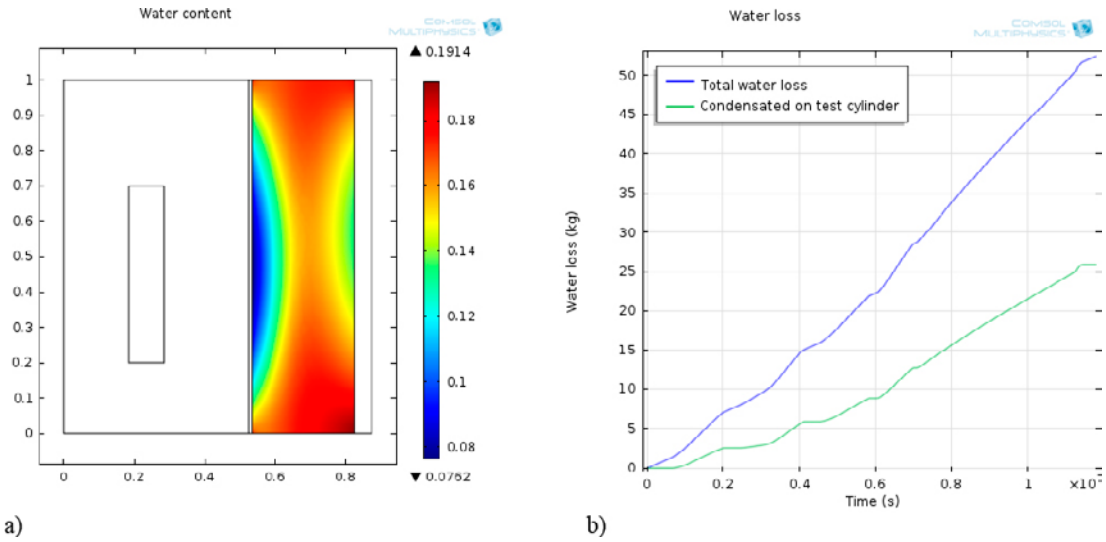

Figure 5-16. *a) A contour plot of the water content in the buffer derived from the simulation of the test. b) The accumulated water loss and the condensed water on the wall.*

6 Conclusions

The test setup represented a section at mid height of the canister in a real repository where most of the heat transfer only occurs in radial direction. At the dismantling and the modelling of the test it was obvious that also a temperature gradient in axial direction was present in the test. It was also obvious that water had disappeared from the blocks. Some of this water had condensated on the outer surface of the test cylinder and gathered on the bottom of the test cylinder where it was then taken up by the bentonite block. This condensation could also be modelled with the Comsol code.

Some of the water had also disappeared from the test setup although efforts at the installation to avoid this were made. In order to get similar water profiles in the models as the measured water content of the buffer, a water leakage must be introduced in the models, both for the Code_Bright and the Comsol code, although the desiccation in the innermost part of the buffer was underestimated in the Code_Bright.

The controlling of the power to the heaters in order to get the required temperatures and temperature gradients did not function properly at the beginning of the test period.

Furthermore, at the end of the test period the temperature on the inner surface of the block was higher and at the outer surface the temperature was lower than the expected in a real repository. The test was also running one month longer than initially planned. The results from the test, in spite of the shortcoming mentioned above, are assumed to be relevant for a real repository. The following conclusions from the test can be made:

1. The increase in temperature and the temperature differences over the buffer in the test have caused a decrease in water content and a reduction in volume resulting in an increased dry density in almost all parts of the bentonite blocks. Exceptions from this are some parts of the buffer at the bottom of the test setup were condensed water has been sucked up by the bentonite causing an increase in water content and a decrease in dry density compared to its initial state.
2. The measured temperatures and water content profiles could fairly well be modelled both with the Code_Bright and Comsol when a leakage of heat from the upper and lower part of the test cylinder and leakages paths of water through the bentonite blocks and out from the test setup are introduced in the models. Despite this the desiccation of the inner part of the buffer was underestimated in the Code_Bright model.
3. It is obvious that a condensation of water has occurred on the inner surface of the test cylinder. This condensation (Rh = 100% close to the inner surface of the test cylinder) together with the temperature fall over the outer gap caused a constant low water content on the outer part of the buffer blocks i.e. a continuous desiccation of the buffer. It is likely that this also will occur in a real deposition hole.
4. The large increase and variation in dry density over profiles in the bentonite blocks i.e. from the inner to the outer part of the blocks is likely the reason for observed cracks in the blocks. The temperature and the temperature gradient have caused shrinkage of the buffer, which the block could not withstand without fissuring.
5. The data from the RH sensors indicate that the desiccation of the buffer started after about 50 days and continued until the end of the test period. However, these measuring do not give any detail information about the desiccation of the buffer as function of time.
6. The modelling of the test and the results from the test show that the transport of water and the desiccation is depending on both the temperature and the temperature differences present in the buffer and gaps.
7. Although large cracks were observed particularly close to the heater no pieces of the buffer had fallen into the inner or outer slot.

The processes observed in the test will most probably exist also in the repository. The extent of the formation of fractures and condensation of water cannot be described based on the reported tests and modelling. Hence the robustness of the installation cannot be fully evaluated based on the results from this single test.

References

SKB's (Svensk Kärnbränslehantering AB) publications can be found at www.skb.se/publications.

Dueck A, 2004. Hydro-mechanical properties of a water unsaturated sodium bentonite: laboratory study and theoretical interpretation. PhD thesis. Lund University, Sweden.

Hökmark H, Fälth B, 2003. Thermal dimensioning of the deep repository. Influence of canister spacing, canister power, rock thermal properties and nearfield design on the maximum canister surface temperature. SKB TR-03-09, Svensk Kärnbränslehantering AB.

SKB, 2010. Design, production and initial state of the buffer. SKB TR-10-15, Svensk Kärnbränslehantering AB.

Wimelius H, Pusch R, 2008. Buffer protection in the installation phase. SKB R-08-137, Svensk Kärnbränslehantering AB.

Åkesson M, Börgesson L, Kristensson O, 2010. SR-Site Data report. THM modeling of buffer, backfill and other system components. SKB TR-10-44, Svensk Kärnbränslehantering AB.

Appendix 1

Description of small scale buffer installation experiments

Buffer installation technique

Membrane experiment and simulation

Ann Dueck, Reza Goudarzi, Ola Kristensson
Clay Technology AB

A1.1 General

After installation of canisters and bentonite blocks in a deposition hole according to the KBS-3V concept, there will be time period of approximately three months before the backfilling of the tunnel, above the deposition hole, is completed. During this time, the bentonite blocks will be covered with a special sheet made of plastic or rubber in order to protect the bentonite from water and high relative humidity. Just before the start of the backfilling, the covering sheet will be removed and the slot between buffer blocks and rock will be filled with pellets.

During the three-month period it is possible that the heat from the canister will affect the buffer blocks and cause a redistribution of the water in the blocks. In order to investigate this phenomenon, introductory laboratory tests in small scale were performed in 2007. In addition, numerical analyses of the processes were made, see Section A1-3.

A1.2 Experiments

A1.2.1 Test description

A1.2.1.1 General

A schematic drawing showing the principal layout of the laboratory tests is provided in Figure A1-1. A ring-shaped bentonite block with an outer diameter of 280 mm, an inner diameter of 110 mm and a height of 100 mm was placed between two lids made of fluoro-polymer. A heater consisting of a copper tube with a diameter of 108 mm was placed in the centre of the block. The temperature of the copper tube was controlled by circulation of heated water, see the photo in Figure A1-2. A rubber sheet (this material is also intended to be used in the full scale) is placed outside the bentonite block. Thermal insulation of foamed polystyrene was placed on the top and bottom surfaces of the block.

A1.2.1.2 Test equipment

To achieve the predetermined temperature gradient over the bentonite cross section the temperature of the heater was controlled. The temperature was measured by two thermo-elements installed on the inner surface and outer surface, respectively of the bentonite block. In order to measure possible high relative humidity in the outer slot, between the bentonite and the rubber sheet, a psychrometer was fixed by the sealing o-ring, between the upper lid and the rubber sheet.

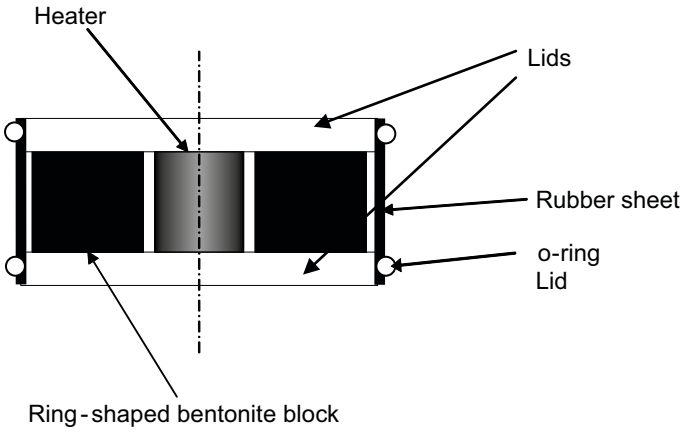

Figure A1-1. *Schematic drawing of the small scale experiment.*

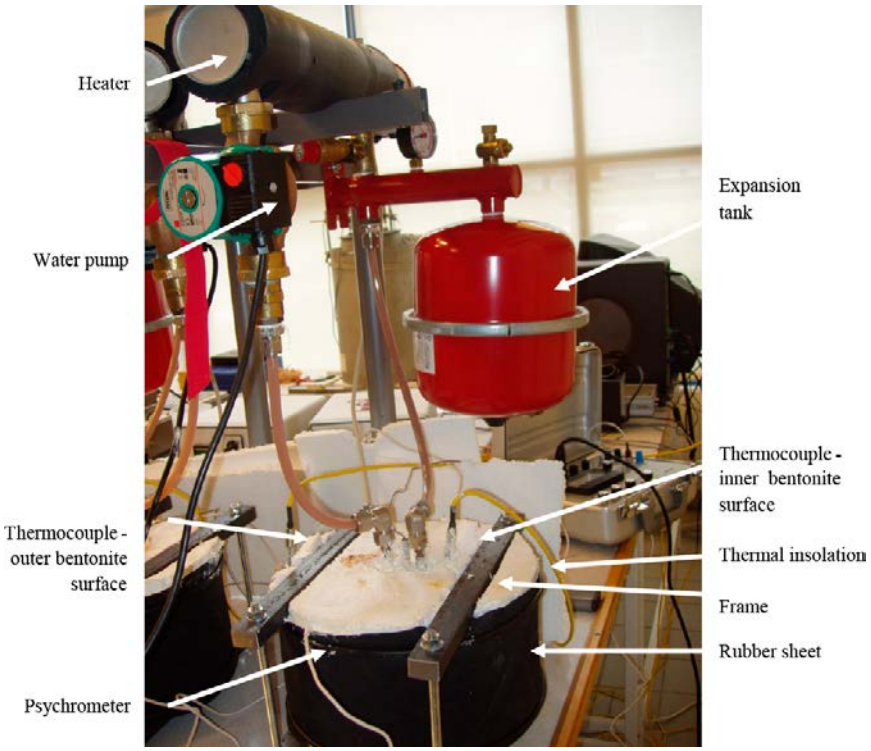

Figure A1-2. *Photo of the small scale experiment. Location of psychrometer, thermocouples and other parts of the equipment indicated.*

A1.2.1.3 Material and methodology

The specimens were made of the commercially available bentonite with the quality label MX-80 (Wyoming bentonite from American Colloid Co.). The initial water content was approximately 10% and tap water was added to reach a water content of 17% before the powder was compacted uniaxial in a rigid mould to blocks. The initial density of the bentonite ring was 2.06 g/cm^3. Each prepared ring was placed between the lids, enclosed by the rubber sheet and sealed by the o-rings. Two sets of lids with different diameters were used, 280 mm and 300 mm. The larger lids were used to keep the prescribed gap between the bentonite and the rubber sheet. The psychrometer and the thermocouples were attached and frames were mounted to keep the lids together. Finally the thermal insulation was put in place.

During the tests the temperatures were measured and controlled continuously. Measurements with the psychrometers were made once a week.

Each test lasted approximately three months. After the tests the bentonite ring was examined regarding cracking and the distribution of water content and density over the cross section were determined. The water content was determined as mass of water per mass of dry substance. The dry mass was obtained from drying the wet specimen at 105°C for 24h. The density was determined from the total mass of a sample and the volume determined by weighing the sample above and submerged in paraffin oil.

A1.2.1.4 Test matrix

Two different versions of the experiment have been performed:

- Test Type 1. The temperature difference between the inner and outer boundary was similar to the full-scaled KBS-3 case.
- Test Type 2. The temperature gradient in the bentonite block was similar to the full scale.

For each of the Test Types above, tests with the gap between the block and the rubber sheet set to 0 and 10 mm were made. The performed tests are shown in Table A1-1.

A1.2.2 Test results

The temperatures at the outer and inner surface of the bentonite measured with thermo-elements are shown in Figure A1-3.

Table A1-1. Test matrix showing the gap, the temperature difference between outer and inner surface of the bentonite ring and the gradient this implies.

Test ID	Test Type	Gap[1] mm	Temperature difference °C	Gradient °C/cm
SA1	1	0	17	2
SA2	2	0	5	0.6
SB1	1	10	17	2
SB2	2	10	5	0.6

[1] Gap between the rubber membrane and the outer surface of the bentonite ring.

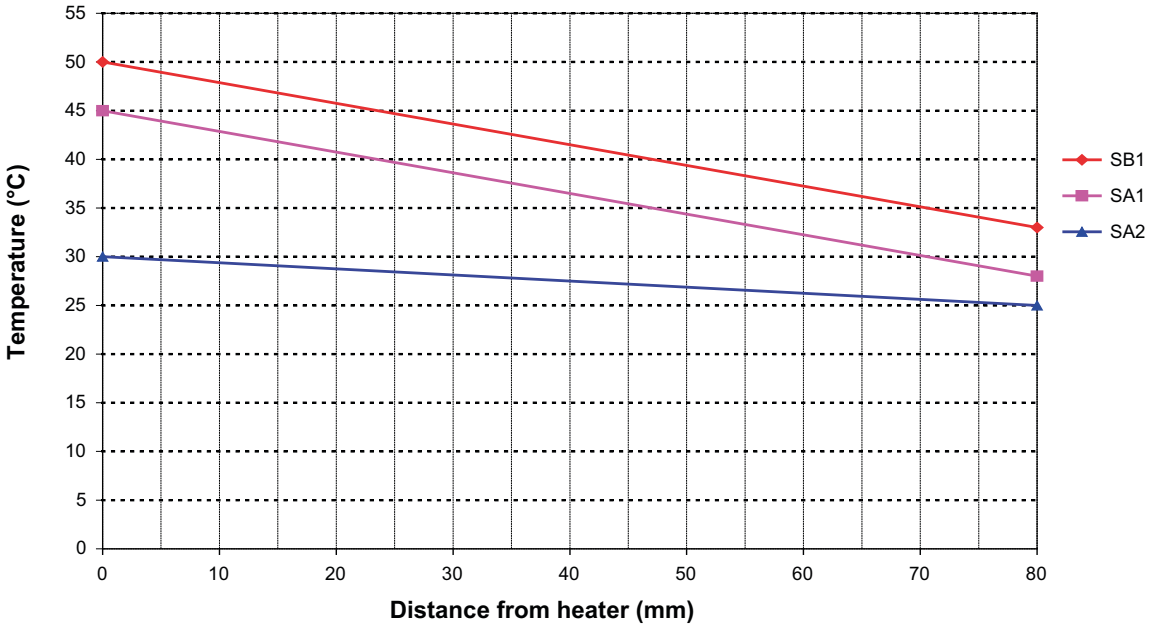

Figure A1-3. *Approximate values of measured temperatures at the outer and the inner surfaces of the bentonite ring.*

The distribution of water content after three month is shown in Figure A1-4 for SA1, SA2 and SB1. Due to problems with leakage from the water circulation in the heater in test SB2 no results were gained from this test.

The distribution of density after three month is shown in Figure A1-5 for SA1, SA2 and SB1. Due to problems with leakage from the water circulation in the heater in test SB2 no results were gained from this test.

At dismantling the rings were examined regarding cracking and the observations are shown in Table A1-2. A photo of specimen SB1 after dismantling is shown in Figure A1-6.

Table A1-2. Observed cracking at termination and psychrometer reading during the test.

Test ID	Observed cracking	Psychrometer reading
SA1	Indications of cracking along the height on the inner surface	No response
SA2	No cracking observed	No response
SB1	Radial cracking according to Figure A1-6	No response
SB2	No results	No results

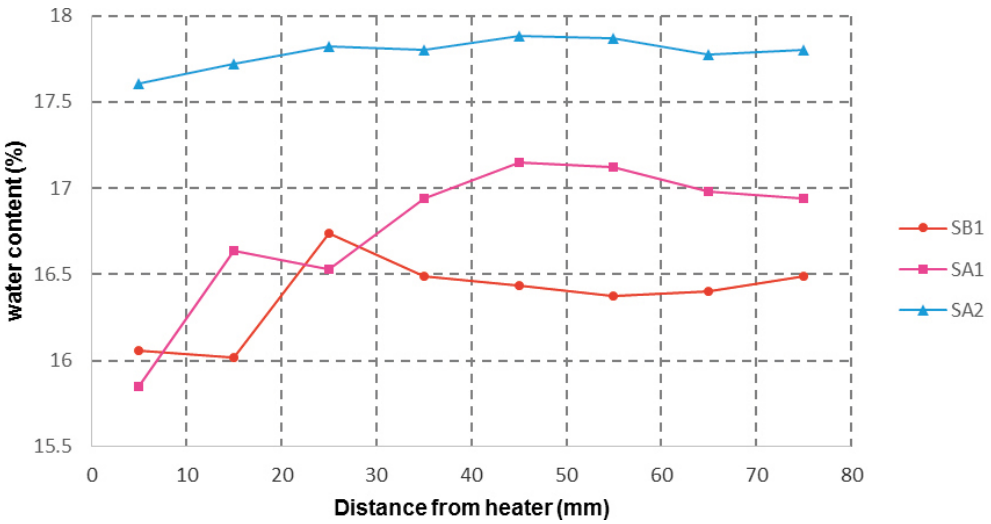

Figure A1-4. *Measured distribution of water content over the bentonite cross section.*

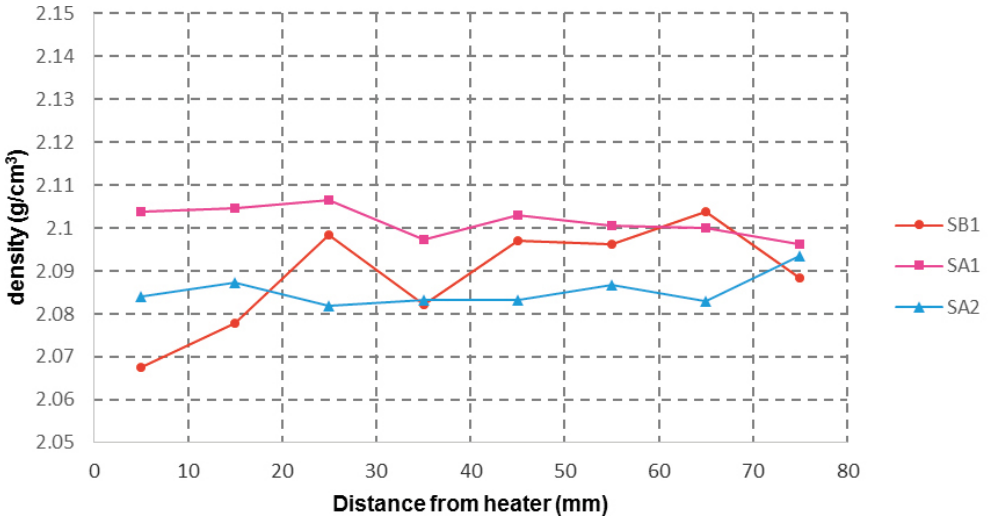

Figure A1-5. *Measured distribution of density over the bentonite cross section.*

Figure A1-6. *Radial cracking seen on specimen SB1 at termination.*

A1.2.3 Discussion

The final water content of specimen SA2 were larger than the initial water content in all parts of the investigated section which might indicate some leakage of water from the water circulation system at the low temperature gradient, Test Type 1. A small gradient over the cross section was seen, Dw = 0.2%.

At the high temperature gradient and no gap, specimen SA1, moisture was transported from the warm part to the colder. At the outer border of the bentonite, outer 20 mm, the final water content, from Figure A1-4, was the same as the initial, i.e. no excess water was present at the outer surface of the bentonite after a test period of three months.

At the high temperature gradient and a gap of 10 mm, specimen SB1, the outer half of the cross section had approximately the same water content which also corresponds to the average of the water contents for this specimen presented in Figure A1-4.

The average of the final water contents of specimen SA1 and SB1, shown in Figure A1-4, was 16.8% and 16.4% respectively. Since the initial water content was 17% it cannot be excluded that the specimens may have suffered some evaporation either during preparation, during installation, at dismantling or by some leakage during the test. The constant values at the outer surface indicate no leakage in that direction.

The relative humidity can be expected to be less than 85% when measured in air in equilibrium with MX-80 at a water content of 17% (Dueck 2004). Since the psychrometer only measures relative humidity above approximately 95% a water content of approximately 30% would have been required to get a measurable value when in equilibrium with the bentonite.

A1.3 Simulations

Here the three experiments A1, A2 and B1 are simulated. By doing this, the processes in the experiment, giving raise to the measured water ratio profiles, may be understood. Alternation of the test setup may also be investigated for future experiments.

A1.3.1 Model description

A1.3.1.1 Geometry

Three different rotational symmetric geometries are used for modelling the three experiments A1, A2 and B1. The geometry representing B1 includes an outer slot, which is not present in the A1 and A2 geometries. Besides this difference, the width w_i of an inner slot, between the heater and bentonite block, also differentiate the models. The inner slot is motivated by the mismatch between the heater diameter and inner diameter of the bentonite ring. Since perfect alignment of the two components is unlikely, this becomes a fitting parameter. The geometry and dimensions of the models are shown in Figure A1-7.

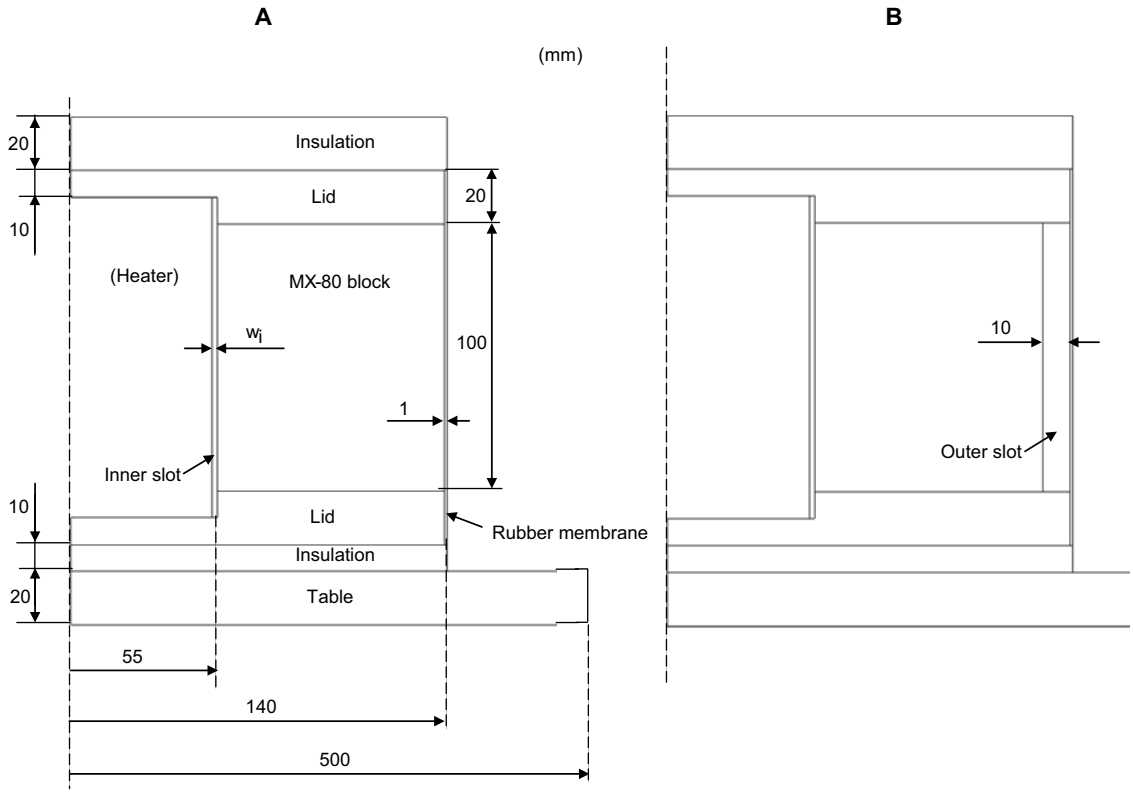

Figure A1-7. *Model geometry.*

The constituents in the models are:

1 **MX-80** block.

2 Upper and lower **Lid**s of polyvinylidene fluoride (PVDF).

3 Upper and lower **Insulation** made out of expanded polystyrene (EPS).

4 **Membrane** of rubber ethylene propylene diene monomer (M-class) rubber (EPDM).

5 **Table**.

6 **Inner slot** (where the width w_i = 0, 0.5 or 2 mm).

7 **Outer slot** (B1 only).

A1.3.1.2 Constitutive laws and parameters

The solid density, specific heat and porosity are given in Table A1-3.

Table A1-3. Solid density, specific heat and porosity.

Parameter	MX-80	Lid	Insulation	Membrane	Table	Inner slot	Outer slot
[kg/m^3]	2,780	920	20	920	650	1.15	1.15
[J/(kg K)]	800	800	800	1,600	1,500	1,005	1,005
n [–]	0.37	0.001	0.001	0.001	0.001	0.001	0.99

Conductive heat flux:

$$\boldsymbol{i}_c = -\lambda \nabla T \tag{A1-1}$$

$$\lambda = \lambda_{sat} S_l + \lambda_{dry}(1 - S_l) \tag{A1-2}$$

It was only the MX-80 material that was assumed to have a conductivity varying with saturation. Thus, $\lambda = \lambda_{sat} = \lambda_{dry}$ for the other materials. The conductivity for the slots was taken as the value obtained by (A1-3), which is dependent on temperature T and slot width a. In (A1-3) the contribution from air conduction and temperature radiation between two parallel surfaces are considered. For the inner slot, the values of conductivity in Table A1-4 are given in the order that corresponds to the slot width order: w_i = 2, 0, 0.5 mm.

When deciding upon the thermal conductivity of the open slots, effective values are used to incorporate the estimated effects from heat radiation in the model, see Hökmark and Fälth (2003). The expression of the effective conductivity is,

$$\begin{aligned} \lambda(T,a) &= \frac{e_1 e_2}{e_1 + e_2 - e_1 e_2} \sigma 4 (T + 273.15)^2 a + \lambda_{air}(T) \\ \lambda_{air}(T) &= 0.024(1 - 0.01T) + 0.00318(0.01T) \end{aligned} \tag{A1-3}$$

where e_1 and e_2 are the emissivity of the two surfaces, $\sigma = 5.66997 \cdot 10^{-8}$ W/(m^{2}K^4) is the Stefan-Boltzamnn's constant, T the slot temperature, a the slot width. Here $e_{bentonite} = 0.9$, $e_{canister} = 0.8$ and $e_{membrane} = 0.9$ were used.

Retention curve:

$$S_l = \left(1 + \left(\frac{S}{p_0} \right)^{1/(1-\lambda)} \right)^{-\lambda} \tag{A1-4}$$

$$S = p_g - p_l \tag{A1-5}$$

The retention curve for the MX-80 material was obtained from using the same λ value as recommended for the buffer ring material in the SR-Site Data report (Åkesson et al. 2010) and finding a p_0 value that gave the correct initial state (w = 0.17, s = 46 MPa). The other materials were given a significantly lower retention curve as compared to the MX-80 material. The used parameter values are shown in Table A1-5.

Table A1-4. Thermal conductivities [W/(m·K)].

Model	MX-80	Lid	Insulation	Membrane	Table	Inner slot	Outer slot
A1	0.7;1.3	0.2	0.035	0.2	0.2	0.24/–/0.17*	–
A2						0.24/–/0.17*	–
B1						0.27/–*	0.07*

Table A1-5. Retention parameters.

Parameter	MX-80	Other
p_0 [MPa]	64.02	0.1
λ	0.48	0.6

Flow through porous medium:

$$\boldsymbol{q}_l = -\frac{kk_{rl}}{\mu_l}\nabla p_l \tag{A1-6}$$

$$\text{(a)} \quad k_{rl} = AS_l^{\,3} \tag{A1-7}$$

$$\text{(b)} \quad k_{rl} = 1 \tag{A1-8}$$

$$\mu_l = 2\cdot 10^{-12}\exp\left(\frac{1808.5}{273.15+T}\right) \tag{A1-9}$$

The MX-80 material was given permeability according to the suggestions in the SR-Site Data report The outer slot was allotted low flow resistance in order to mimic an open slot. The other materials were equipped with high flow resistance. The values of the permeability are shown in Table A1-6.

Vapor diffusion:

$$\boldsymbol{i}_g^w = -(n\rho_g S_g D_m^w)\nabla\omega_g^w \tag{A1-10}$$

$$S_g = 1 - S_l \tag{A1-11}$$

$$D_m^w = \tau 5.9\cdot 10^{-6}\frac{(273.15+T)^{2.3}}{p_g} \tag{A1-12}$$

In the MX-80 and outer slot, vapour diffusion efficient by maximizing the tortuosity according to the adopted theory was made. The other materials were made quite impermeable by using a low value of tortuosity. Used tortuosity values are shown in Table A1-7.

Table A1-6. Permeabilities.

Parameter	MX-80	Outer slot (B1)	Other
k [m^2]	$2.4\cdot 10^{-21}$	$1\cdot 10^{-10}$	$1\cdot 10^{-30}$
k_{rl}	A = 1 [(a)]	(b)	A = 0.001 [(a)]

Table A1-7. Tortuosities.

Parameter	MX-80	Outer slot (B1)	Other
τ	1	1	$1\cdot 10^{-5}$

A1.3.1.3 Initial/boundary conditions

The initial conditions are given by $T_0 = T_{room}$ (shown below in Table), $p_{l0} = -45.9$ MPa.

The thermal boundary conditions are prescribed as shown below in Figure A1-8. The measured heater temperature is prescribed at the inner boundary of the model and the measured room temperature is prescribed at the outer boundary by using a heat transfer coefficient γ.

Hydraulically, the boundaries are closed.

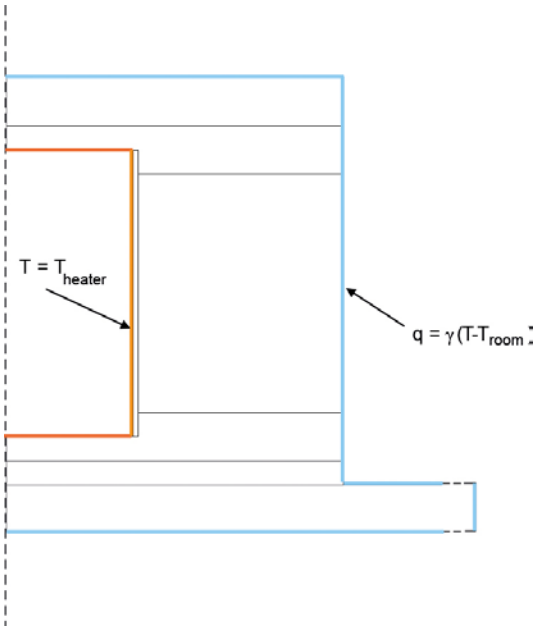

Figure A1-8. *Indication of the used thermal boundary conditions.*

A1.3.2 Thermal calibration

The temperature field significantly governs the vapor transport in the current experimental setup. Therefore, it is of great importance that the thermal process is captured accurately in the model. From the experiment following temperatures are known:

1. The heater temperature (here considered homogeny over the heater surface).
2. The temperature at the outer surface of the block at mid-height.
3. The room temperature.

For the three different experiments the following temperatures given in Table A1-8 were measured:

The strategy how to calibrate the models was to apply the room temperature together with a constant heat transfer coefficient of 10 W/(m^2·K) at the outer surface of the models and find an inner slot width in the interval {0, 2} mm that gave the correct outer block temperature. The heater temperature was prescribed at the inner surface of the slot and the top/bottom of the heater.

For one simulated experiment (A2) it was necessary to decrease the heat transfer coefficient to 6 W/(m^2·K) in order to calibrate the model.

Below in Figure A1-9 the calibration process is shown by indicating a temperature rage close to the outer block temperature given by the experimental data. The models producing the rightmost figures were taken as the starting point when developing the TH-models.

Table A1-8. Measured temperatures.

	Heater temp. °C	Outer block temp. °C	Room temp. °C
A1	44.1	26.4	18.4
A2	29.4	24.3	19.4
B1	50.0	32.5	18.4

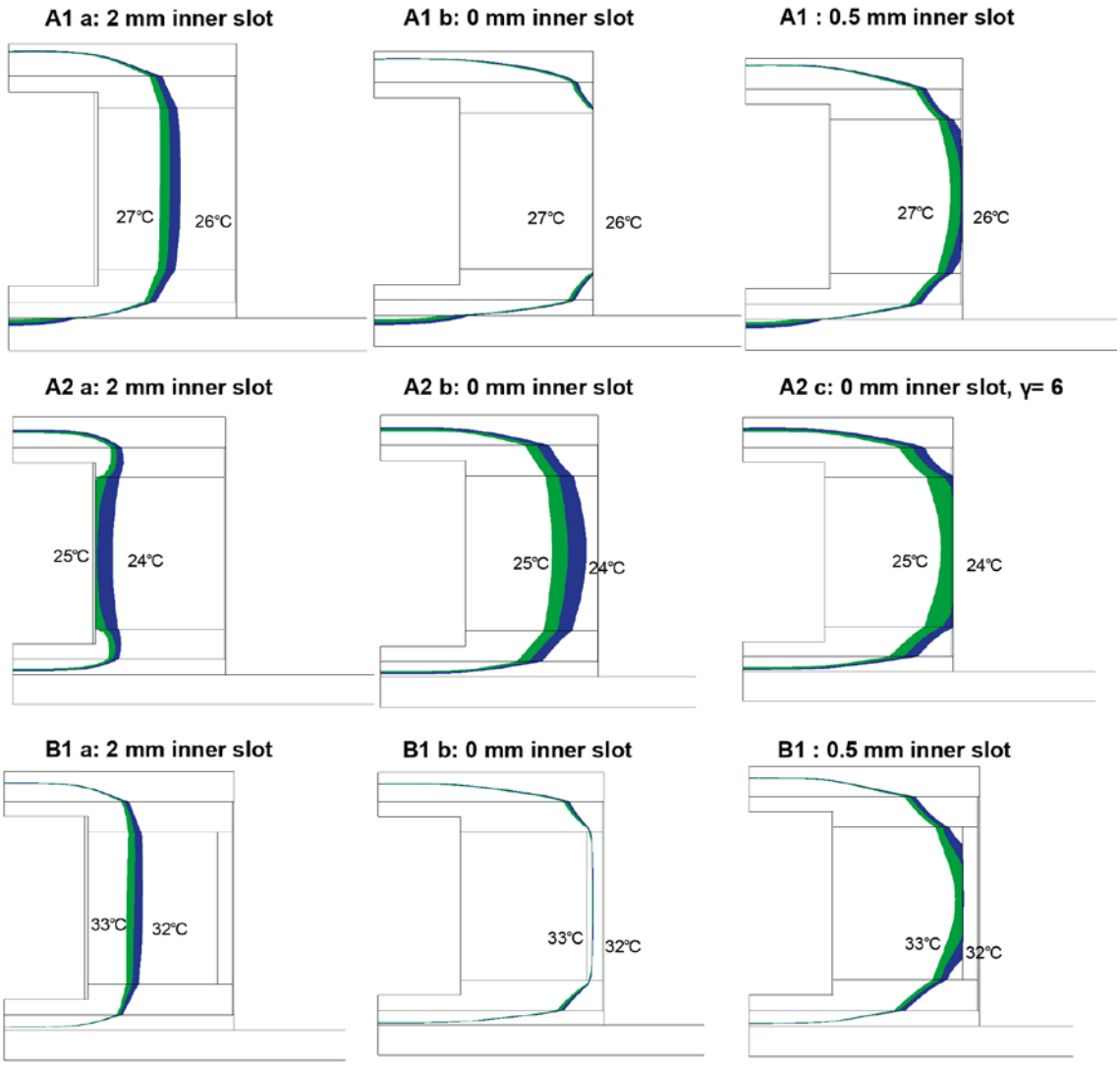

Figure A1-9. *Schematic view of the thermal calibration process (left to right) for the three simulated experiments (A1 top, A2 middle and B1 bottom).*

A1.3.3 Thermal – Hydraulic simulations

The outputs from the thermal calibration process, the calibrated thermal models, were equipped with hydraulic logic.

When evaluating the modelled results against the experimental results, the process of how the experimental results were obtained was mimicked.

In the experiment, the block was cut twice vertically so that a segment of the ring-shaped block was obtained. The water ratio was evaluated in the upper half of this segment. The material was then cut at a number of radial distances and for each obtained sample the water ratio was determined.

The model results were treated to mimic the experimental evaluation. The volume average of the water ratio was calculated in the volumes corresponding to the samples that were evaluated experimentally.

It should be mentioned that the initial water ratio was not measured with high accuracy in the experiment and therefore quantitative comparisons of high accuracy are not possible.

A1.3.3.1 A1

The experimental and simulated water ratio profiles are shown in Figure A1-10 for experiment A1. For comparison, the volume averages of the experimental and simulated profiles are given and also the initial water ratio in the simulation.

It can be seen that the profiles matches reasonably well at radii < 0.1 m. At the outer part of the block, radii > 0.1 m, the experimental data is below that of the modelled result. The averages of the data are not too far apart with the experimental below that of the simulation.

To investigate the origin of the decrease in water ratio in the outer part of the block two additional cases were modelled:

1. It was assumed that the block, after 100 days in the experimental setup, was subjected to cooling and a constant surrounding RH = 72% (equal to the initial RH in the block) for 3 hours.
2. It was assumed that the block, after 100 days in the experimental setup, was subjected to cooling and a surrounding RH starting at 72% and decreasing to 60% during 3 hours.

The first additional case could correspond approximately to the block put in a plastic bag. The second additional case could correspond to the block subjected to indoor climate. The resulting water ratio profiles are shown in Figure A1-11 and Figure A1-12.

Here the water can be seen to be redistributed comparing with the base case profile. The outer part has lost some water and the inner part has gained some water. Comparing the average water ratios indicate that, in total, no water is lost or gained.

In the second additional case the average levels show that water is lost. The entire curve is lowered and both ends of the profile points more downward as compared to the base case profile.

The trends of the experimental and simulated (the additional cases) profiles in the outer part of the block indicate that redistribution/loss of water is likely to have happened. Water may have been lost during the operational phase of the experiment and/or after the operational phase.

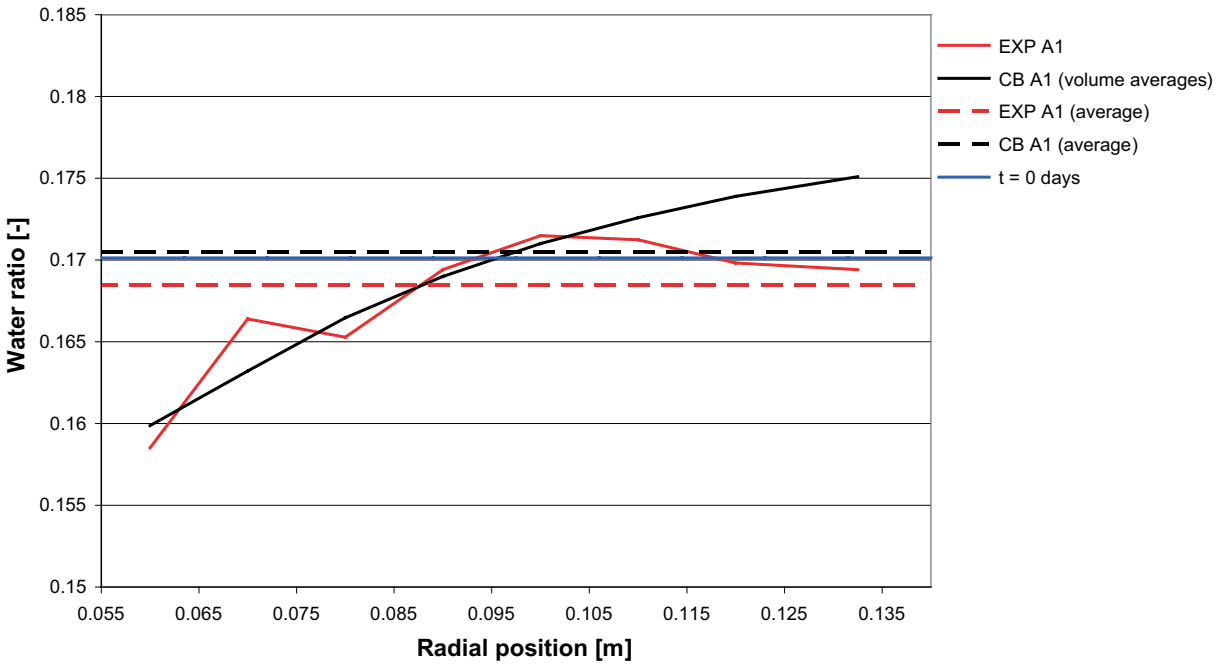

Figure A1-10. *Water ratio profiles for A1 (Base Case).*

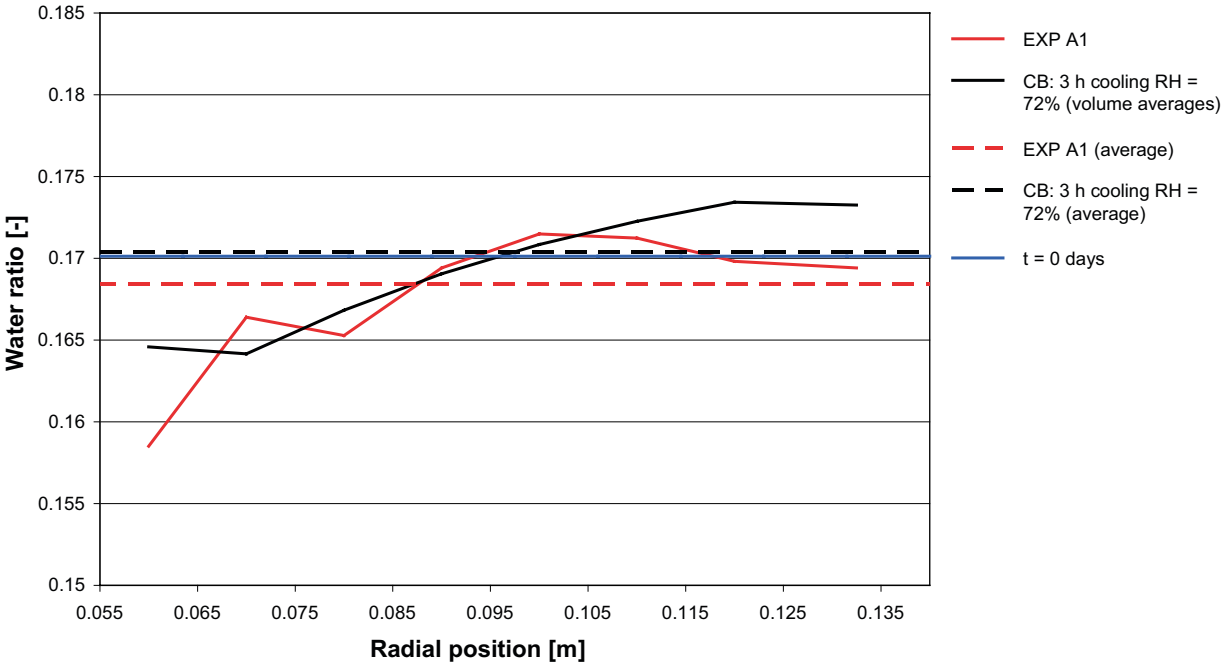

Figure A1-11. *Water ratio profiles for A1 (water redistribution case).*

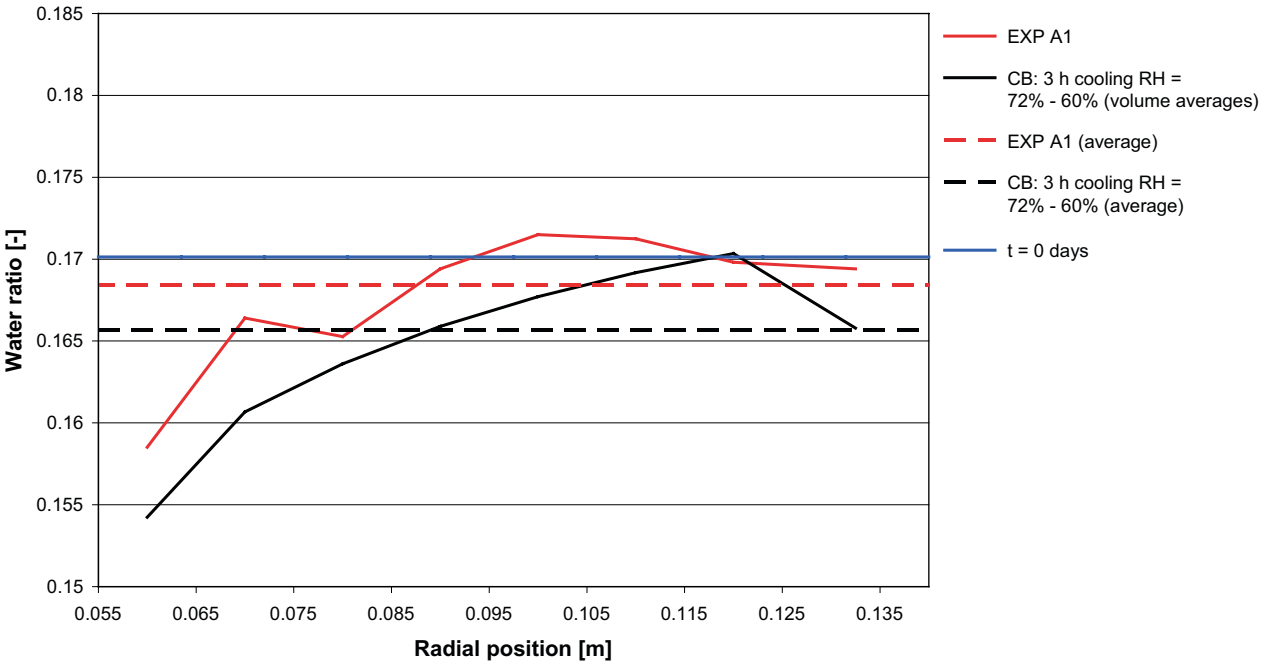

Figure A1-12. *Water ratio profiles for A1 (drying case).*

A1.3.3.2 A2

The experimental and simulated water ratio profiles are shown in Figure A1-13 for experiment A2. For comparison, the volume averages of the experimental and simulated profiles are given and also the initial water ratio in the simulation.

The average of the experimental water ratio indicates high initial water ratio or gain of water. Gain of water is unlikely in the present experiment (The heater contains water so there could have been some leakage, but it is not very likely for A2.). Due to the small temperature gradient used in A2 the redistribution of water has been less as compared to A1. The experimental profile compares to the simulated profile as in A1, the profile in the outer part is lower (as compared to the average value).

A1.3.3.3 B1

The experimental and simulated water ratio profiles are shown in Figure A1-14 for experiment B1. For comparison, the volume averages of the experimental and simulated profiles are given and also the initial water ratio in the simulation.

What have been seen in the previous cases is also seen here. The average water ratio does not correspond well between the experiment and simulation. The experimental water ratio profile is closer to the corresponding average value in the outer part.

A1.3.4 Conclusions

When comparing the trends of the experimental and simulated profiles in the outer part of the block there are indications that redistribution/loss of water is likely to have happened. Either, water is lost during the experiment or, in between the block being in the test setup and values of the water ratio have been determined.

A1.3.4.1 Notes for how to design similar experiments in the future

- Determine the initial water ratio carefully.
- More insulation could reduce the simulation work (the problem becomes closer to radial).
- Hurry when demounting the experiment and determining the water ratios.
- Wrap the material in plastic to prevent drying.
- Make sure the equipment does not leak.

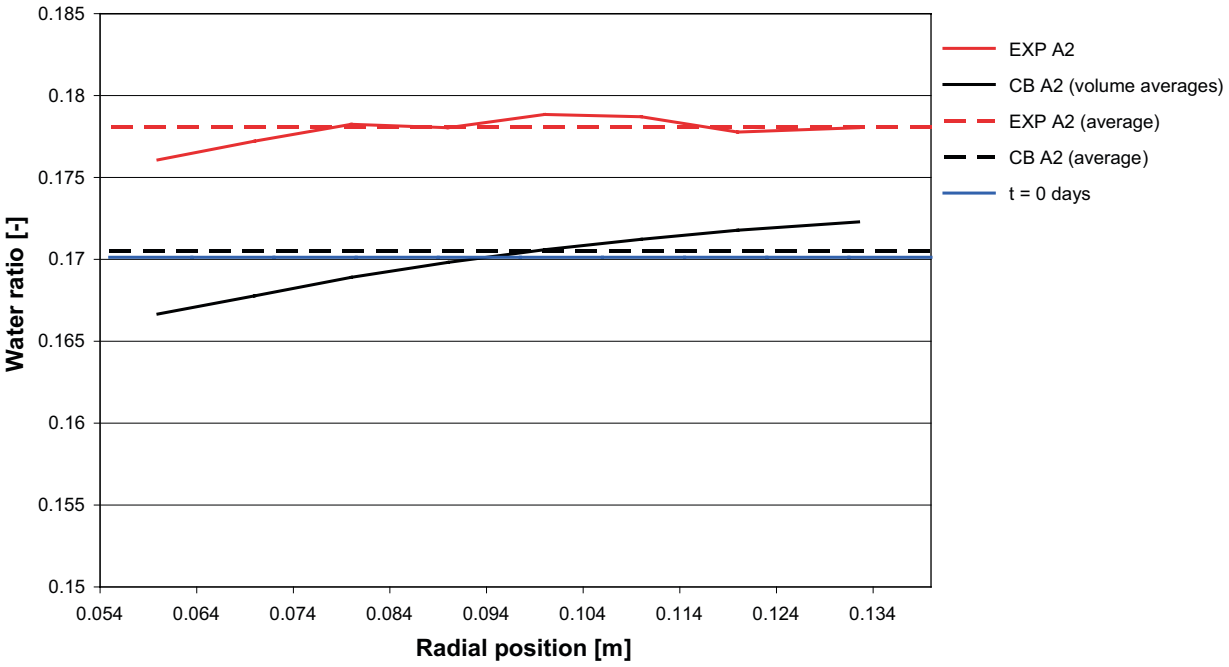

Figure A1-13. *Water ratio profiles for A2.*

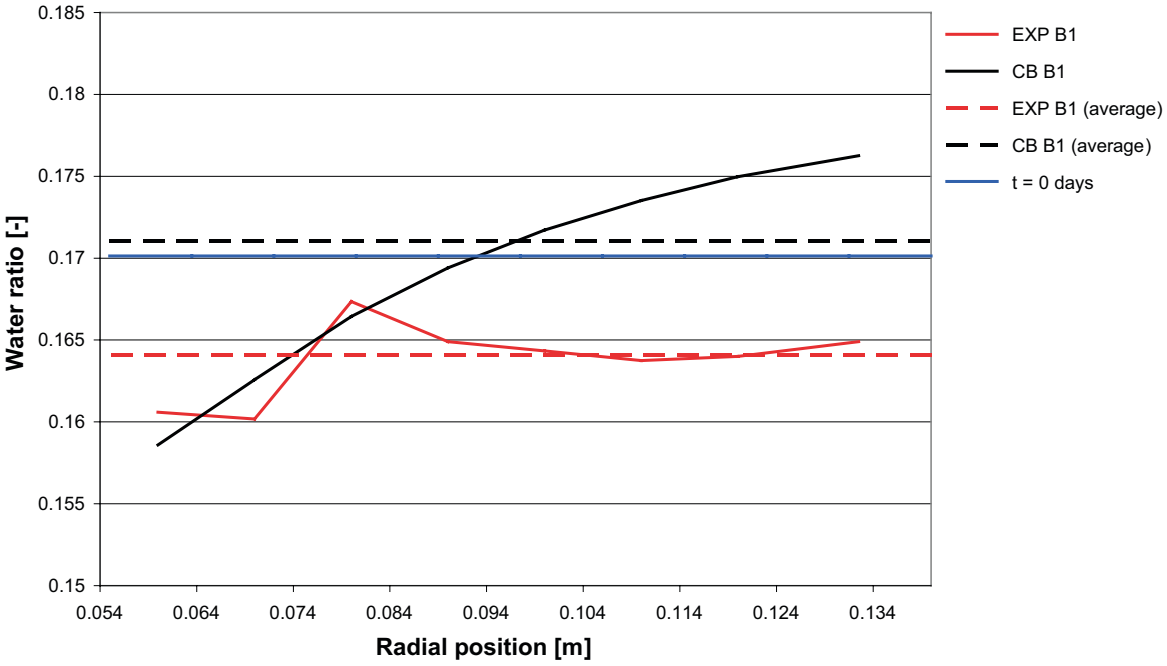

Figure A1-14. *Water ratio profiles for B1.*

Appendix 2

Description of models used in the pre operational simulations

A2.1 Thermal KBS-3V model

An axisymmetric model geometry containing canister, open slots, bentonite blocks and surrounding rock was used as a point of departure to study the thermal conditions, see Figure A2-1. The existing model was equipped with an outer empty "pellet-slot", since the pellets are not to be installed during the time that was analysed.

Linear heat conduction has been used in the model. The canister power input, $P(t)$, was a linear fit to the expression:

$$P(t) = P(0)\sum_{i=1}^{7} a_i \exp(-t/t_i) \qquad \text{(A2-1)}$$

Here $P(0)$=1,700 W and the decay function coefficients, shown below in Figure A2-2, corresponds to 35 year old fuel.

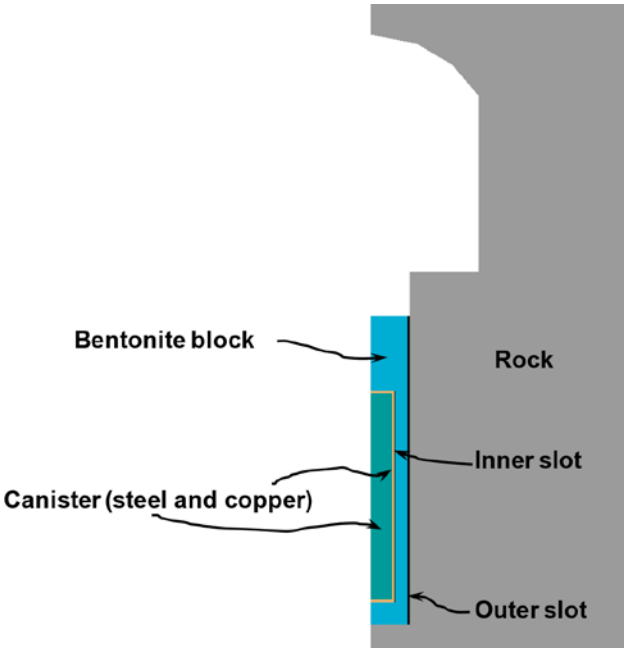

Figure A2-1. *Close up of the geometry of the tunnel and deposition hole in the KBS-3V model.*

i	t_i [years]	a_i
1	20	0.060
2	50	0.705
3	200	-0.055
4	500	0.250
5	2,000	0.025
6	5,000	-0.009
7	20,000	0.024

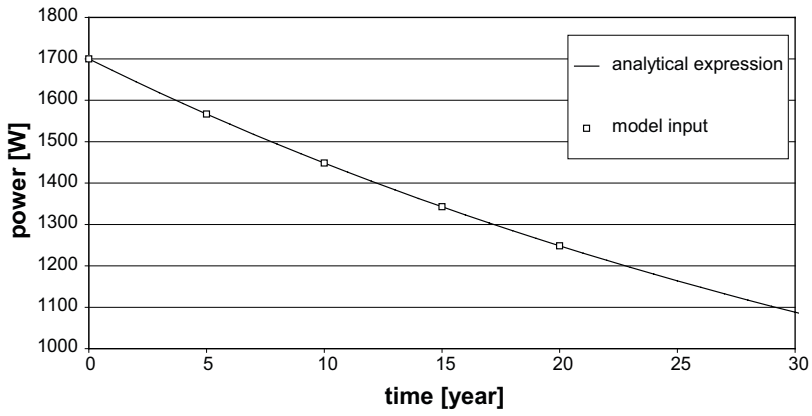

Figure A2-2. *Decay function coefficients and the corresponding graph for the 35 year old fuel.*

The initial temperature was 10°C in the entire model. The boundary conditions were adiabatic at all model boundaries except for the tunnel where a convection heat transfer coefficient of γ = 10 W/(m^{2}K) was used.

The material parameter values: solid density ρ; specific heat capacity c; thermal conductivity λ; and porosity n; used in the model are shown in Table A2-1.

To account for effects of heat transfer by radiation in the open slots and still only use the format of conductive transfer, an estimate of an effective conductivity,

$$\lambda_{eff}(T) = \frac{e_1 e_2}{e_1 + e_2 - e_1 e_2}\sigma 4(T+273)^3 a + \lambda_{air}(T), \qquad \text{(A2-2)}$$

based on the Stefan-Boltzmann law, was used. In the expression, e_1 and e_2 are the emissivity of the two parallel surfaces, $\sigma = 5.66997 \cdot 10^{-8}$ W/(m^{2}K^4) is the Stefan-Boltzmann constant, T the average temperature in the slot, a the slot width, and

$$\lambda_{air}(T) = 0.024(1 - 0.01T) + 0.0318(0.01T), \qquad \text{(A2-3)}$$

the adopted relation describing the air conductivity. The emissivity used for the surfaces of the heater, bentonite block, and rock wall are; e_h = 0.1, e_b = 0.8, and e_{rw} = 0.8, respectively.

Initial estimations λ_{in}^0 and λ_{out}^0 of the effective conductivity of the inner and outer slot, respectively, were used in the first simulation. The temperature field T^0 obtained after 3 months gave new slot conductivities λ_{in}^1 and λ_{out}^1.

If there was too much mismatch between the two sets of conductivities $\{\lambda_{in}^0, \lambda_{out}^0\}$ and $\{\lambda_{in}^1, \lambda_{out}^1\}$, the latter was used in a new simulation.

When two sequential sets of conductivities were close enough, $\{\lambda_{in}^i, \lambda_{out}^i\} \approx \{\lambda_{in}^{i+1}, \lambda_{out}^{i+1}\}$, convergence was obtained. At convergence the obtained temperature field T^i was adopted as the temperature at deposition hole installation, $T_{inst} = T^i$.

Table A2-1. Material parameter values used in the KBS-3V model.

No	Material	ρ (kg/m^3)	c (J/(kg·K))	λ (W/(m·K))	n (–)
1	Cast iron	7,200	500	40	0
2	Copper	8,930	390	390	0
3	Inner slot	1.3	1,000	0.0379	0
4	Empty pellet slot	1.3	1,000	0.2446	0
5	Bentonite	2,780	800	1.1	0.355
6	Backfill	2,500	780	1.5	0.5
7	Rock	2,770	770	3.63	0

A2.2 Hydro-Thermal 2D model of the deposition hole at canister mid-height

In Figure A2-3 the geometry of the model is shown. The model is aimed at representing a disc of the experiment at mid-height, i.e. the symmetry surface.

The used material parameter values of; solid density ρ_s; specific heat capacity c; and porosity n; are shown in Table A2-2.

Figure A2-3. *Geometry of the 1D_T experiment model.*

Table A2-2. Solid density, specific heat capacity, and porosity.

Parameter	MX-80	Slots
[kg/m^3]	2,780	1.15
[J/(kg·K)]	800	1,005
n [–]	0.37	0.99

It was only the MX-80 material that was assumed to have a thermal conductivity, λ, varying with saturation, S_l. Thus, $\lambda = \lambda_{sat} = \lambda_{dry}$ for the slot materials, see Table A2-3. The conductivity for the slots was taken as the values obtained in the modeling of the KBS-3V.

$$\boldsymbol{i}_c = -\lambda \nabla T \tag{A2-4}$$

$$\lambda = \lambda_{sat} S_l + \lambda_{dry}(1 - S_l) \tag{A2-5}$$

Table A2-3. Thermal conductivity parameters.

Parameter	MX-80	Inner slot	Outer slot
λ_{dry} [W/(m·K)]	0.7	0.0397	0.2446
λ_{sat} [W/(m·K)]	1.3		

The retention curve for the MX-80 material was obtained from using the same parameter value for λ (not to be mixed up with the thermal conductivity) as recommended for the buffer ring material in the "SR-Site Data Report" and finding a p_0 value that gave the correct initial state in terms of water content, $w_0 = 0.17$, and suction, $S_0 = 46$ MPa. Suction is given by the pore pressures of gas and liquid, p_g and p_l, respectively. The slot materials were given a significantly lower retention curve as compared to the MX-80 material. The parameter values are given in Table A2-4.

$$S_l = \left(1 + \left(\frac{S}{p_0}\right)^{1/(1-\lambda)}\right)^{-\lambda} \tag{A2-6}$$

$$S = p_g - p_l \tag{A2-7}$$

Table A2-4. Water retention parameters.

Parameter	MX-80	Slots
p_0 [MPa]	64.02	0.1
λ	0.48	0.6

The MX-80 material was given intrinsic and relative liquid permeabilities, k and k_{rl}, according to the suggestions in the "SR-Site Data Report" and the slots were allotted with a low flow resistance, see Table A2-5. The liquid viscosity, μ_l, was taken as given by (A2-11).

$$\boldsymbol{q}_l = -\frac{k k_{rl}}{\mu_l} \nabla p_l \tag{A2-8}$$

(a) $$k_{rl} = A S_l^{\,3} \tag{A2-9}$$

(b) $$k_{rl} = 1 \tag{A2-10}$$

$$\mu_l = 2 \cdot 10^{-12} \exp\left(\frac{1808.5}{273.15 + T}\right) \tag{A2-11}$$

Table A2-5. Flow through porous media parameters.

Parameter	MX-80	Slots
k [m^2]	$2.4 \cdot 10^{-21}$	$1 \cdot 10^{-10}$
k_{rl}	$A = 1$ [(a)]	(b)

In the MX-80 and slots, vapor diffusion was made efficient by maximizing the tortuosity, τ, according to the adopted theory, see Table A2-6.

$$\boldsymbol{i}_g^w = -(n\rho_g S_g D_m^w)\nabla \omega_g^w \tag{A2-12}$$

$$S_g = 1 - S_l \tag{A2-13}$$

$$D_m^w = \tau 5.9 \cdot 10^{-6} \frac{(273.15+T)^{2.3}}{p_g} \tag{A2-14}$$

The gas density is given by $\rho_g = \theta_g^a + \theta_g^w$, where θ_g^a and θ_g^w are defined below. When expressing the gas density the parameters: molar mass of air (M_a); molar mass of water (M_w), and constant of gases (R) are used.

$$\tilde{\theta}_g^a(p_g, T) = \frac{\left(p_g - \tilde{p}_g^{\,w}(T)\right)M_a}{R(273.15+T)} \tag{A2-15}$$

$$\tilde{\theta}_g^w(p_l, p_g, T) = \frac{\tilde{p}_g^{\,w}(T)M_w}{R(273.15+T)} \exp\left(\frac{-(p_g - p_l)M_w}{R(273.15+T)\tilde{\rho}_l(p_l, T)}\right) \tag{A2-16}$$

$$\tilde{p}_g^{\,w}(T) = 136075 \exp\left(-5239.7/(273.15+T)\right) \tag{A2-17}$$

$$\tilde{\rho}_l(p_l, T) = 1002.6 \exp\left(4.5 \cdot 10^{-4}(p_l - 0.1) - 3.4 \cdot 10^{-4} T\right) \tag{A2-18}$$

Table A2-6. Tortuosities.

Parameter	MX-80	Slots
τ	1	1

A2.2.1 Prescribed conditions

The gas pore pressure, p_g, was prescribed to 0.1 MPa. The initial conditions were given by $T_0 = 10$°C, and $p_{l0} = -45.9$ MPa.

The thermal boundary conditions were:

- A constant heater power of 265 W/m prescribed at the axial symmetry line.
- A water tank temperature according to the protocol given below, prescribed in the outer white section in Figure A2-3.

Hydraulically, the boundaries were prescribed as closed.

Table A2-7. Water tank temperature protocol.

Interval no.	Start (day)	End (day)	Water temperature (°C)
1	0	15	20
2	15	23	24
3	23	34	28
4	34	53	32
5	53	74	36
6	74	90	38

Water content and dry density profiles (B1,10°)

Measured water content and density for the lower block (B1) at direction 10°.

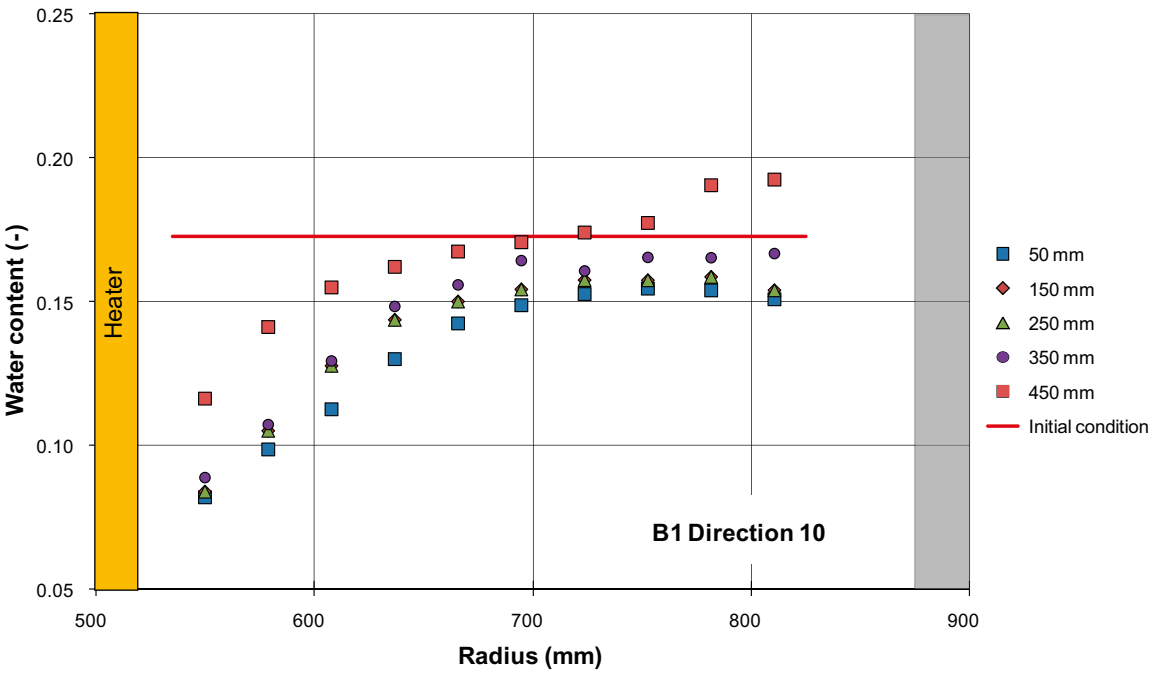

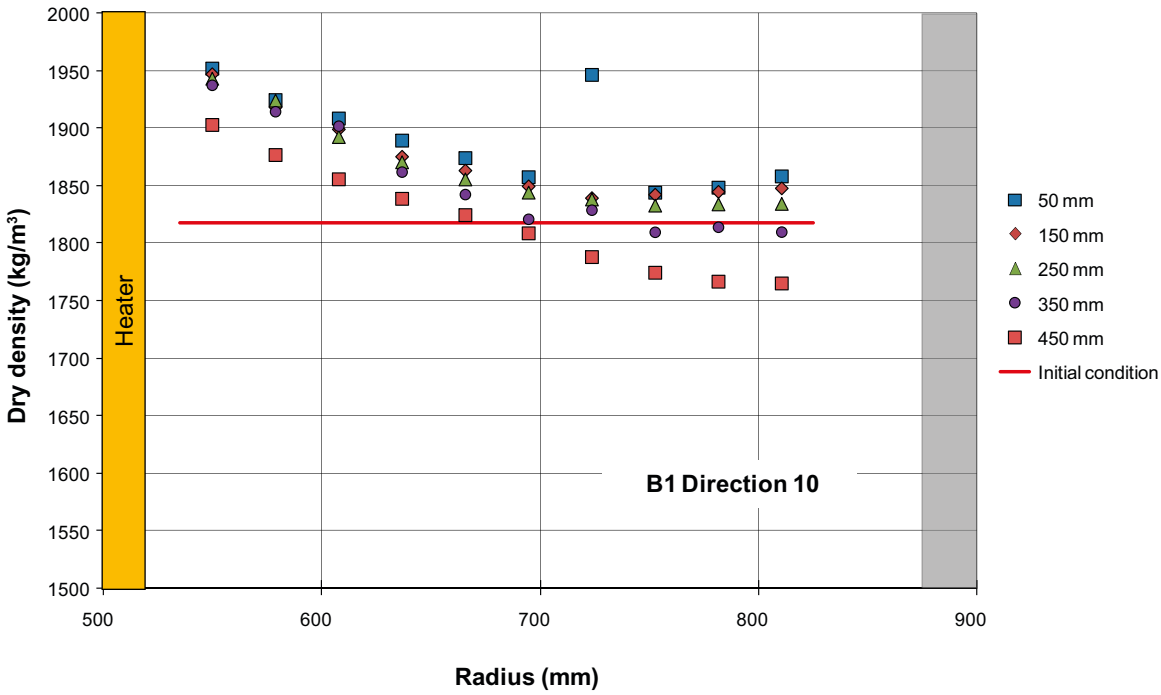

Water content and dry density profiles (B1,100°)

Measured water content and density for the lower block (B1) at direction 100°.

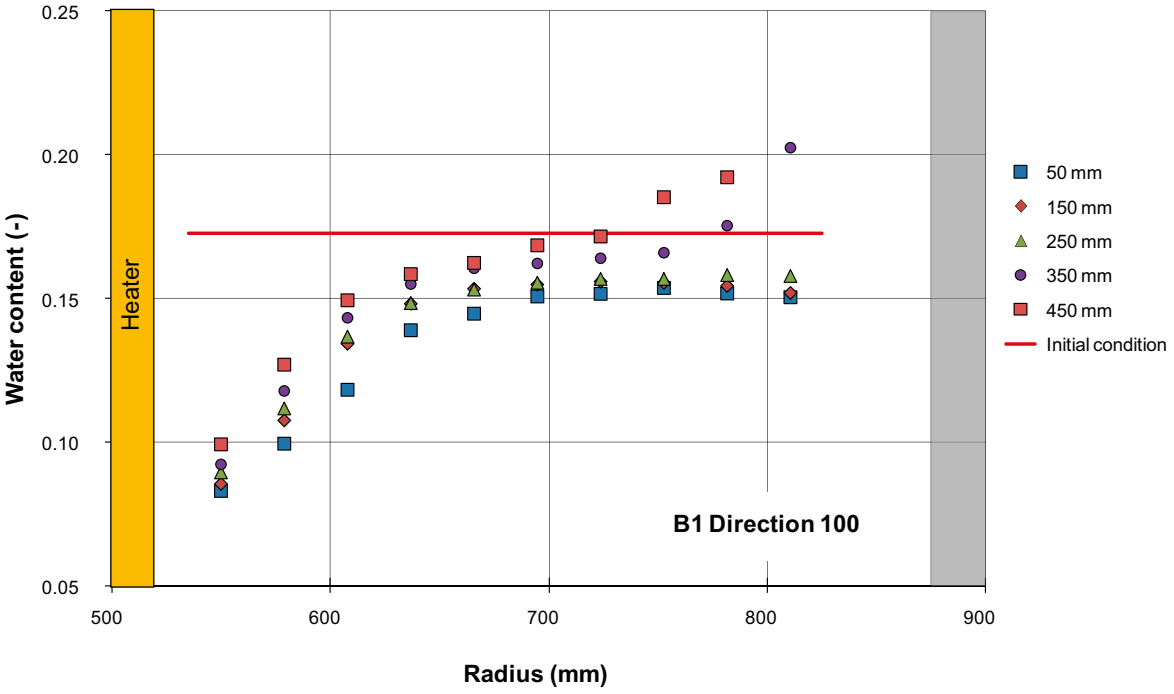

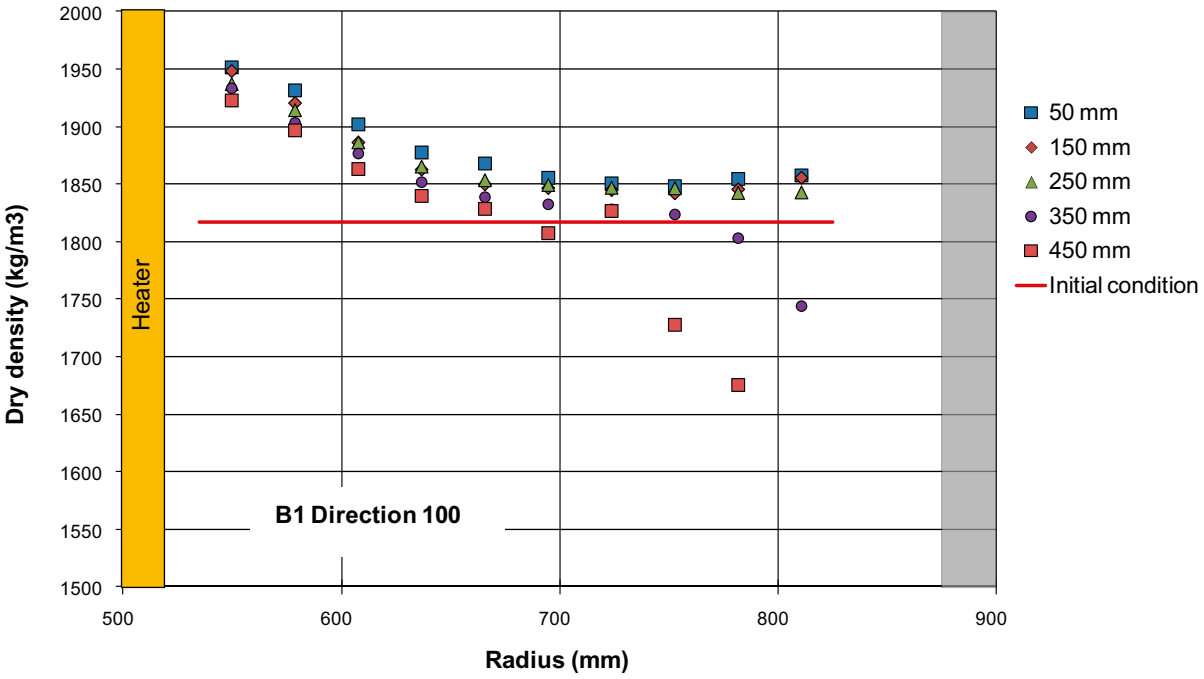

Appendix 5

Water content and dry density profiles (B1,190°)

Measured water content and density for the lower block (B1) at direction 190°.

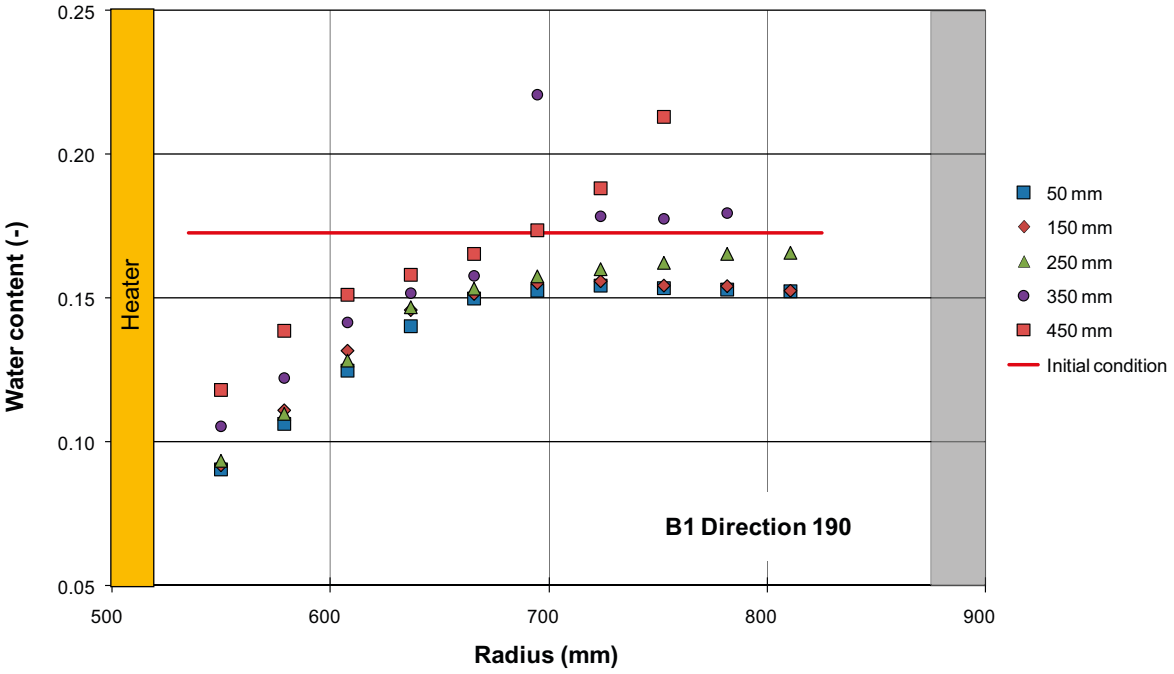

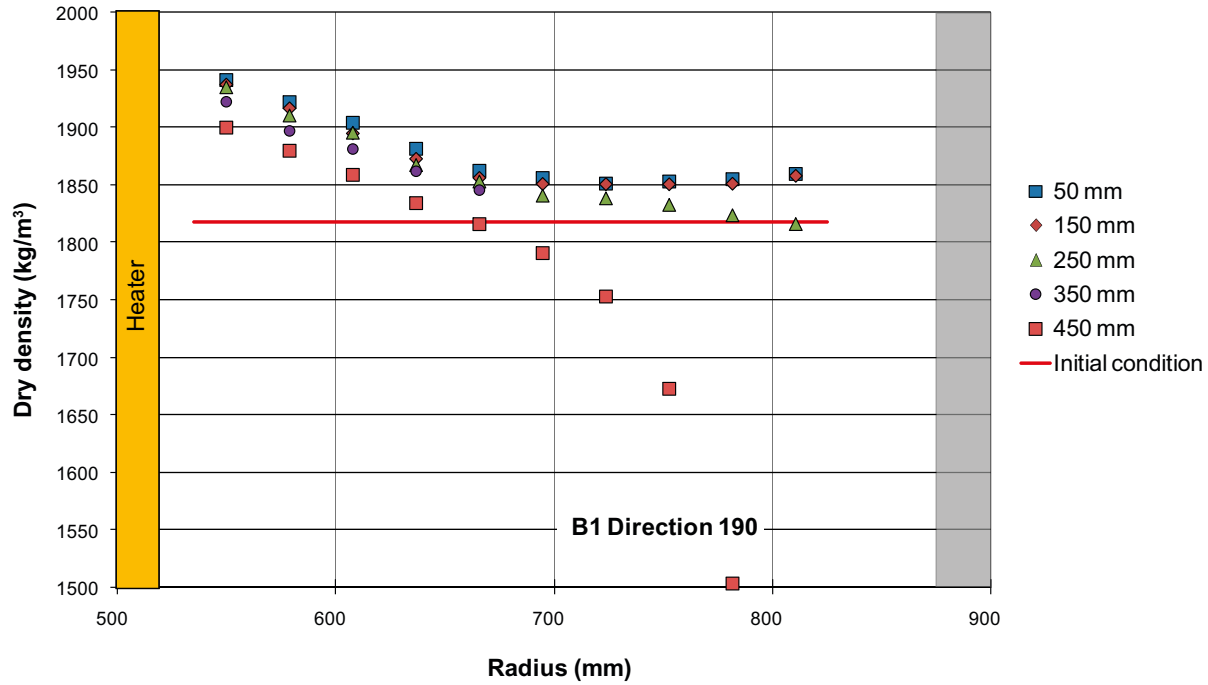

Water content and dry density profiles (B1,280°)

Measured water content and density for the lower block (B1) at direction 280°.

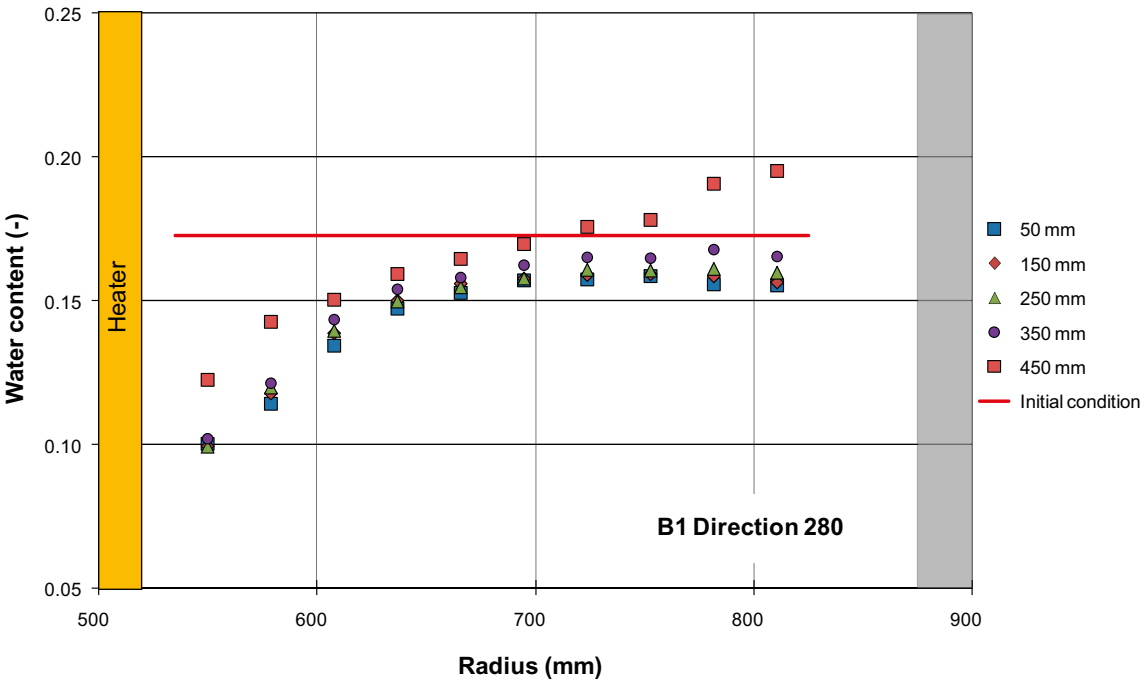

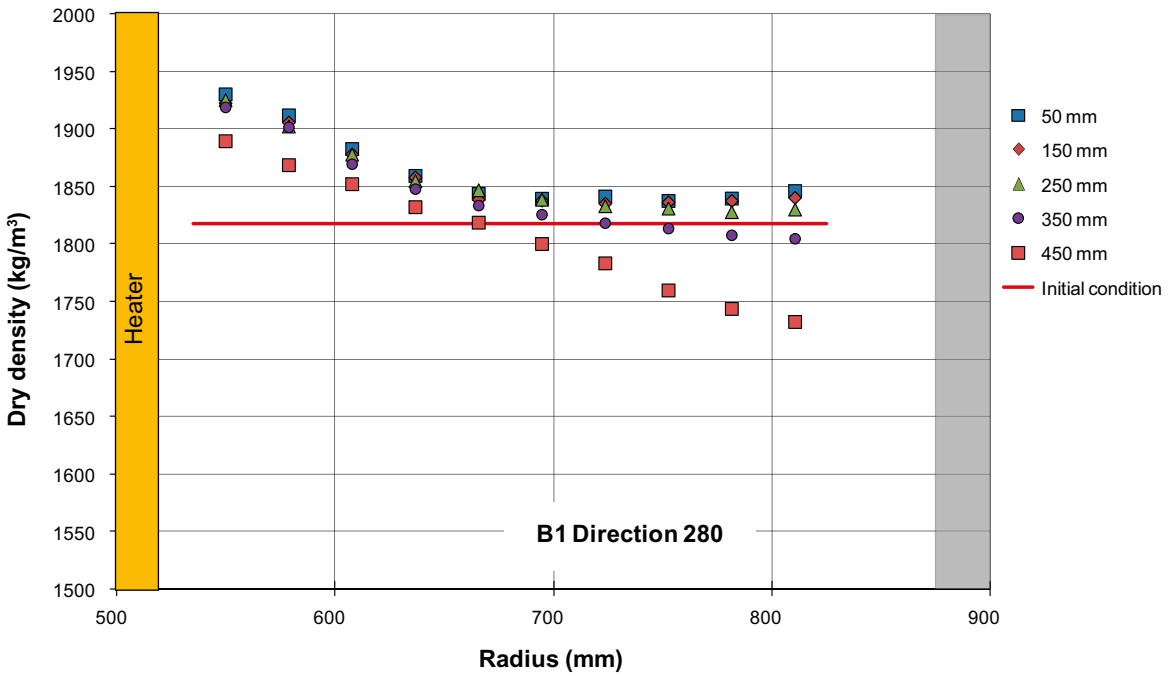

Water content and dry density profiles (B2,10°)

Measured water content and density for the lower block (B2) at direction 10°.

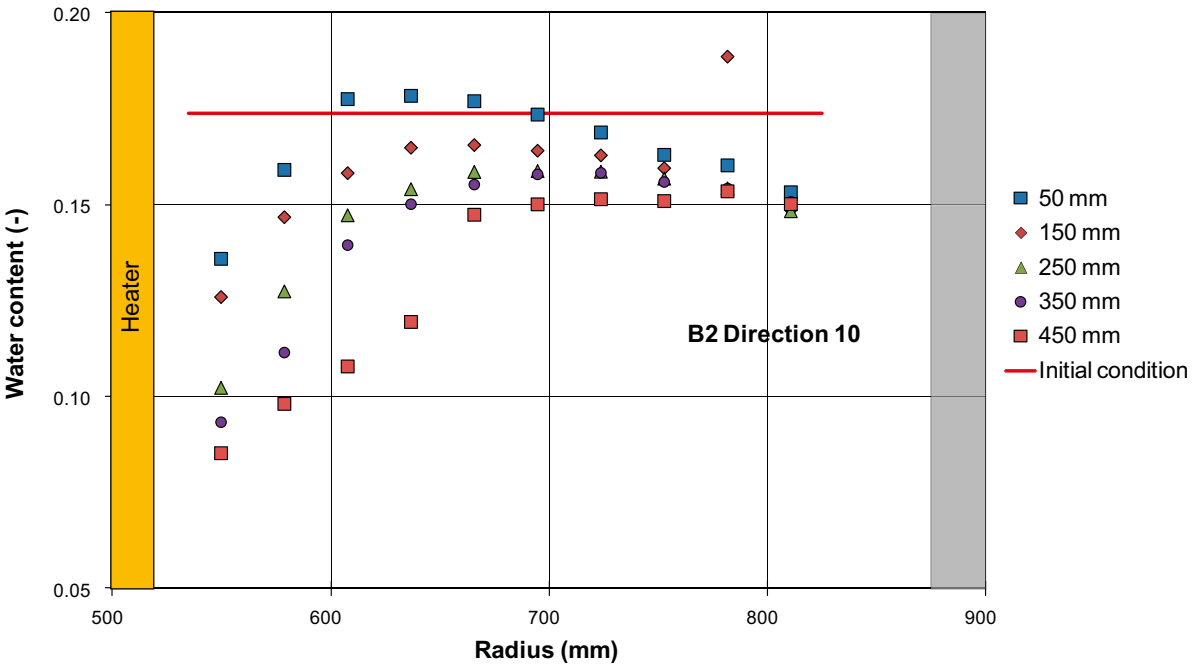

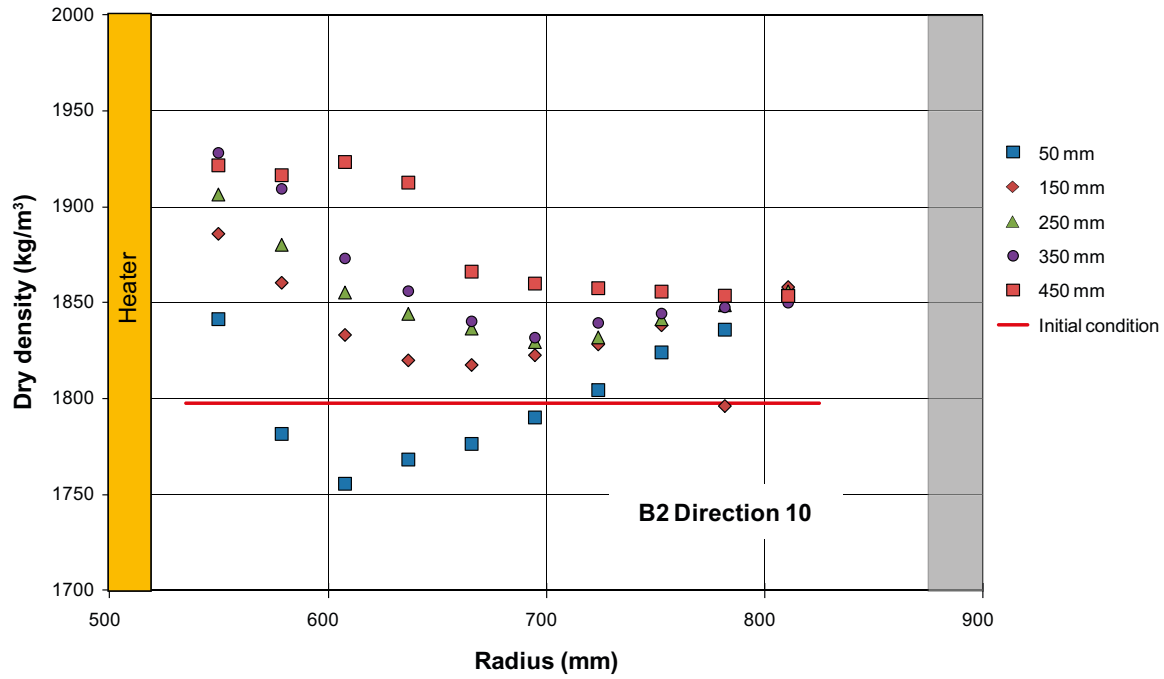

Water content and dry density profiles (B2,100°)

Measured water content and density for the lower block (B2) at direction 100°.

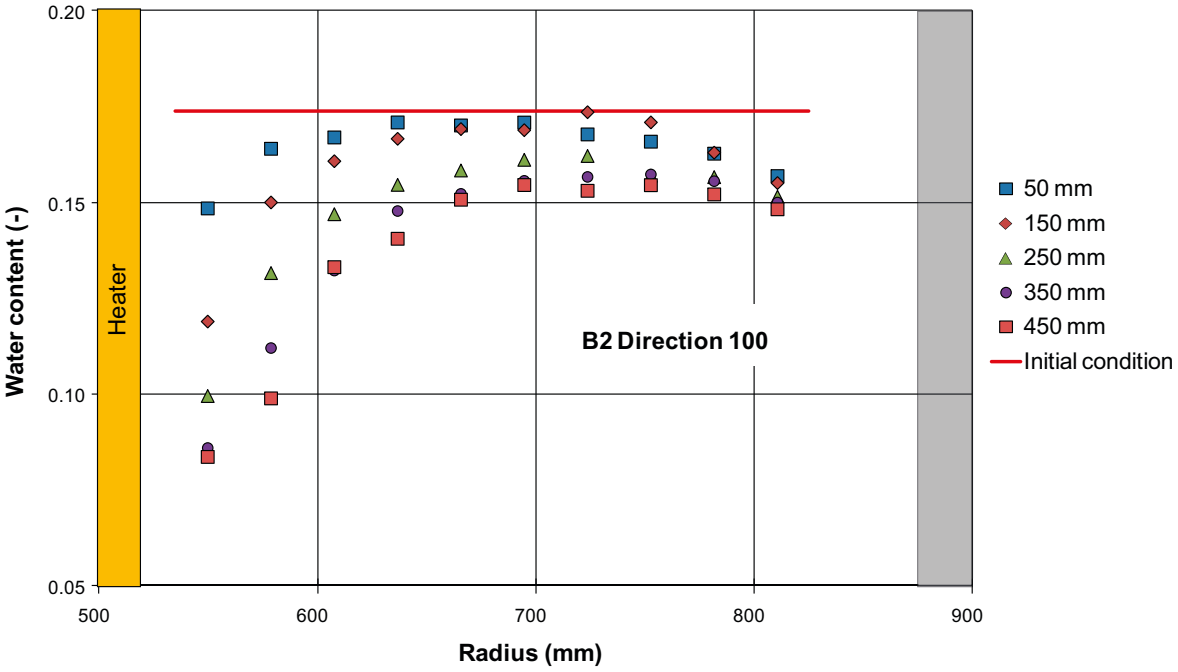

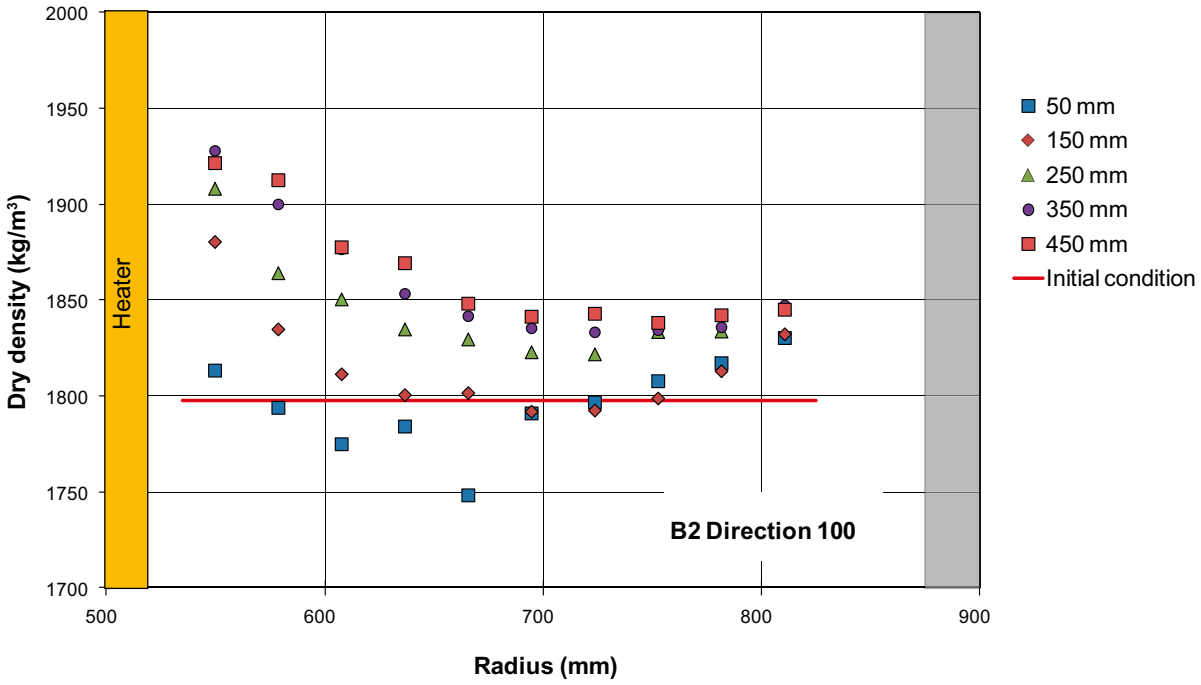

Water content and dry density profiles (B2,190°)

Measured water content and density for the lower block (B2) at direction 190°.

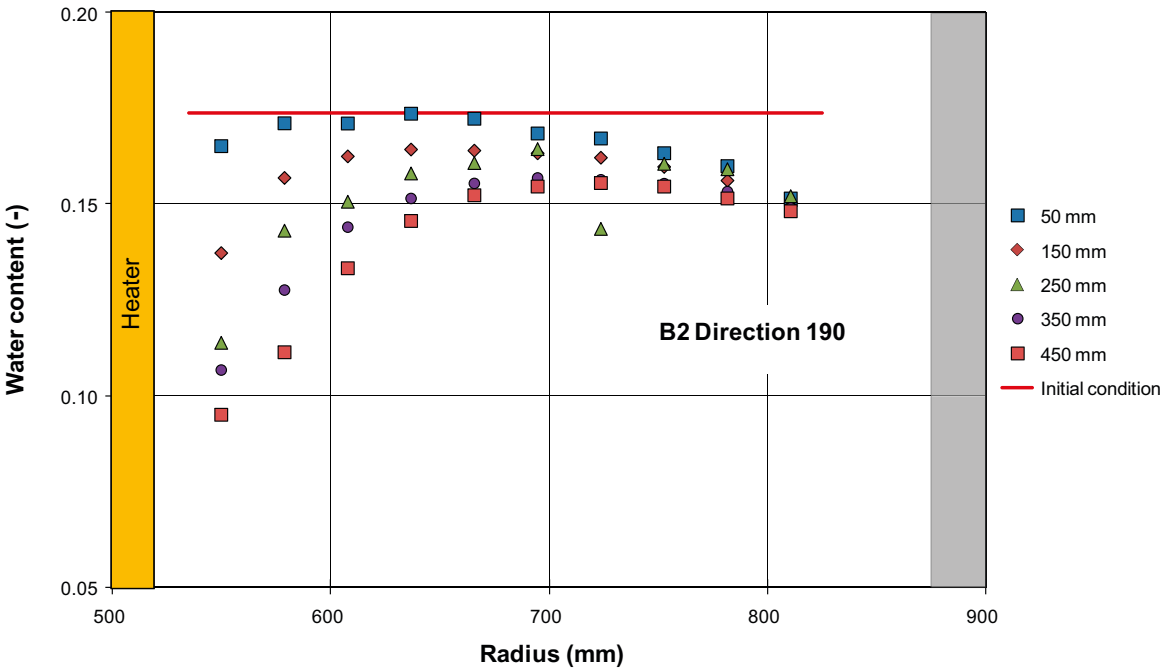

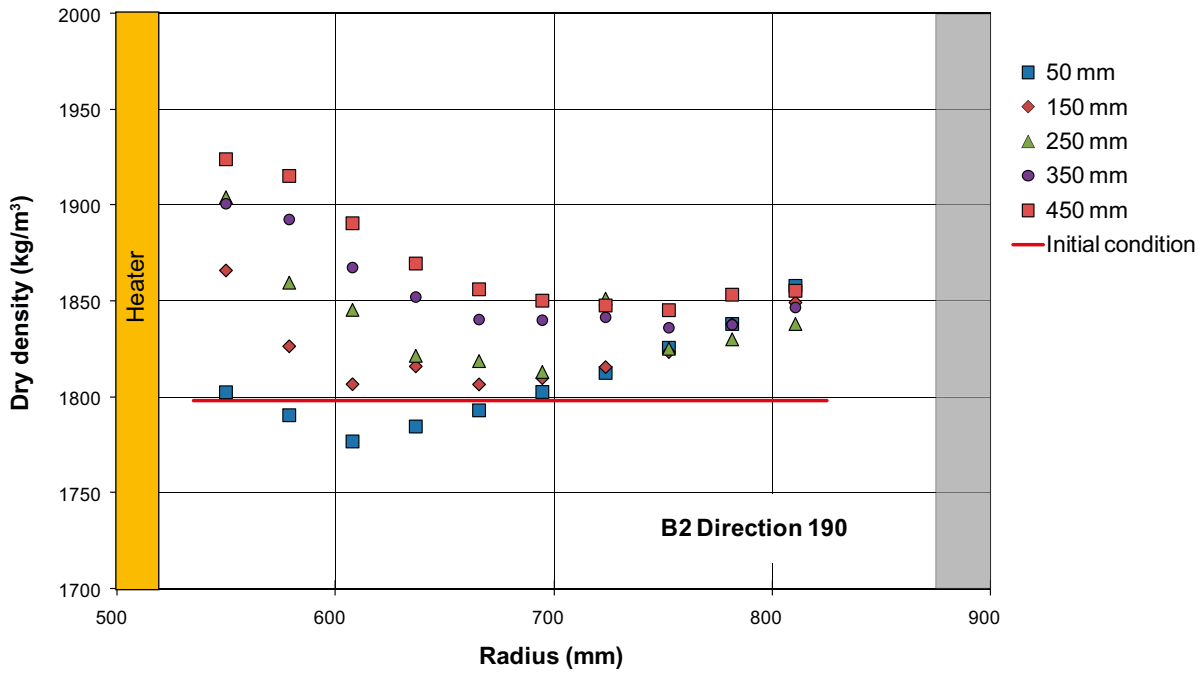

Water content and dry density profiles (B2,280°)

Measured water content and density for the lower block (B2) at direction 280°.

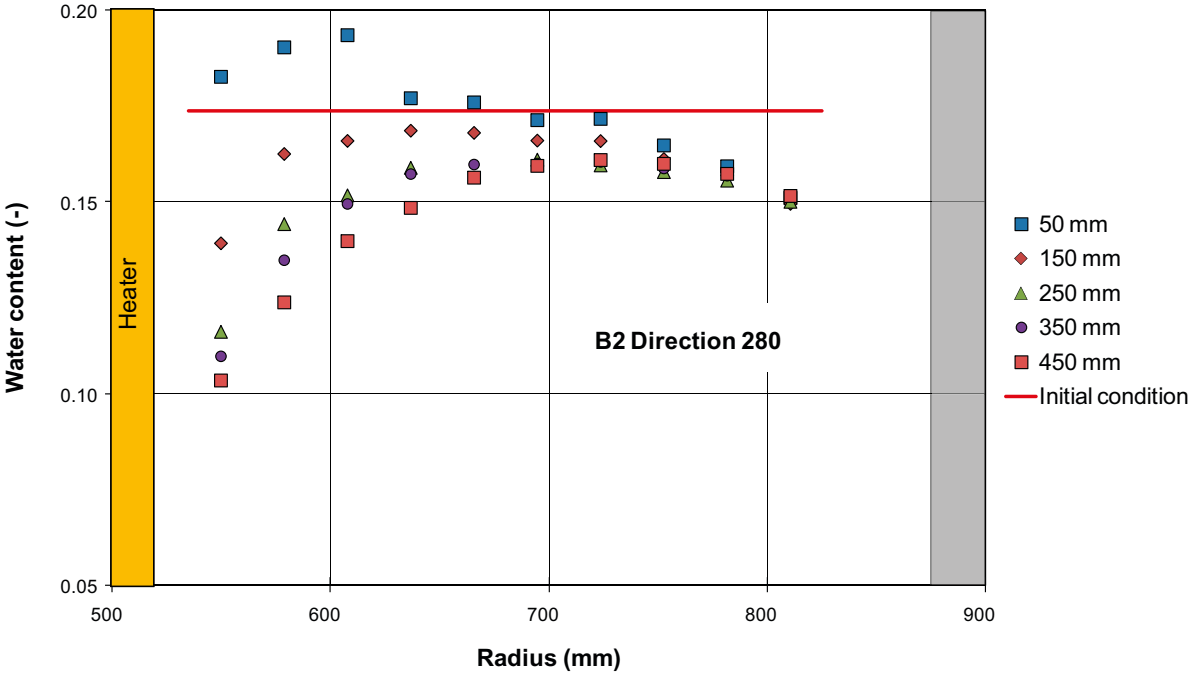

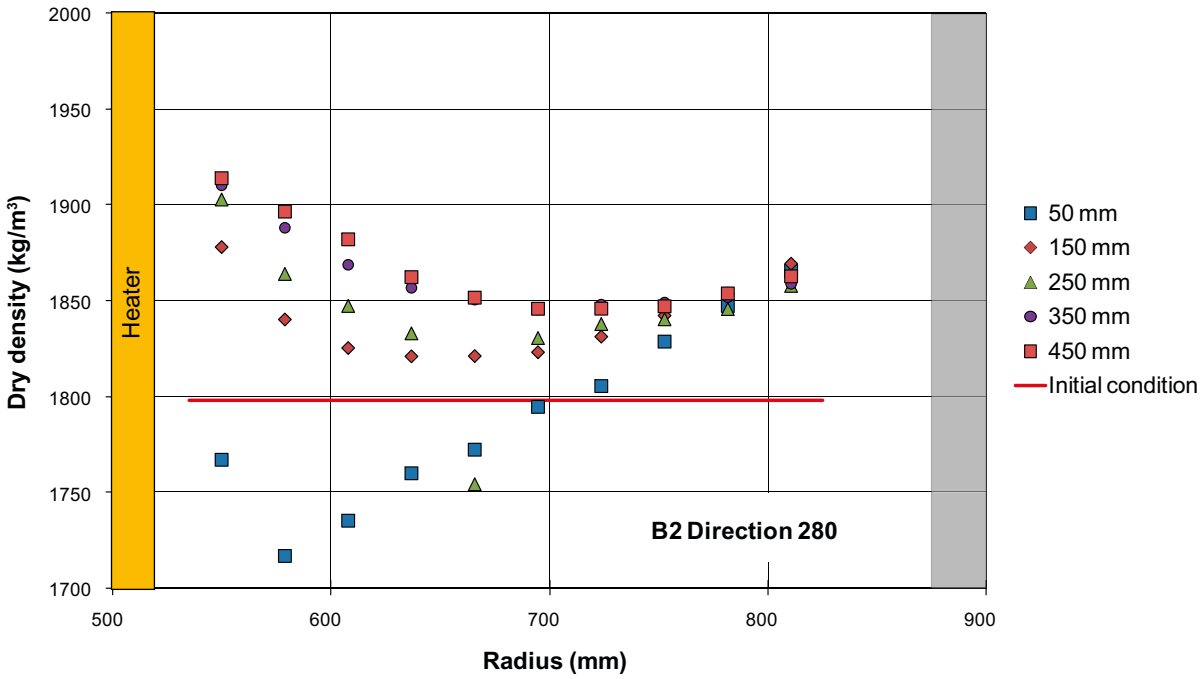

Water content and dry density maps at 10°

Contour plots of water content and density at direction 10°. The initial average water content and dry density of the buffer blocks were 17.3% and 1,810 kg/m^3 respectively.

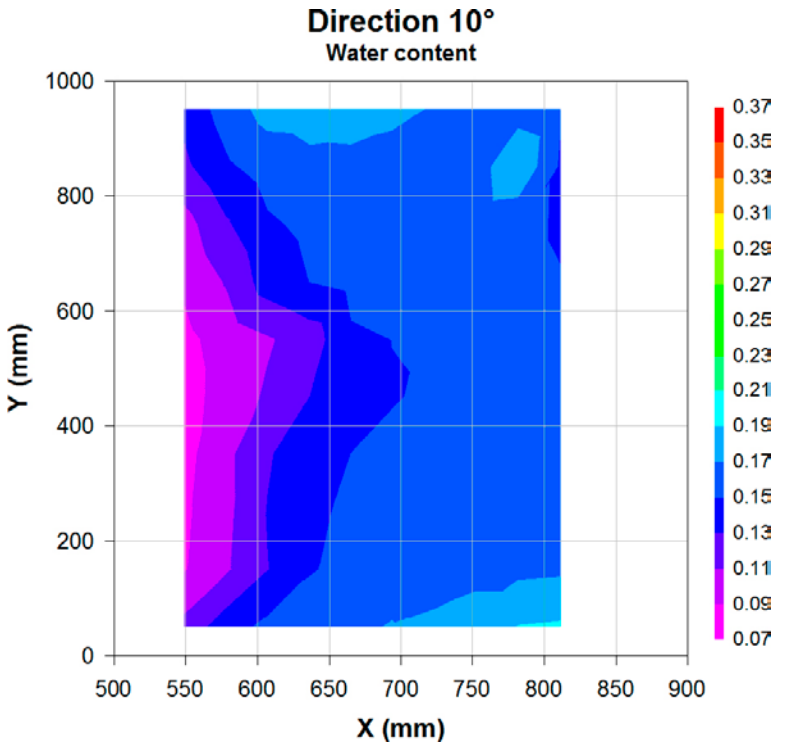

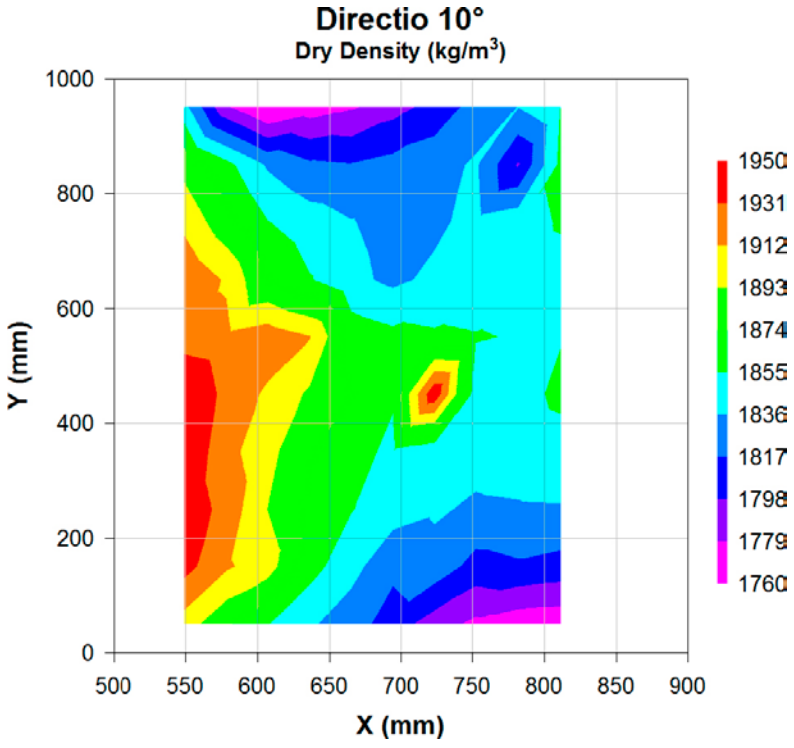

Water content and dry density maps at 100°

Contour plots of water content and density at direction 100°. The initial average water content and dry density of the buffer blocks were 17.3% and 1,810 kg/m^3 respectively.

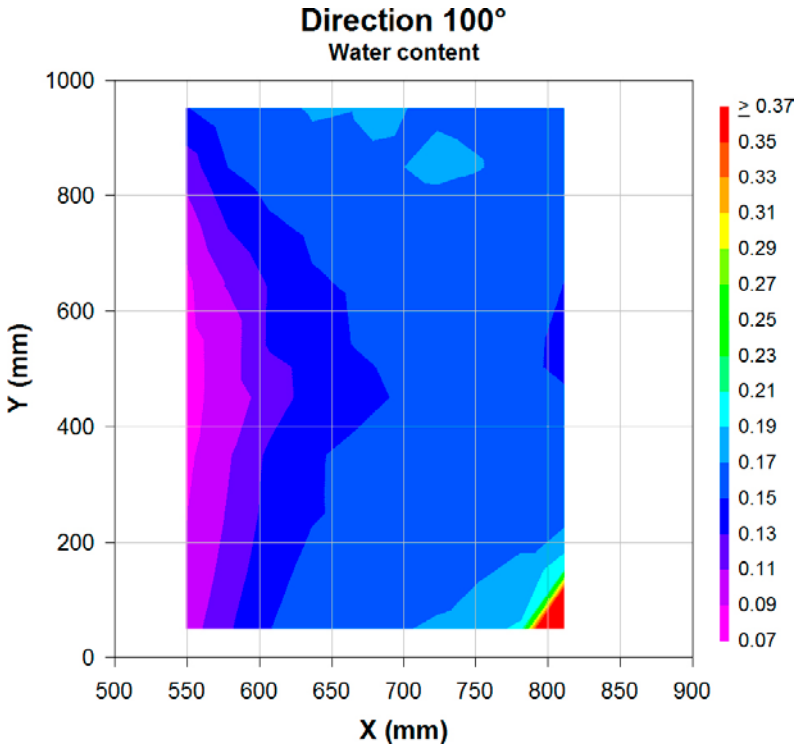

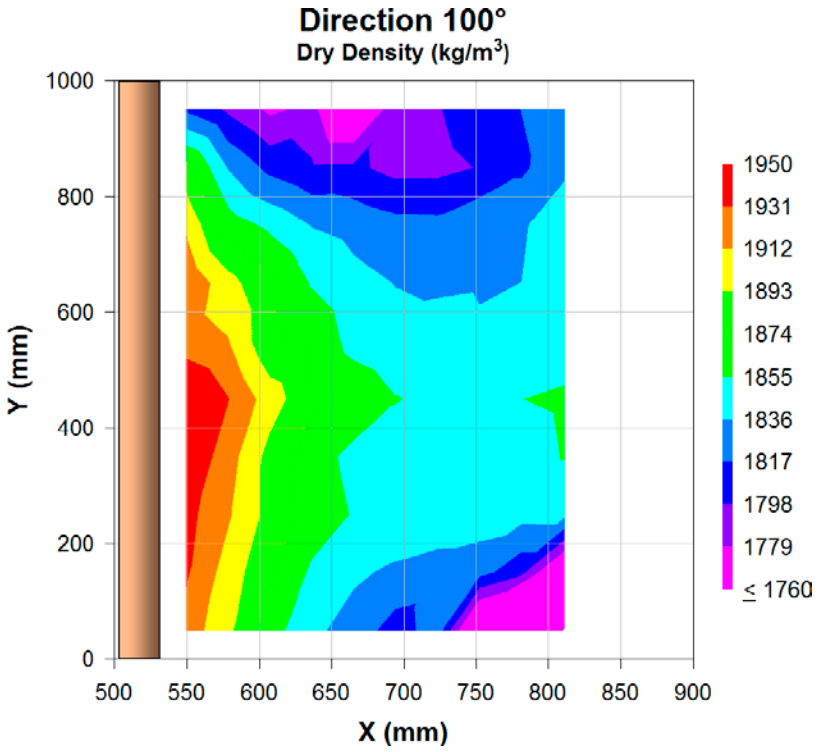

Water content and dry density maps at 190°

Contour plots of water content and density at direction 190°. The initial average water content and dry density of the buffer blocks were 17.3% and 1,810 kg/m^3 respectively.

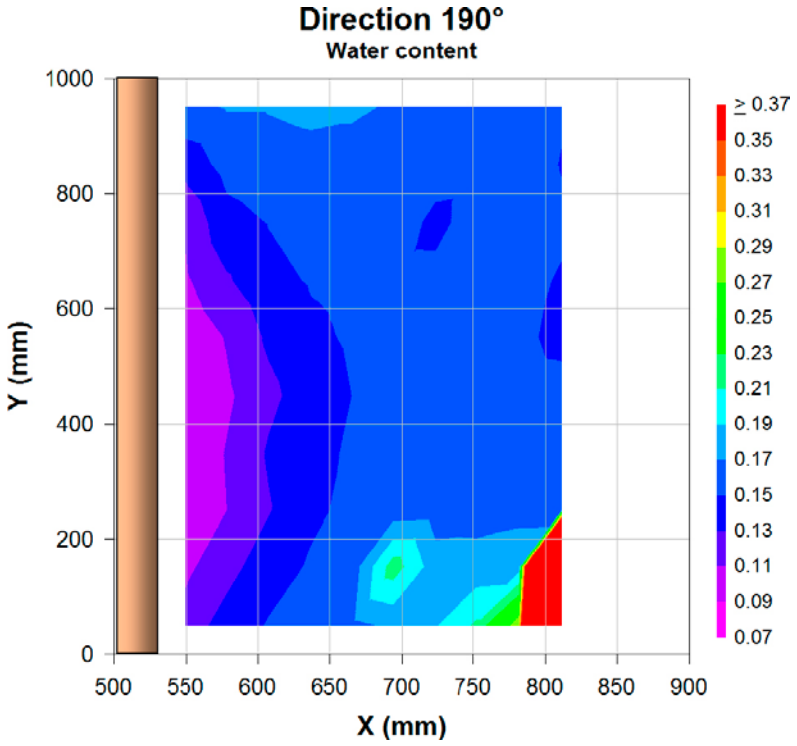

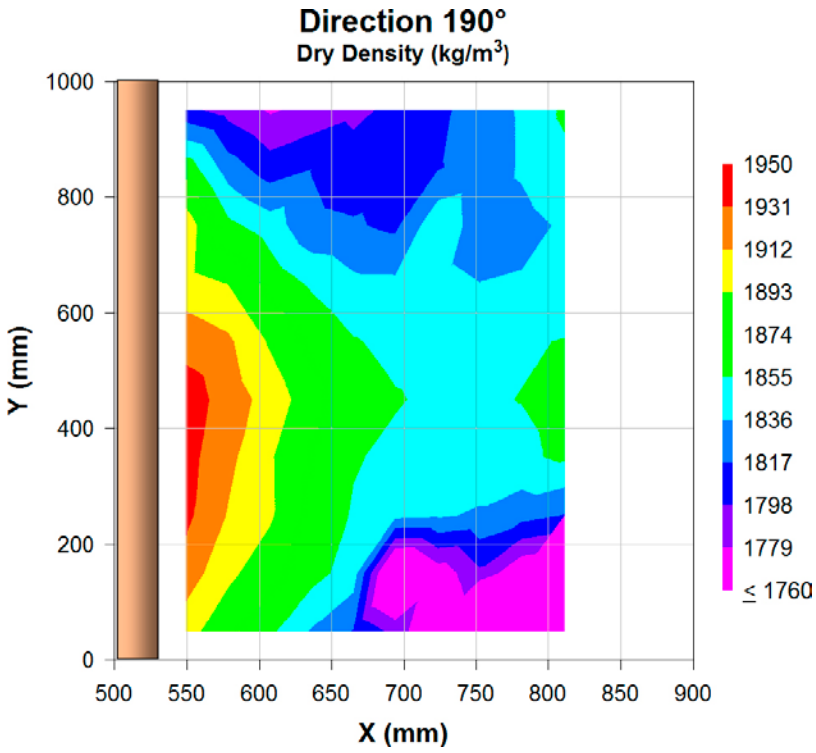

Water content and dry density maps at 280°

Contour plots of water content and density at direction 280°. The initial average water content and dry density of the buffer blocks were 17.3% and 1,810 kg/m^3 respectively.